

東京大学 修士論文

Enhancing the Performance of Linear Metro Driven Railway
-- Energy-saving through ATO Running-curve and
Improvement of Secondary Design of
Linear Induction Motor --

リニア駆動都市鉄道の高性能化の研究
--ATO の活用とリニア誘導モータの二次側構造改良に
よる省エネルギー化--

By

NINH VAN CUONG
(37-126517)

Supervisor

Professor Takafumi Koseki

Department of Electrical Engineering
THE UNIVERSITY OF TOKYO
February 2014

Acknowledgements

First of all, I would like to express my deep gratitude to my supervisor, Professor Takafumi Koseki, for not only his invaluable supervision on this research but also his passionate concern and help in everything since the first day I came to Japan. He has always encouraged me to think and do what a researcher should do. I cannot imagine how could I accomplish this study without his kind support. To be under his supervision has become a great opportunity of my life.

Secondly, I would also like to thank Hitachi Co., Ltd, for their technical support, discussion and advice through joint-research with our laboratory. It was the very field trip to Hitachi Research Laboratory and a lot of discussion with Mr. Eisuke Isobe, Mr. Iwataki Masato, Mr. Masuda Seikichi, and Mr. Yuichiro Nozaki that initiated a part of my research on Linear Induction Motor and the development of ATO for linear metro.

I would then like to sincerely thank my laboratory's Technical staff, Mr. Yasuhiro Takada, for his kindly support on the super computer as well as many other research items for me to carry out the LIM simulations, data processing, which enabled me to smoothly finish my thesis.

Personally, I highly appreciate my sempai, an ex-lab member, Mr. Yuta Yamamoto, and two current M2 companions, Shoichiro Watanabe and Ryuri Watanabe for not only our interesting discussion on research but also their kind help for me to find a job in Japan.

It is certain that I would not be able to accomplish all my tasks during three years without my professor and all lab members. Thank you all the members of Koseki Laboratory: Post-doctor Valerio, Dr. Ong, Dr. Shin, M2 Travis, M2 Duc, M1 Zhao, M1 Mori, M1 Luo, B4 Matsuoka, and B4 Ohashi. Thank you so much for sharing all difficulties and happiness of the laboratory life with me.

I would like to express my special thanks to Panasonic Scholarship Co., Ltd., not only for their financial supports during my three years in Japan but also for giving me a lot of activities to study Japanese culture.

My sincere thank is given to Ms. Yukako Matsuzaki, our laboratory's secretary who has spent much time in supporting me with financial documents for my conference travelling despite the fact that she always has loads of work to do.

Finally, for their emotional support and encouragement, I would like to thank my family, especially thank to my wife for her all the time encouragement and trust in me so that I could have made difficult decisions in my life.

Abstract

The main contribution of this thesis is the research on improving the performance of linear metro - one kind of railway system - through the research on high performance of linear induction motor and energy-saving ATO running curve design. This significant result of ATO running curve design can be applied for linear metro in particular and for normal railway system in general. The thesis is organized in four chapters as follows:

Chapter I will present the background and motivation of the research. Currently due to the demand to energy saving, environmental friendliness and low construction cost, linear metro has appeared to be a good solution for urban transportation system. In order to improve the performance of this system for energy saving, high efficiency linear induction motor should be designed. In addition, the designing for one for the most effective methods for energy saving and improving the transportation efficiency - ATO - is also mentioned.

Chapter II & Chapter III will discuss the main parts of the research as figured out in the chart below; and Chapter IV is the conclusion of the thesis as well as suggestion for further research in the future.

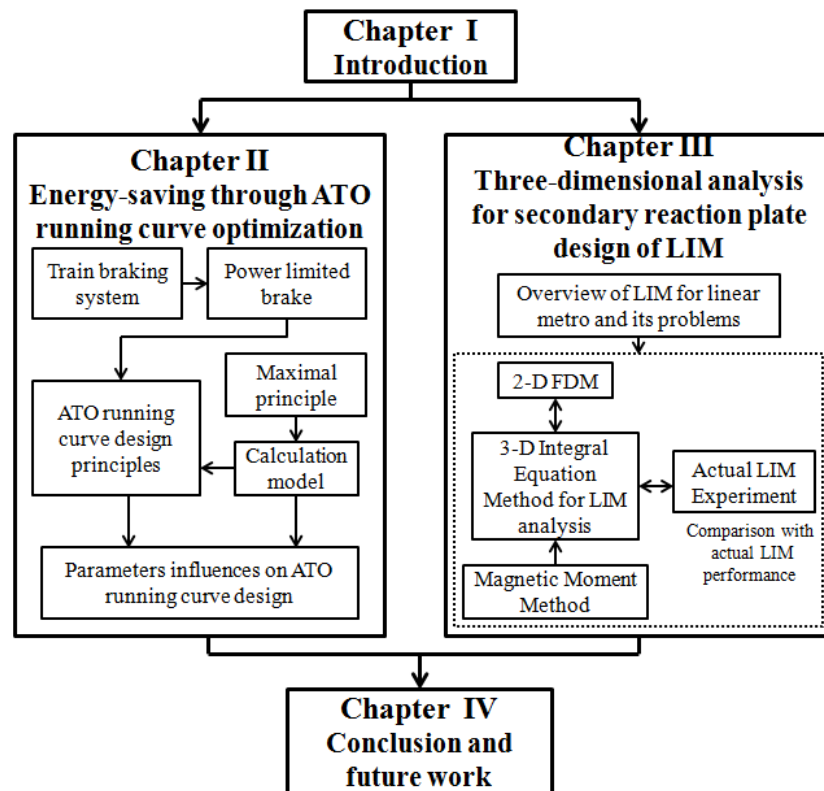


Table of contents

Acknowledgements.....	i
Abstract.....	ii
Chapter 1. Introduction.....	1
1.1. Electric railway and linear metro.....	1
1.2. Research trend on linear metro for energy saving.....	3
1.3. Research purpose.....	4
Chapter 2. Energy saving through ATO running curve optimization.....	5
2.1. Introduction.....	5
2.2. Braking system for electric railway.....	6
2.2.1. Mechanical brake system.....	6
2.2.2. Air brake system.....	7
2.2.2.1. Automatic air brake system.....	7
2.2.2.2. Straight air brake system.....	8
2.2.3. Electric brake system.....	9
2.2.4. Power limited brake for better used of electric brake.....	9
2.2.4.1. Problems of electric brake.....	9
2.2.4.2. Power limited brake.....	10
2.3. Models and simulator.....	11
2.3.1. Models.....	11
2.3.1.1. ATO module.....	12
2.3.1.2. Motor/Generator.....	13
2.3.1.3. Dynamic system module.....	14
2.3.1.4. Energy consumption.....	16
2.3.2. Maximal principle for dynamic system.....	16
2.3.3. Case study for simulation.....	18

2.3.3.1. Simulation conditions.....	18
2.3.3.2. Equation of motion.....	19
2.3.3.3. Simulation results.....	20
2.3.3.4. Possible of energy saving through running curve design.....	29
2.4. Parameter influence on ATO running curve design.....	31
2.4.1. Influence of coasting distance.....	32
2.4.2. Influence of coasting and notch off speed when considering speed limitation.....	33
2.4.2.1. Influence of primary coasting.....	34
2.4.2.2. Influence of primary notch off speed.....	37
2.4.3. Influence of upper and lower speed at constant speed control.....	41
2.4.4. Influence of the combination of some different parameters.....	42
2.5. Chapter summary	44

Chapter 3. Three-dimensional analysis for secondary reaction plate design of LIM...45

3.1. Introduction.....	45
3.2. Overview of LIM for linear metro.....	46
3.2.1. Construction and principle of LIM.....	46
3.2.2. LIM problems.....	47
3.2.2.1. End effect.....	47
3.2.2.2. Edge effect.....	48
3.2.2.3. Eddy current problem.....	48
3.3. Numerical analysis method for LIM analysis.....	49
3.3.1. 2-D finite different method.....	50
3.3.2. 3-D integral equation method using magnetic moment method.....	52
3.3.3. LIM calculation using numerical analysis.....	53
3.3.3.1. Derivation of basic equation.....	53
3.3.3.2. Magnetic flux density calculation.....	54
3.3.3.3. Forces calculation.....	55
3.3.3.4. Impedance calculation.....	56

3.4. 3-D integral equation method model and results.....	58
3.4.1. LIM model for 3-D IEM analysis.....	58
3.4.2. Numerical results.....	61
3.4.2.1. Air gap magnetic flux density.....	61
3.4.2.2. Two dimensional forces.....	66
3.4.2.3. Inter-linkage flux.....	66
3.4.2.4. Eddy current distribution.....	67
3.4.2.5. 2-D FEM and 3-D IEM result comparisons.....	68
3.5. Actual LIM experiment and comparisons.....	69
3.6. Chapter summary.....	73
Chapter 4. Conclusion and future work.....	74
4.1. Conclusion.....	74
4.2. Future work.....	75
References.....	76
Publication list.....	78

Chapter I: Introduction

1.1. Electric railway and Linear Metro

Environmentally friendly energy solutions are growing in demand in global development. Such solutions are also required in railway systems that are already considered as one of the most energetically efficient transportation systems. Because of its social role in the era of motorization since the later half of the 20th century, electric railway systems are growing as an important key in energy saving and environmentally friendly consumption, Fig.1.1 [1]

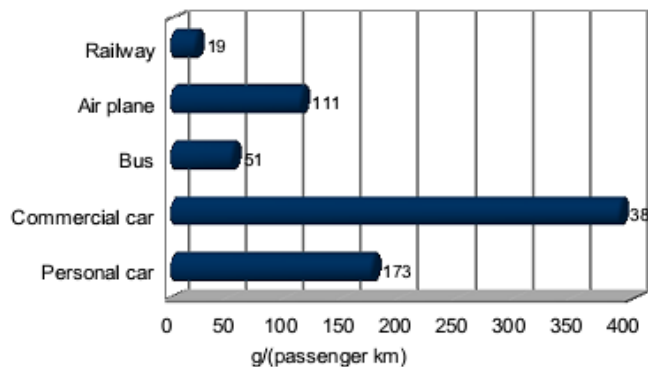


Fig.1.1. CO2 emission of different transportation models

In order to meet the requirement of reducing the construction, maintenance, and operating cost, Linear Metro has appeared to be the best solution for urban transportation systems. Driven by a Linear Induction Motor (LIM) and employing a steel wheel/steel rail track system, the Linear Metro is an advanced urban transportation system offering a wide range of features that are not available on other train systems. The Linear Metro has already been operated in Canada, Japan, China, Korea, Austria, and other countries. In Japan, Linear Metro has been developed since the 1990s, and it is a good solution for the big cities like Tokyo, Osaka, Yokohama, Kobe, Fukuoka and the newest one in Sendai, Fig.1.2. Exploiting all the advanced features of Linear Metro including low-noise inverter equipment and automatic operation system, the cars offer enhanced intelligence as a new subway transport systems for the 21st century.

In comparison with conventional railway systems, Linear Metro has some remarkable features[2]:

- (1) easy to navigate at steep gradients and sharp curves;
- (2) able to reduce cross section of subway tunnels;
- (3) saving of maintaining cost and operation cost;
- (4) unaffected by weather conditions on train operation;
- (5) reducing gear and ignorant of revolving motor.



Fig.1.2. Linear Metro in Fukuoka

With the features described above, Linear Metro meets all requirements of the next generation of urban transportation systems. Ideal urban transportation requirements and Linear Metro features are described in Fig.1. 3.

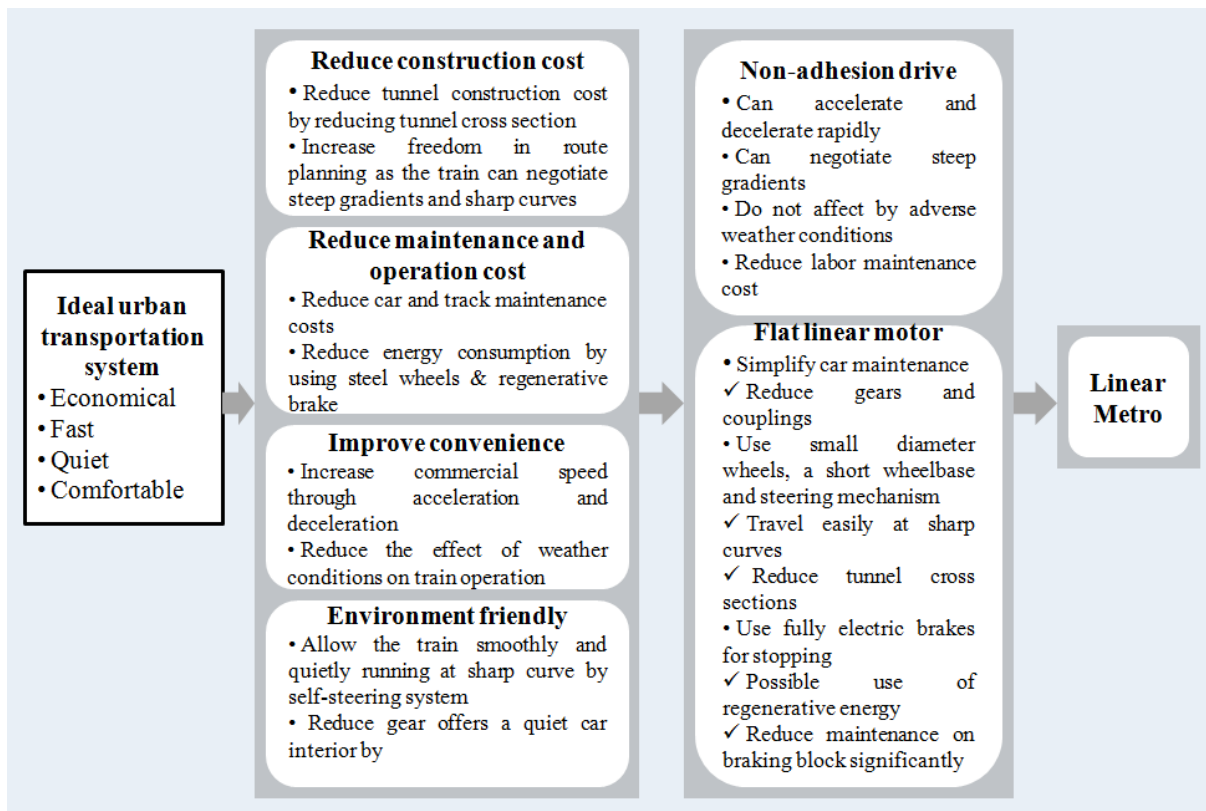


Fig.1.3. Advantages of Linear Metro system

1.2. Research trend on Linear Metro for energy saving

In order to reduce energy on Linear Metro operation, many researches have been conducted in both hardware and software bases. For example, researches on improving the performance of driven part - Linear Induction Motor (LIM) design and control; traction inverters using IGBTs to minimize noise; light and low cost on board energy storage devices, improving transportation efficiency through Automatic Train Control (ATC), and Automatic Train Operation (ATO) for better use of regenerative brake or Train Intelligent Management Systems (TIMS). Mainly current develops for energy saving on Linear Metro are illustrated in Fig.1.3.

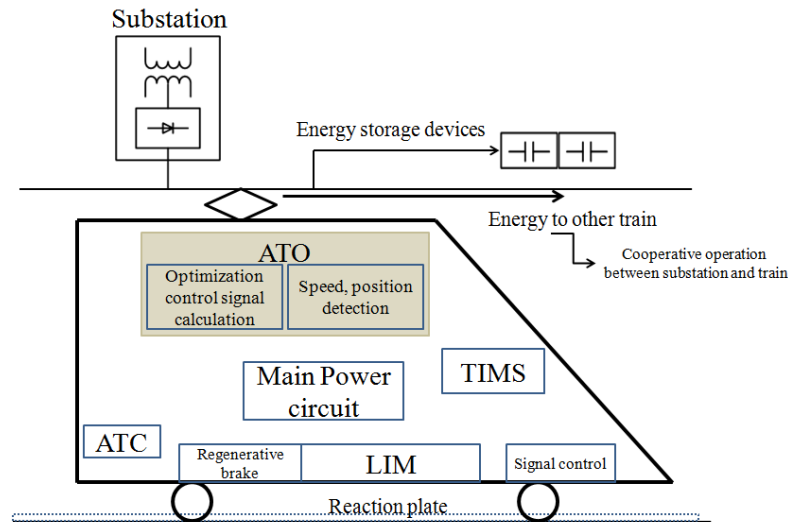


Fig.1.3. Research trend on Linear Metro

1.3. Research purpose

Due to the requirement of energy saving on Linear Metro, this research focuses on two problems:

- i. Energy saving through ATO running curve optimization

While most of the railway systems, including Linear Metro systems, have the function for regenerative brake, Linear Metro has no function for regenerative power from the railway to commercial power network. Therefore, regenerative power cannot be used when there are no other simultaneous accelerating trains near the braking train. Consequently, the effective usage of regenerative power is less than initial expectation since power squeezing and cancellation of regenerating brake often occur. To solve this problem, running curve for better use of regenerative brake has been considered in the first part of this thesis. Thanks to the support of ATO devices, the design of running curve can be considered in both total energy consumption and braking power, which can be applied not only for Linear Metro but also for normal railway systems.

ii. Three-dimensional analysis for secondary reaction plate design of LIM

The cars are powered by a bogie frame-mounted primary LIM that permits reduction of the car floor size. In addition, LIM is capable of navigating at steep gradients and sharp curves. The LIM was designed for maximal efficiency and the same principal was applied to secondary reaction plates mounted on the sleepers. In LIM analysis and design, since two-dimensional (2-D) analysis cannot express the influence of transverse edge effect caused by the finite width of the electromagnetic problem; in this thesis, by using 3-D dynamic analysis for accurate dynamic characteristics, the influence of the finite length of the primary part and the finite width of the secondary part will be examined in LIM performance.

The research purposes are illustrated in Fig.1.4.

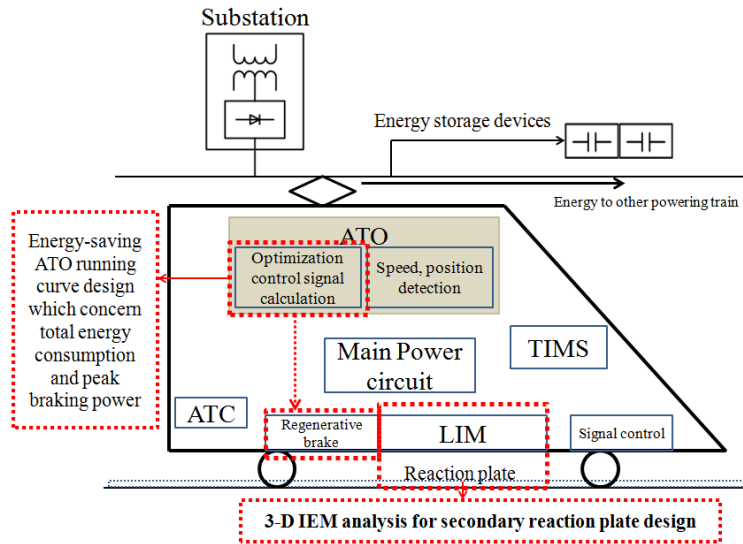


Fig.1.4. Illustration for research purposes

Chapter II

Energy-saving through ATO running curve optimization

2. 1. Introduction

Automatic Train Operation (ATO) system has been known as one of the most effective methods for saving energy and improving the transportation efficiency, especially in urban transportation systems [3]. Together with the rapid improvement of technologies, more and more ATO systems have been put into railway operation, including in Linear Metro [4]. This new system does not only operate the train according to the running plan, but it can also control the braking pattern to stop the train smoothly and accurately while still be able to save energy.

While most of the railway systems have the function for regenerative brake, most substations for DC-electrification have no function for regenerative power from the railway to commercial power network. Therefore, regenerative power cannot be used when there are no other timely accelerating trains near the braking train. Consequently, the effective usage of the regenerative power is less than initial expectation since power squeezing and cancellation of regenerating brake often occur. In an attempt to solve this problem, several studies have been conducted recently on reducing peak power by utilizing regenerative energy. Power-limited brake for better use of regenerative brake at high-speed operation has also been proposed in recent researches [5][6]. Fundamental advantages of this method have been confirmed through various experimental studies. Although limitation still exists on the braking point, this method will be more useful in designing new ATO systems.

In order to find the running curve for the purpose of energy saving, mathematical models have been applied based on optimal control techniques. In [7] the optimal speed profile is calculated with the maximum principle. The study in [8] considers the problem of optimal driving strategy based on a generalized equation of motion that can be used in discrete and continuous control but the result is a theoretical approach. The study in [9] developed a discrete dynamic programming algorithm to avoid the difficulties of resolving the optimal control problems. In [10], Bellman's dynamic programming has also been used to optimize the running profile of train. Because of the simplification of the tracks, trains and driving models of these methods, they cannot be applied for optimal design of subway ATO running curve that has complicated braking force characteristics and short inter-stations [11].

One of the most important requirements for railway system is customer satisfaction of time accuracy. However, as total energy can be reduced when the running time is increased, total energy consumption reduction has been considered in [12] by assigning a little more time to stopping time. In this sense, this method has apparently negative affect on customer satisfaction.

Purpose

The main purpose of this chapter is to show the benefits of the regenerative brake through power limited brake and energy optimized through running curve design when looking at energy consumption and peak power of regenerative brake.

Methods

The study is carried out through both literature review of previous studies and practical methods of calculation and simulation.

2.2. Braking system for electric railway

Any rolling stock has some forms of braking devices, so it can decelerate and stop when necessary. Since most passenger trains are electric trains, the braking system is usually a combination of air brake system and dynamic brake system which is able to generate electricity.

2.2.1. Mechanical brake system

The basic braking devices used by mechanical brake system are: wheel-tread brake, Fig. 2.1; axle-mounted disc brake, Fig. 2.2; and wheel-mounted disc brake, Fig. 2.3. All these mechanisms use an object (a brake shoe or lining) that applies friction to the disc. The applied pressure is adjusted to control the braking force. In the wheel-tread brake, the brake shoe applies friction to the wheel tread, creating a sliding effect. High-speed trains cannot use this type of brake because of the damage to the wheel-tread. Instead, axle- or wheel-mounted disc brakes have been used. In addition, axle-mounted disc brakes are used on trailer bogies, because they have sufficient space to accommodate in such systems. Wheel-mounted disc brakes are often used on motor bogies that must accommodate the traction motor and have insufficient space for an axle-mounted brake. In both systems, compressed air or oil is applied to a brake cylinder that forces the brake lining against the disc. Brake discs are dead weights that are useful only during braking, so operators are keen to install lighter discs. Carbon/carbon-composite multi-discs and aluminum composite discs offer lighter weights and are viewed with considerable interest. The carbon/carbon-composite multi-disc has alternative sections of carbon-fiber rotors and stators. During the braking mode, they rub against each other to create a frictional force that slows down the wheel or axle. The disc is lighter than conventional materials and has excellent heat resistant properties, as shown in Fig. 2. 4 [13].

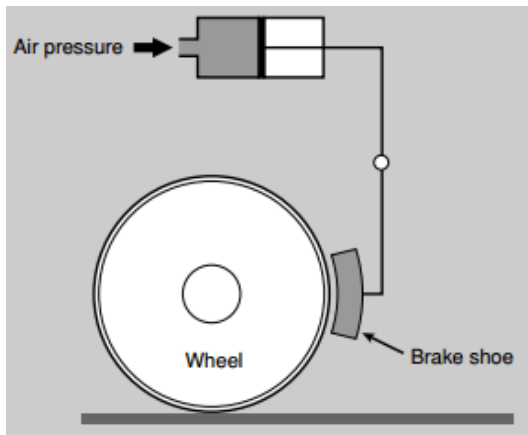


Fig. 2.1. Wheel-tread brake system

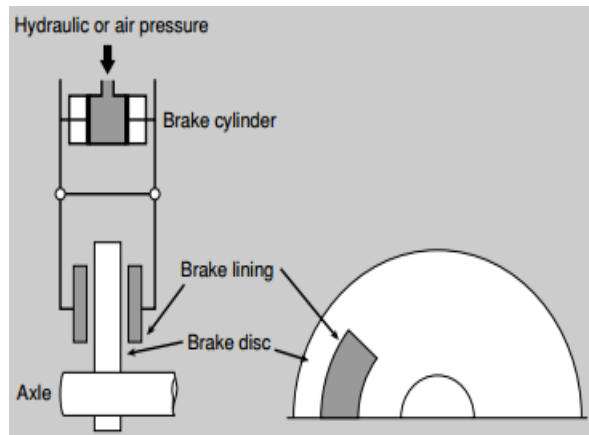


Fig. 2.2. Axle-mounted disc brake system

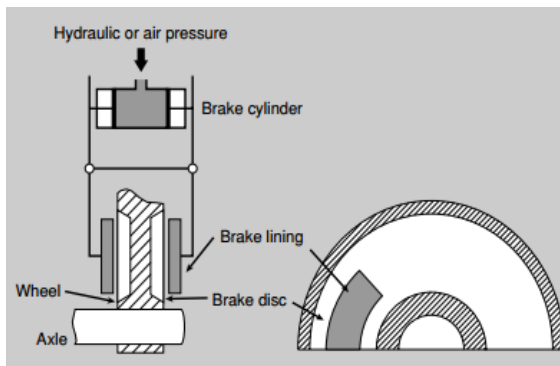


Fig. 2.3. Wheel-mounted disc brake system

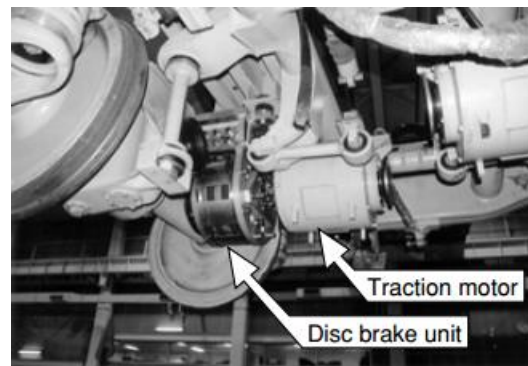


Fig. 2.4. Carbon/carbon-composite multi-disc system

2.2.2. Air brake systems

2.2.2.1. Automatic air brake system

Fig. 2.5 shows the arrangement of an automatic air brake system. Air compressors mounted every two for four cars supply compressed air to the air brakes. The air, which is compressed from 700 kPa to 900 kPa, is piped under the car floors to main air reservoirs. The air pressure is lowered to 490 kPa by a pressure regulator and the air is fed via the brake valve, brake pipes and control valves to the auxiliary air reservoirs. When the compressed air in the brake pipes and auxiliary air reservoirs of each car is at 490 kPa, the brakes are not activated. However, the activated brake valve cuts the flow of air from the pressure regulator, so the air pressure in the brake pipes falls. The fall of air pressure is detected by the control valves on each car. The control valves regulate the flow of compressed air from the auxiliary air reservoirs to the brake cylinders. The brake cylinders

activate the basic braking mechanisms to slow down and stop the car. The control valves regulate the flow of air from the auxiliary air reservoirs to the brake cylinders at a pressure that is proportional to the pressure drop in the brake pipes [13].

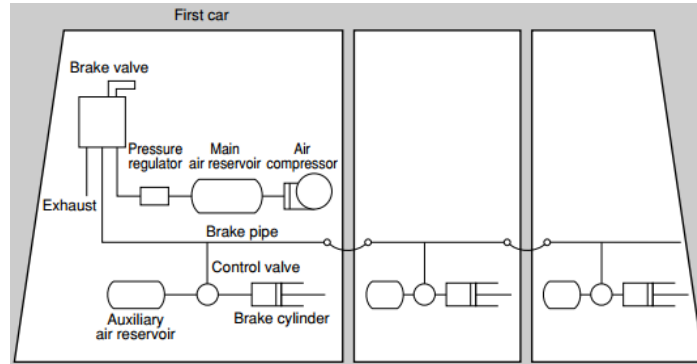


Fig. 2.5. Automatic air brake system

2.2.2.2. Straight air brake system

Fig. 2.6 shows a straight air brake system. Different from the automatic air brake system, the straight air brake system does not have a control valve or auxiliary air reservoir in each car. The activation of the brake valve forces compressed air through the straight air pipe to the brake cylinders, activating the basic mechanical brake.

However, since the straight air pipes do not contain compressed air during normal running conditions, the brake would fail if the cars become uncoupled. In order to avoid this problem, the straight air brake system can be used in conjunction with the automatic air brake system. It can also be avoided by running another pipe from the first to the last car. The air pressure in this pipe acts like the compressed air in the brake pipes of the automatic air brake system. If the compressed air in this main air reservoir pipe falls, or if it leaks from air pipes or from air hoses between cars, etc., the pressure drop is detected and the brakes are applied automatically.

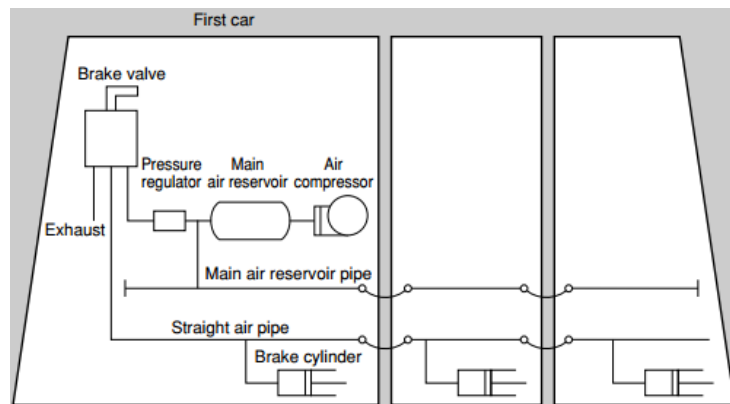


Fig. 2.6. Straight air brake system

2.2.3. Electric brake system

Nowadays, with the demand on energy saving, electrical dynamic systems have been widely used. The electrical system can convert the motor into braking generator dissipation the kinetic energy as heat. Fig. 2.7 shows the principles of the electrical traction, dynamic braking and regenerative braking systems. Although the traction motor drives and accelerates the train during braking mode, it acts as an electric generator instead of forming a part of a circuit that consists of a main resistor (rheostat), armatures and a field system. Electricity flows through the circuit and is consumed by the main resistor that converts the kinetic energy of the train into heat and thereby acts as a brake [13].

Regenerative brake uses the same type of circuit, but the main resistor does not consum the electricity generated through braking. Instead, it is transmitted to the overhead wire. A controller under the pantograph that opens and closes with split-second timing control the flow of this electricity. The problem with electrical brake system is that they can occasionally malfunction because they have complex circuits. For this reason, they cannot be used as emergency brakes. In an electrical braking system, the braking force of the traction motor is transmitted to the wheel via gears. The generated electricity is adjusted to control the braking force.

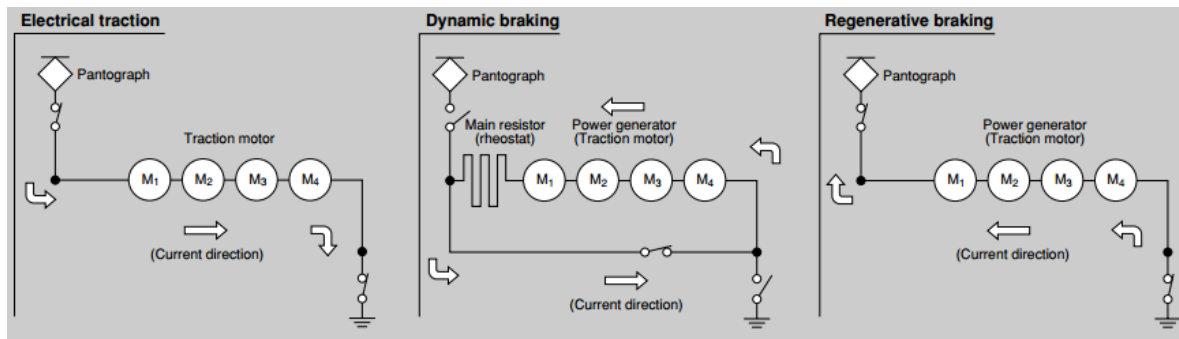


Fig. 2.7. Principle of electric braking system

2.2.4. Power limited brake for better use of electric brake

2.2.4.1. Problems of electric brake

The advantages of electric brake as regenerative brake have been tested and approved in real railway systems. It is possible to reduce the operation maintenance, the wheels of the brake shoe and to increase the energy saving effect.

However, the regenerative brake cannot operate successfully by external loading conditions as described in Fig. 2.8, the graphic of braking pattern and pantograph voltage in train system [14]. As shown in this figure, at position A - the initial of braking point, when

braking command value is small, the braking force is also required to be small on the train. For this reason, pantograph voltage is less than the overhead voltage value (1650V), and it is possible to use full regenerative brake. However, when the braking command increases in position B, pantograph voltage also increases to over 1650V, and the braking force of electric brake makes larger aperture. There are many standards to control the narrow regeneration of overhead line voltage, but because of the large regenerative power, regenerative power cannot be obtained by powering train. In this case, the output of the regenerative brake is suppressed to protect the electrical equipment, and mechanical brake must be used instead.

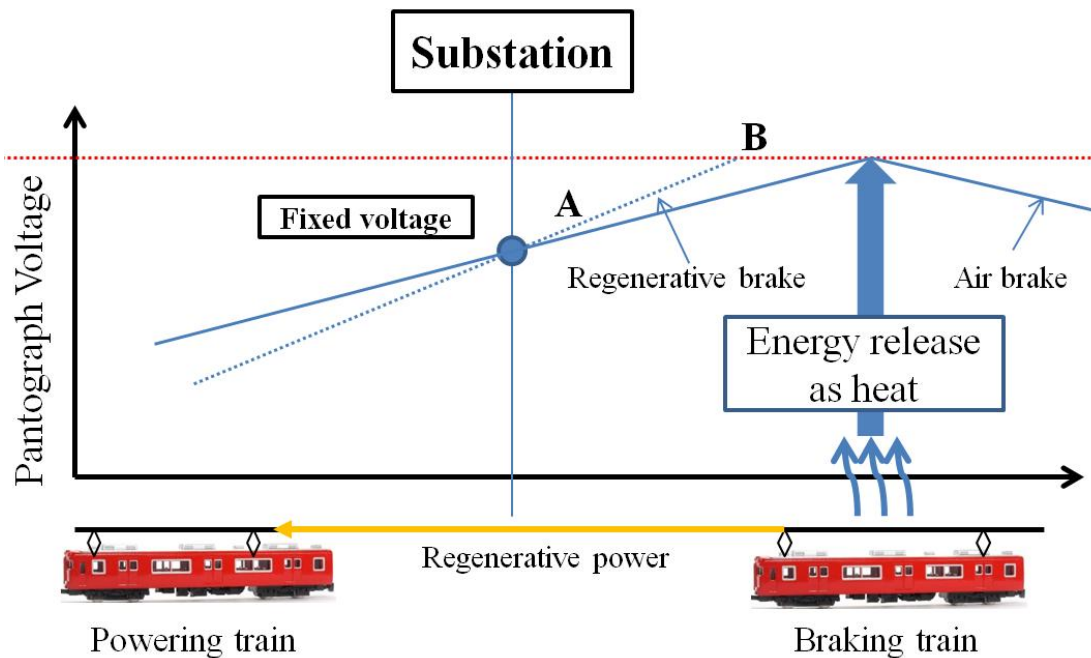


Fig. 2.8. Graphic of braking pattern and pantograph voltage

2.2.4.2. Power limited brake

The restriction on energy loss and protecting power of electronic components of conventional braking pattern has made researchers keep on considering a substation method for braking pattern. Based on the idea of previous researches, braking pattern appropriate for energy saving train operation is schematically represented in Fig. 2.9 - the power limited brake. The solid line is conventional braking command with constant deceleration. The 'plus' solid line stands for motor specification. The 'dot' line represents the different power-limited brakes. Braking force is kept as motor specification at low speed. At high speed, braking power is kept constant at power-limited value, so the braking force is reduced in proportion to $1/v$ at high speed.

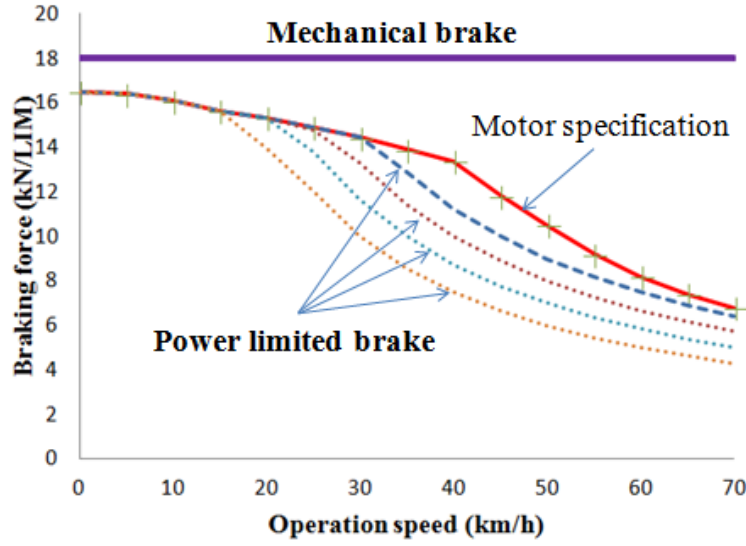


Fig. 2.9. Different braking modes

2.3. Models and simulator

2.3.1. Models

When designing the energy-efficient running curve, running time, energy consumption and braking power must be considered in a mutual relation. The proposed design method is based on the accurate simulation of all the possible combination of ATO running curve for each inter-station in order to obtain precise results of these variables. To achieve this accuracy, the simulation model has been modularized. Each module represents the different subsystems of a real train, Fig. 2.10.

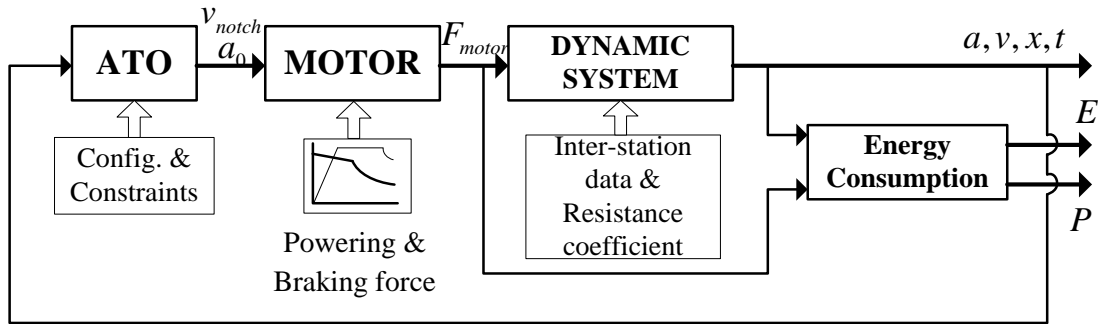


Fig. 2.10. Blog diagram of the modularized model simulator with ATO module

The simulation is composed of four modules: ATO equipment simulator, defined and set up the input notch-off speed and acceleration; motors, generated accelerate and decelerate force; train dynamic systems, based on real parameters; and train consumption

model. This modular architecture allows the validation of each module separately and an easy adjustment for specific features of a particular ATO. In addition, the simulator input interface is designed to enable the definition of track layout, train characteristics and ATO system configuration.

The ATO model represents the control logic of the driving schemes. At each simulation step, the position and speed of the train is input. Then, an acceleration set value is calculated depending on the state of the train (powering, braking to target speed, braking to stop, etc.). This value is sent to the motor module that translates it as the ratio between required force and maximal traction force corresponding to the speed at each simulation step. Motors need the mass of the train plus the traction force depending on speed operation to calculate the force needed to follow the acceleration set value of the ATO module. Then, a jerk limitation checks to make sure that there are no abrupt changes in force transitions in order to assure comfort for passengers. Subsequently, the new acceleration/deceleration, speed and position of the train must be calculated through train dynamic system with inter-station data and resistances. The resistances include departure resistance, running resistance, gradient resistance and curve resistance. Depending on each inter-station and train configuration, different coefficients of resistances are determined.

Finally, the energy consumption E is calculated according to the time increment Δt , traction force and speed at each simulation step. Train velocity, acceleration, traction or brake force and energy consumption are computed at each simulation step and they would be the input data for the next simulation step.

2.3.1.1. ATO (Automatic Train Operation) module

ATO system is an operational safety enhancement device used to help automate operation of trains. To guarantee the limited speed, stop position and running time, the expectation for ATO system is to make a better running curve with more possibility of energy saving. In order to satisfy this requirement, the functions of control command of ATO devices are described in Fig. 2.11[15].

- Running plan function: the main function is to make the running plan from current position to stop position. For example, powering, constant speed, coasting and braking mode are calculated thanks to this function. By using the train dynamic model in consideration of the vehicle's actual performance, it is possible to obtain the better drive plan, and possible to adjust the running time with high accuracy. Furthermore, within the predetermined running time, coasting mode is kept as long as possible, and the strength of powering and braking are set by notch step by step. By adjusting the notch, it is possible to reduce total energy consumption.
- Running control function: the main function is to determine the control command based on the prediction result of the movement of the train and travel plan. Basically, notches are chosen according to travel plan. However, when the train travels close to the speed

limitation, notches are selected in order not to exceed the speed limitation based on train speed prediction. When the train reaches the station, the notch is selected based on stop position prediction and stop target position. For better stop action, accuracy with a small notch switching which considers the reaction delay for braking force has been used.

- Vehicle characteristics estimation function: the main function is to estimate the vehicle characteristics by changing the train speed and control command.

For these different functions of ATO model, running plan function is used for running curve design in this chapter.

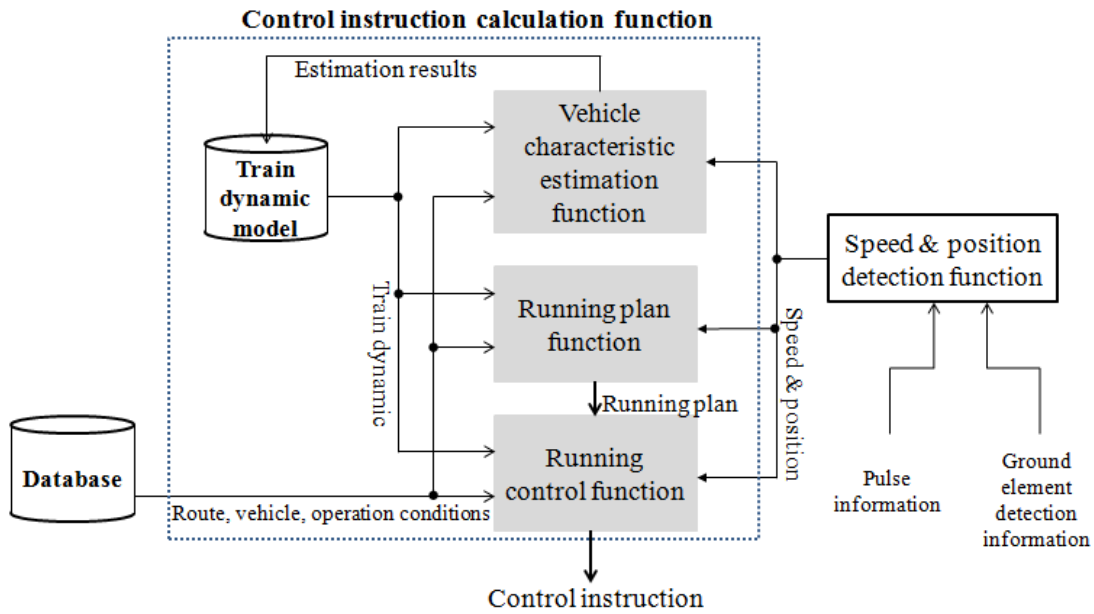


Fig. 2.11. Functional architecture of ATO equipment

2.3.1.2. MOTOR/ GENERATOR

The traction and braking force characteristics with different customer rates of motor and generator are shown in Fig. 2.12 and Fig. 2.13. The nominal forces are determined at the wheel periphery and at steady state with no acceleration/deceleration. Because of the end-effect, traction force decreases at high-speed operation.

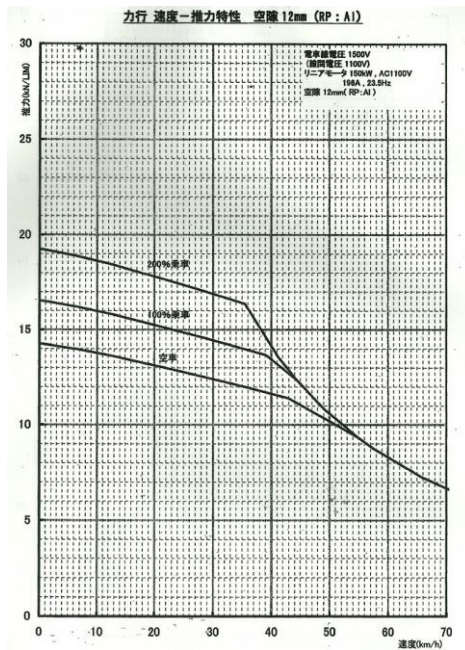


Fig. 2.12. Traction force in speed relation

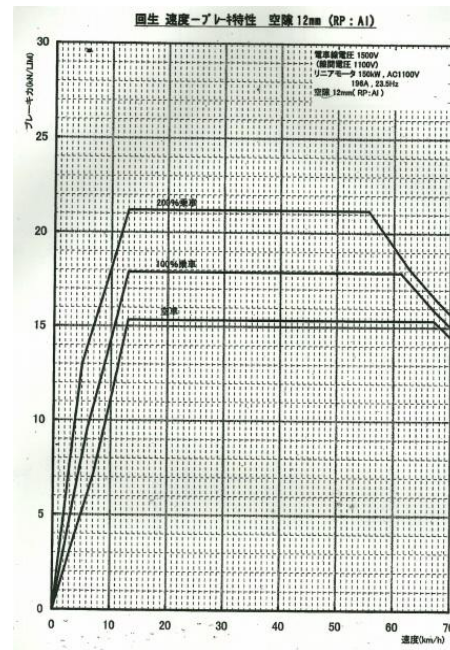


Fig. 2.13. Braking force in speed relation

2.3.1.3. DYNAMIC SYSTEM module

Calculation of the dynamic system is based on the block diagram illustrated in Fig. 2.14. Numerical simulations are realized in some constrained conditions: upper limited speed and maximal acceleration.

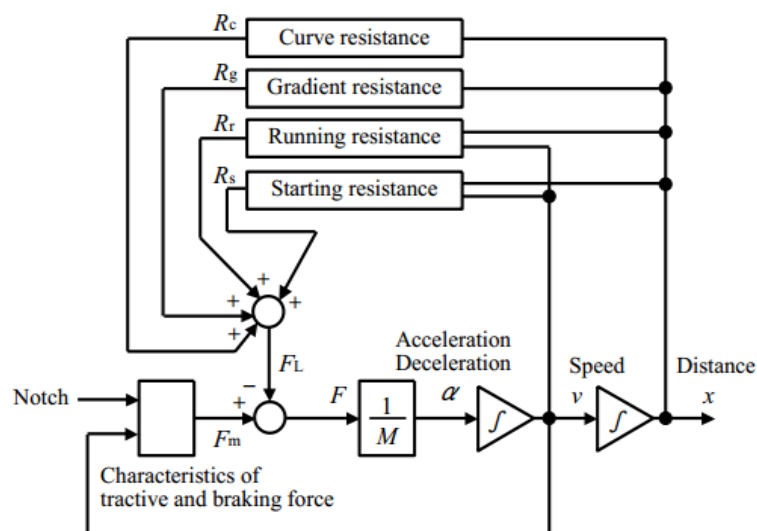


Fig. 2.14. Dynamic system of a train motion

Where the parameters in the block diagram are explained as in table 2.1. below:

Table 2.1

Symbol	Parameter
M (ton)	Mass of rolling stock
M_M (ton)	Mass of power car
M_T (ton)	Mass of non-power car
v (m/s)	Speed
n	Number of cars
i	Gradient ratio
L_t (m)	Full length of rolling stock
L (m)	Length of slope or curve

Consequently, the dynamic system is based on the following equation:

$$M \frac{dv}{dt} = F(v) - \sum R \quad (2.1)$$

Different resistances in case of linear metro are expressed as below:

a) Departure resistance

Departure resistance is considered at the departure moment with operational speed smaller than 3km/h.

$$R_s = 9.8 \times 4M \quad (2.2)$$

b) Running resistance

In case of Linear Metro, running resistance is a function of speed as:

$$R_r = 9.8 \times (2.07 + 0.039v + 0.00021v^2) \times M \left\{ 1 + 0.2 \left(\frac{v_f}{v} \right)^2 \right\} \quad (2.3)$$

Where v_f is a certain area terminal speed (m/s), determined by experimental results as follow:

$$\begin{cases} v \leq 12.5 \text{ m/s} \rightarrow v_f = v \\ v > 12.5 \text{ m/s} \rightarrow v_f = 12.5 \end{cases} \quad (2.4)$$

c) Gradient resistance

$$R_g = 9.8M \times \left(\frac{i}{1000}\right) \left(\frac{L}{L_t}\right) \quad (2.5)$$

Because linear metro is widely used for urban transport with lack of tunnel resource and high gradient of downhill and uphill sections, gradient ratio can be up to 8%, so gradient resistance has strong effect on train operation.

d) Curving resistance

$$R_c = 9.8 \left(\frac{600}{r}\right) \left(\frac{L}{L_t}\right) \quad (2.6)$$

2.3.1.4. ENERGY CONSUMPTION

Energy consumption at powering mode is calculated by equation (2.6), while the regenerative energy is calculated as in equation (2.7) where F_m, F_b are respectively traction force and regenerative braking force of linear metro system. In Fig. 2.12 and Fig. 2.13, $\eta(v)$ is the coefficient depending on motor and inverter efficiency. In case of LIM, this coefficient strongly depends on speed operation.

$$E_p = \frac{1}{\eta(v)} \int F_m(v) v dt \quad (2.7)$$

$$E_r = \eta(v) \int F_b(v) v dt \quad (2.8)$$

2.3.2. Maximal principle for dynamic system

Dynamic system and energy consumption are described by equations from 2.1 to 2.8 as presented above. However, the traction force and braking force in Fig. 2.12 and 2.13 generate a question: what kind of force and speed characteristics are suitable for energy saving? Pontryagin's maximal principle has been used to solve this problem [16][17].

Consequently, the following different equations describe the state equations of train motion and energy consumption:

$$\frac{dx}{dt} = v \quad (2.9)$$

$$M \frac{dv}{dt} = F(\gamma, v) - R(x, v) \quad (2.10)$$

$$\frac{dE}{dt} = \frac{dE_p}{dt} - \frac{dE_r}{dt} = \eta(\gamma, v)F(\gamma, v)v \quad (2.11)$$

The problem is to find out the traction and braking curve in limited region, $F(\gamma, v) \leq F(\gamma_0, v)$, which satisfies the condition: with planned running time T , the optimal energy saving problem is formulated as

$$\min_{\gamma} E$$

And constrained conditions:

$$x(0) = 0, v(0) = 0, x(T) = L_0, v(T) = 0 \quad (2.12)$$

Where

γ is control input (as Fig. 2.15)

With the variables relations as (2.9) to (2.11) and constrained conditions (2.12), after defining the Hamiltonian function, dynamic programming based on Pontryagin's maximum principle calculate the control input for minimum E purpose.

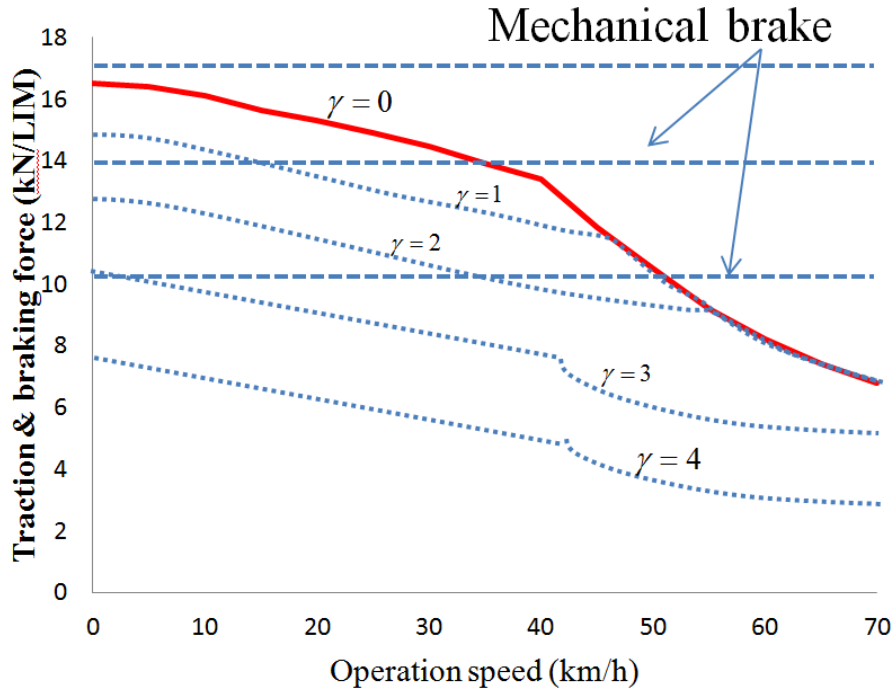


Fig. 2.15. Powering and braking force with different control units

2.3.3. Case study for simulation

2.3.3.1. Simulation conditions

A case study for simulation based on the parameters of Nanakuma-line (Fukuoka), the longest station between Beppu and Chayama, Fig.2.16. Maximal speed of LIM is 70km/h (19.5m/s) and maximal acceleration is 1.1 m/s/s. The influences of running, curving and gradient resistance have also been considered in the simulation. Simulation conditions are described in Table 2.2.

Table 2. 2. Simulation conditions

Train	3000 Series (Nanakuma line)
Distance	1 (km)
Number of cars	4
Number of motors	2 per car
Maximal speed	70 (km/h)
Maximal acceleration	1.1 (m/s/s)
Maximal panda voltage	1500 (V)
Maximal motor power	150 (kW)
Running resistance	Yes
Curving resistance	Yes
Gradient resistance	Yes
Customer conditions	Full customer (100% passenger)
Driving safety equipment	ATO/ATC

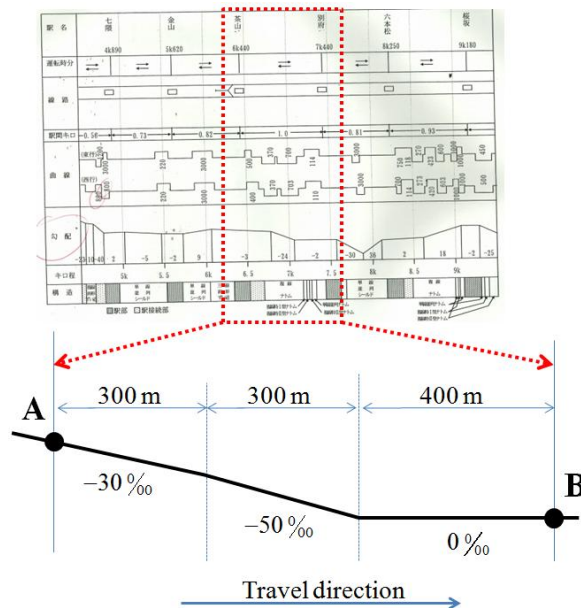


Fig. 2. 16. Running condition

2.3.3.2. Equation of motion

Acceleration during powering mode for each time step Δt_i is calculated by:

$$a_i = \frac{F(0, v)_i - R(x, v)_i}{M} \quad (2.13)$$

During coasting mode:

$$a_i = \frac{-R(x, v)_i}{M} \quad (2.14)$$

During braking mode:

$$a_i = -\frac{F(0, v)_i + R(x, v)_i}{M} \quad (2.15)$$

Speed is calculated for each time step i by:

$$v_{i+1} = v_i + a_i \Delta t_i \quad (2.16)$$

And the travel distance is:

$$L_0 = \sum_{i=1}^n \Delta x_i = \sum_{i=1}^n \left(v_i + \frac{a_i}{2} \Delta t_i \right) \Delta t_i \quad (2.17)$$

Current power:

$$P_i = F(0, v)_i \cdot v_i \quad (2.18)$$

Total energy consumption:

$$E_p = \sum_{i=1}^n \eta(0, v_i) P_i \Delta t_i = \sum_{i=1}^n \eta(0, v_i) F(0, v)_i v_i \Delta t_i \quad (2.19)$$

2.3.3.3. Simulation results

a) Different running curves with different braking patterns

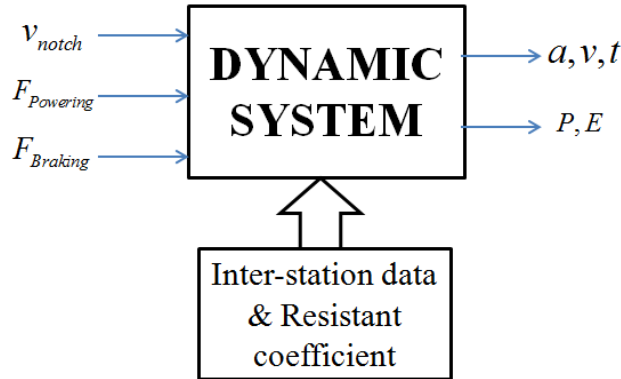


Fig. 2.17. Input and output illustration

In the first simulations, maximal speed in powering mode and braking pattern are firstly established in order to determine the speed-distance-time relation, acceleration and deceleration characteristics, and power distribution. Based on maximal principle, speed, running time and power distribution are calculated in response to running conditions.

The responses of speed, acceleration, deceleration, power, running time and resistances are illustrated in their relations from Fig.2.18 to Fig.2.23.

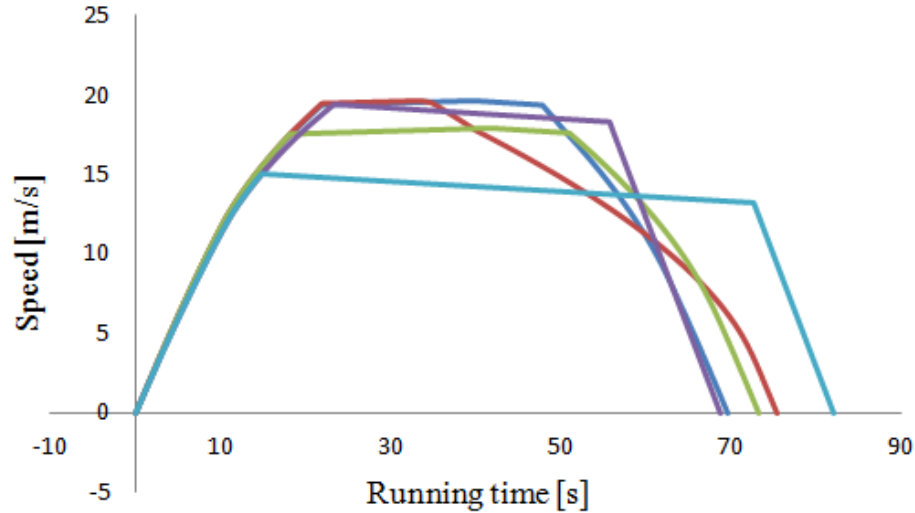


Fig. 2.18. Speed and running time relations

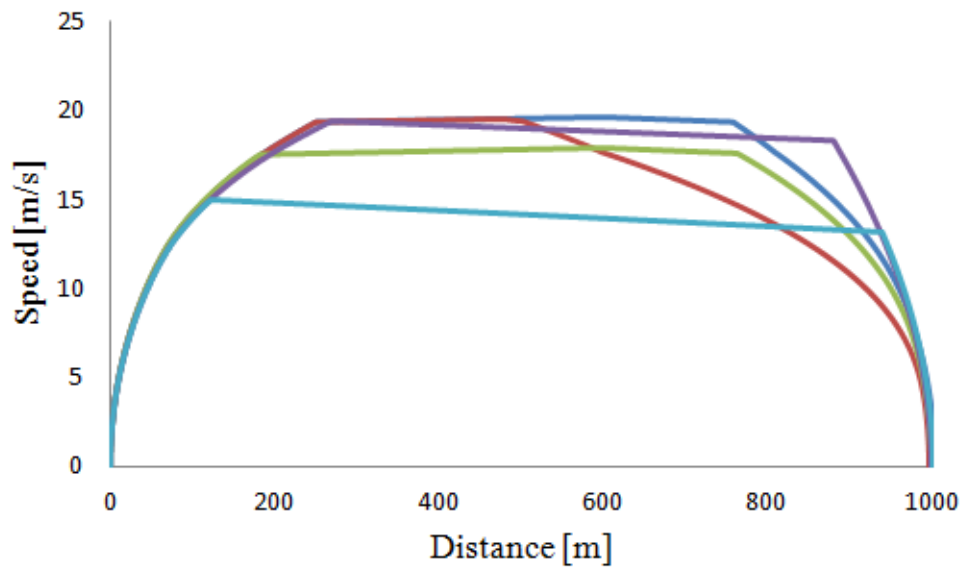


Fig. 2.19. Speed and distance relations

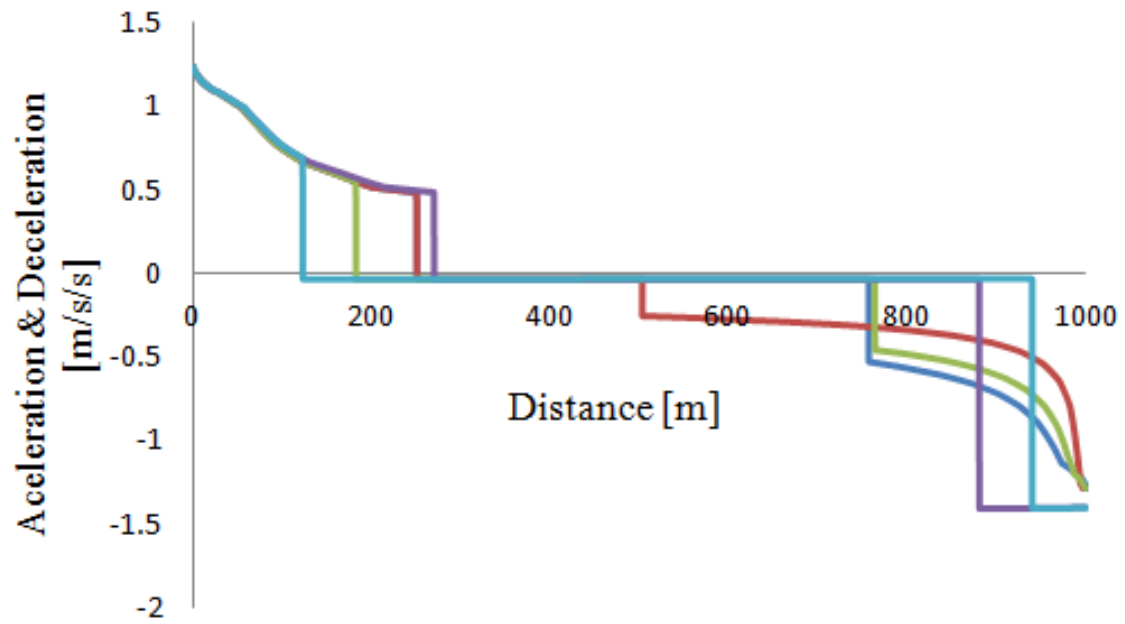


Fig. 2.20. Acceleration, deceleration and distance relations

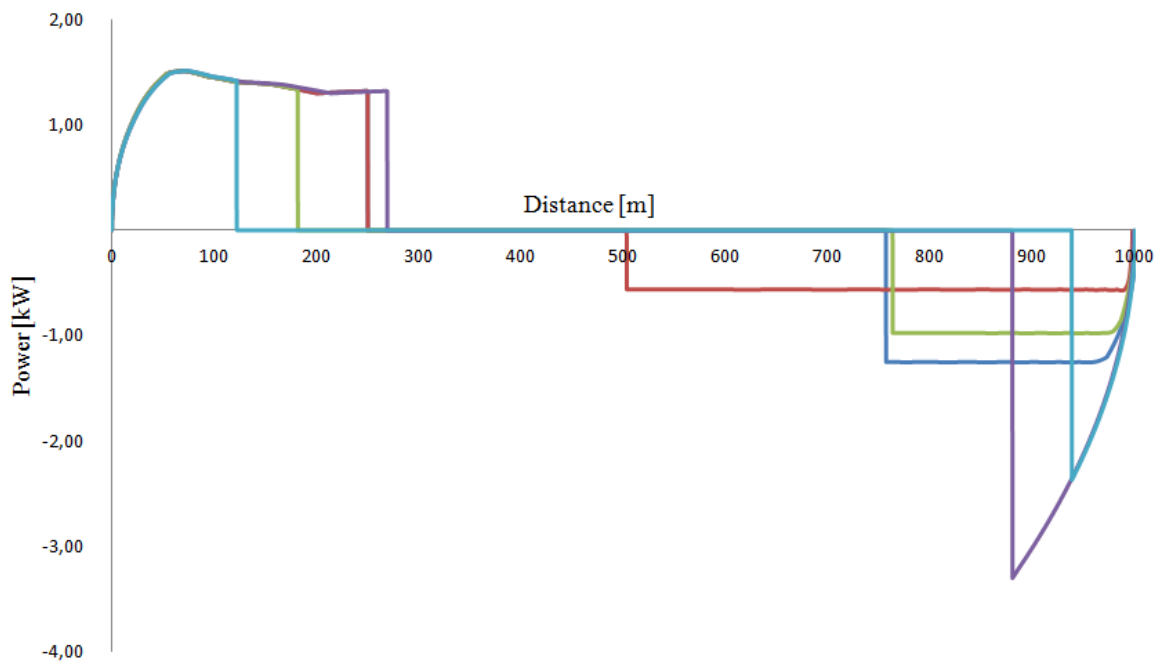


Fig. 2.21. Power and distance relations

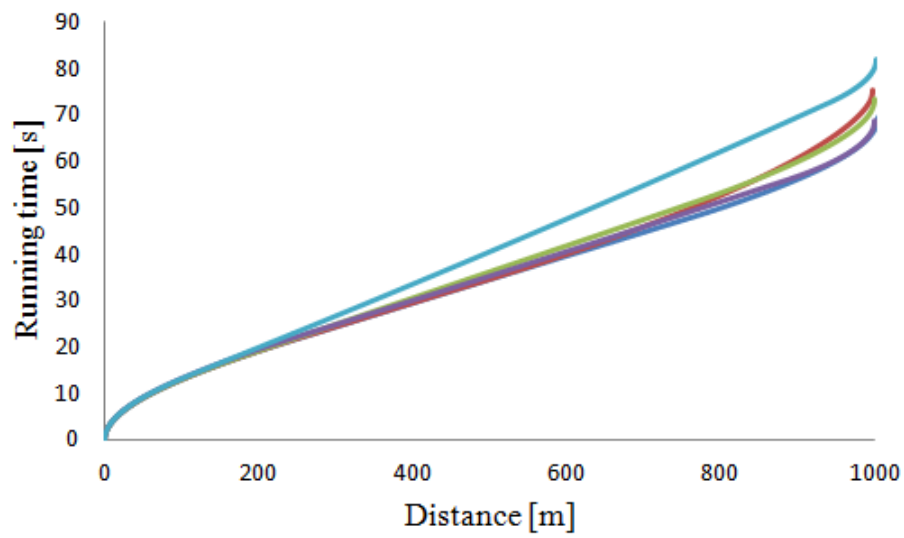


Fig.2.22. Running time and distance relations

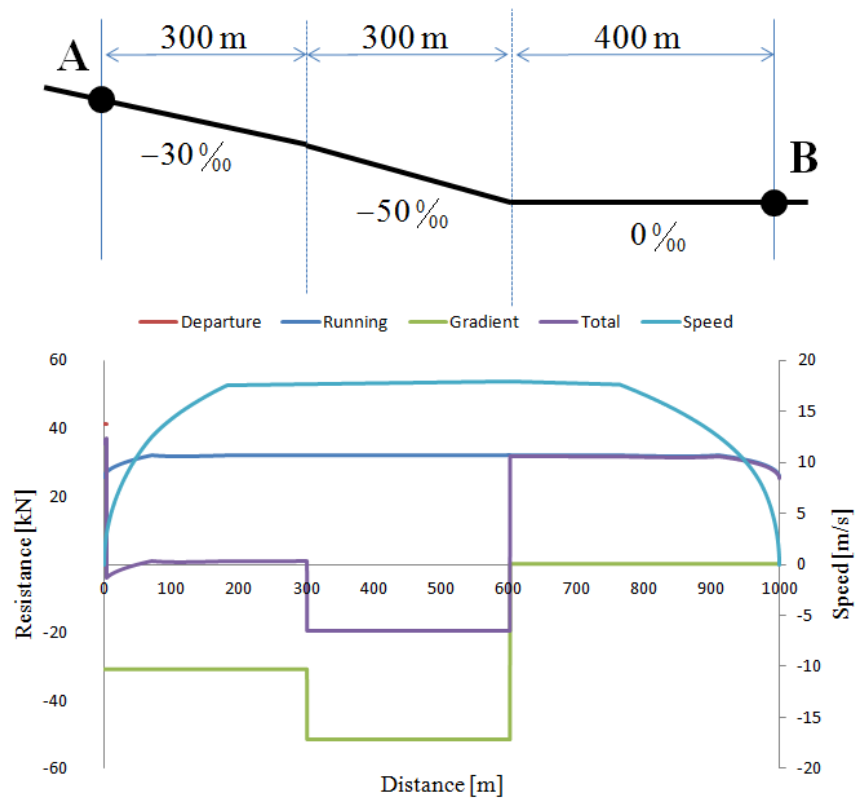


Fig.2.23. Resistances and distance relations

b) Running curve with different power limited brake

In the second simulation, as illustrate in Fig.2.24 with input and output variables, instead of different braking modes, different power limited brakes, Fig. 25, are chosen to calculate the responses.

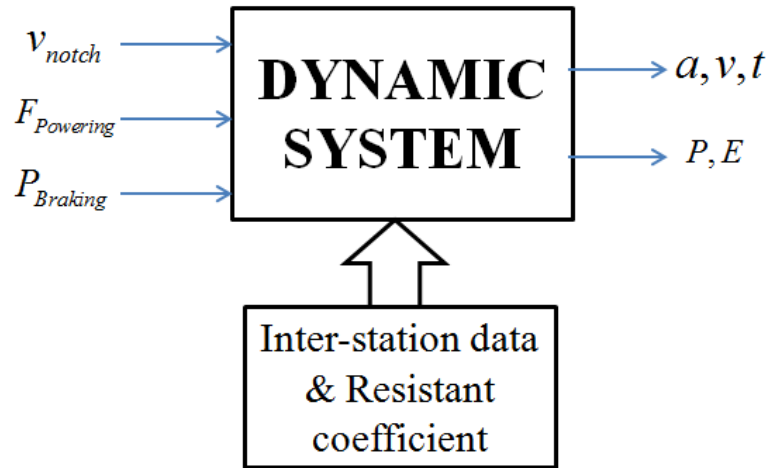


Fig.2.24. Input and output illustration

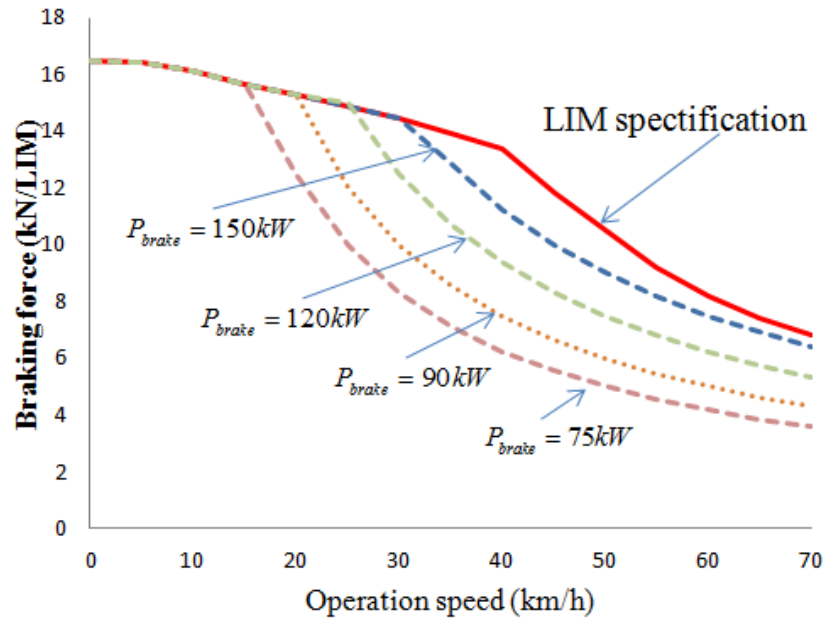


Fig. 2.25. Different power limited brakes

At the same notch-off speed

Running curves with different braking power are expressed in Fig.2.26. Small braking power means more braking time is needed. On the other hand, large braking power means short braking time.

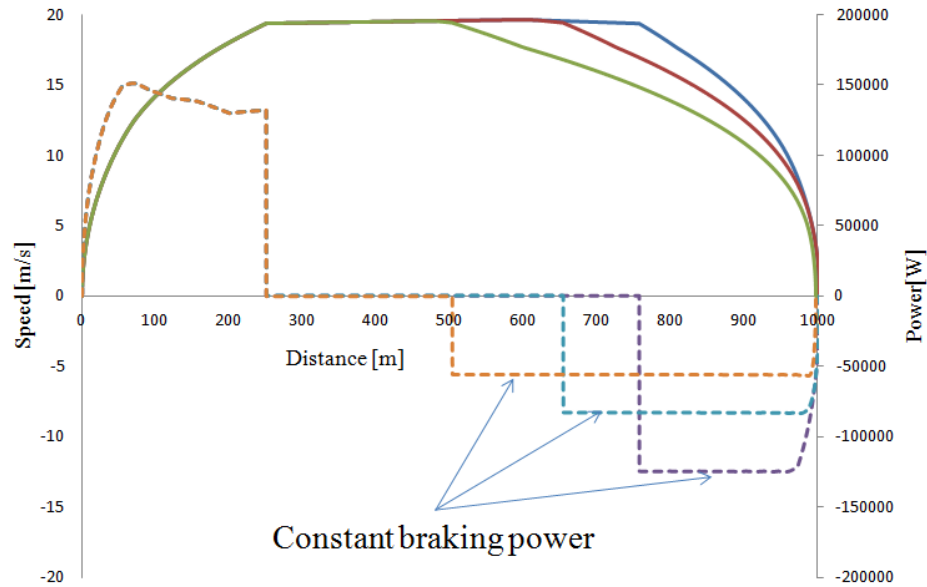


Fig. 2.26. Running curve at the same notch-off speed

With the same notch-off speed, running time, braking time, braking power and possibility of regenerative energy are expressed in Table 2.3:

Table 2.3. Performance at the same notch-off speed

Running time (s)	Braking time (s)	Braking power (kW)	Regenerative energy (kWh)
69.61	21.78	150	12.16
70.58	27.14	125	12.01
71.77	31.12	100	11.89
73.32	35.86	80	11.59
75.34	41.78	65	11.46

From this result, the relation of possible regenerative energy and total running time at the same notch-off speed and different power limited brakes can be expressed in Fig. 2.27.

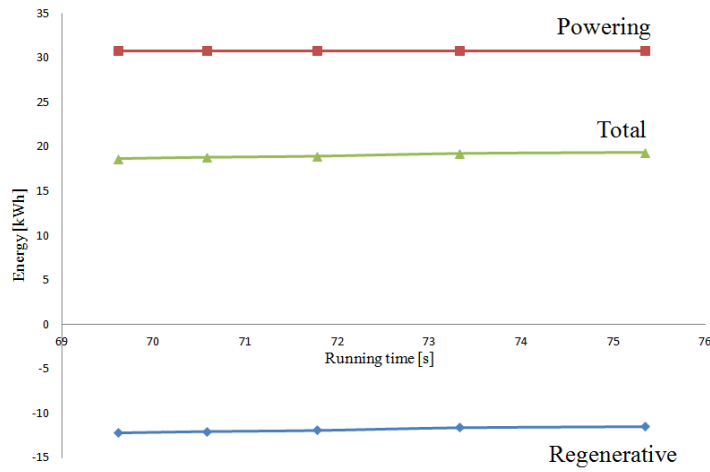


Fig.2.27. Energy and running time relation at the same notch-off speed

As described above, regenerative energy can be calculated as in (2.8). It seems that we can obtain the same regenerative energy at the same notch-off speed because small braking means long braking time and vice versa. For this reason, with the same notch-off speed, the same total energy consumption from substation is necessary.

At different notch-off speed and same braking power

Different running curves, power distribution and energy at different notch-off speed and same braking power are expressed in Fig.2.28, Fig.2.29 and Table 2.4.

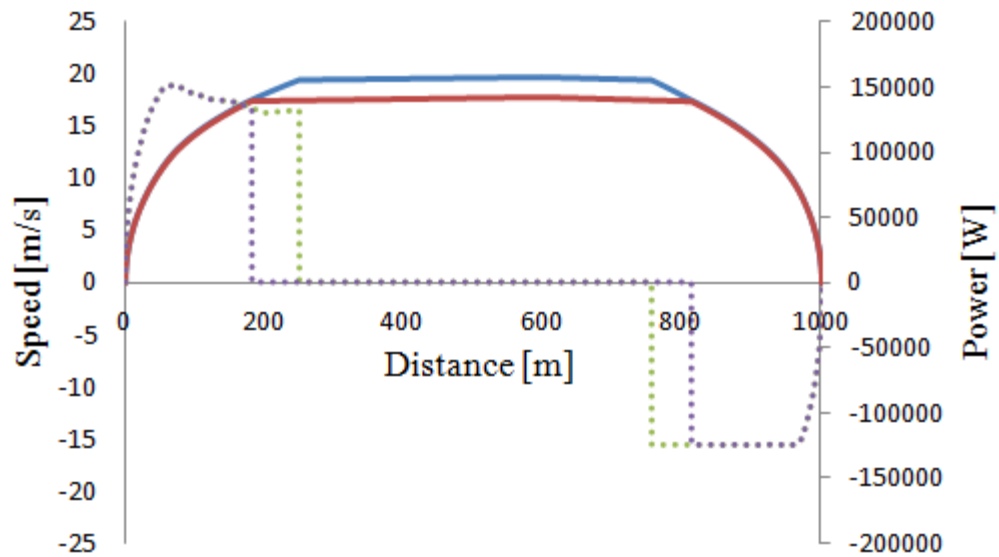


Fig.2.28. Running curve at different notch-off speeds

Table 2.4. Calculation results at different notch-off speeds

Running time [s]	Braking time [s]	Braking power [kW]	Powering energy [kWh]	Reg. Energy [kWh]	Total Energy [kWh]
85.12	11.25	150	15.86	4.12	11.74
82.92	12.22	150	18.19	5.07	13.11
79.52	13.15	150	21.02	6.47	14.54
75.84	15.67	150	24.84	8.14	16.7
73.32	17.58	150	28.26	9.57	18.68
70.57	20.34	150	32.96	11.18	21.77

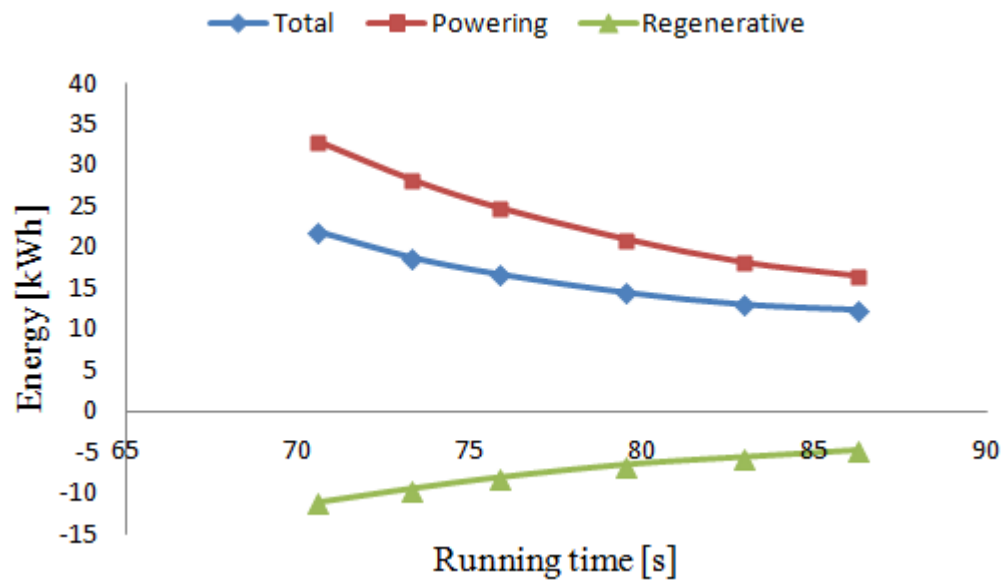


Fig.2.29. Energy and running time relations at different notch-off speeds

From these results we can see that at lower notch-off speed, we can reduce powering energy, but we will obtain smaller regenerative energy. However, in general, total energy consumption can be reduced. It is also important to note that reduction of notch-off speed means increase in running time. Consequently, total energy consumption at substation can be reduced by increasing running time.

At different notch-off speeds and different braking power

By combining the results in the two cases above, we can have relations between powering energy, regenerative energy, total energy consumption and running time at different notch-off speeds and different braking power, Fig.2.30.

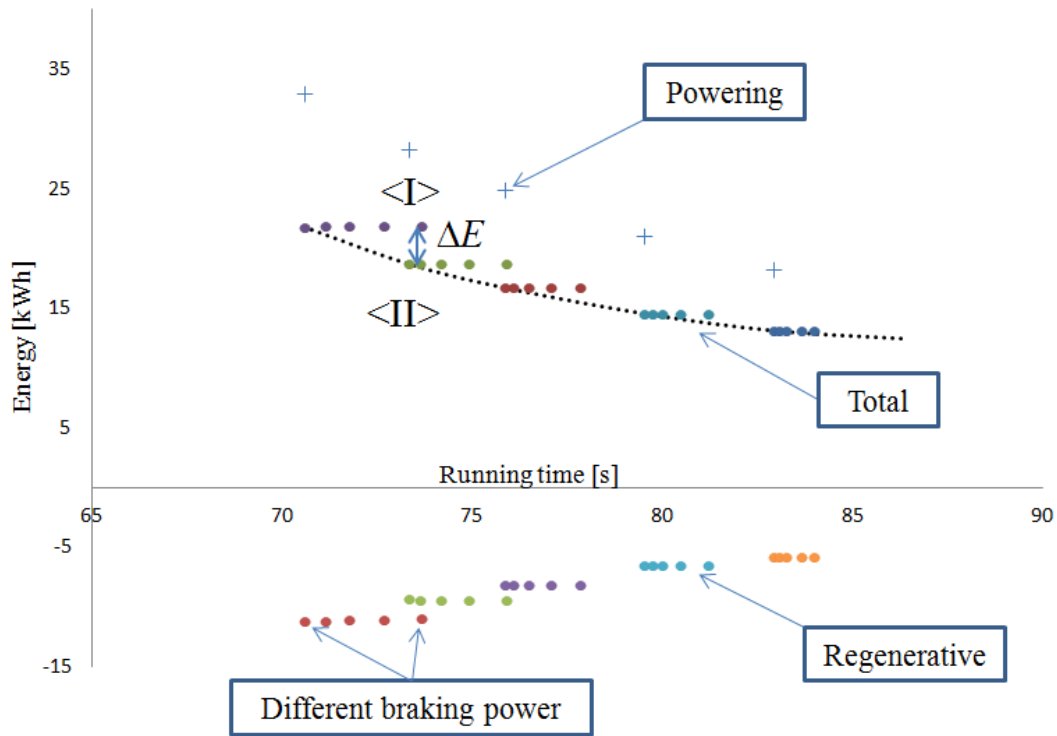


Fig.2.30. Energy and running time relations

c) Influence of gradient on energy consumption

Linear metro is well known as a good solution for urban transportation system where there are a lot of slopes. While the normal railway systems are limited at 3% of gradient, linear metro can run at the place up to 8% of gradient thanks to the support of non-adhesive drive system. In this case, the running time when the train goes up the slopes and operation speed exceeding limitation value when the train runs down the slopes must be considered in train operation. Energy consumption and running time relations of flat line as well as maximal of upward and downward slopes are expressed in Fig.2.31. The supposition in these simulations is that the train runs along the upward or downward of the rail track.

Regenerative brake and conventional brake (air brake) are used for these simulations based on which the difference of energy consumption at flat line and slope line can be determined. As we can imagine, larger energy consumption and longer running time are required in upward slopes. On the other hand, smaller energy consumption and shorter running time are required in downward slopes. There is a significant difference in the shortest time when using mechanical brake and electrical brake in case the train runs on an upward slope. This value reduces with the reduction of the gradient.

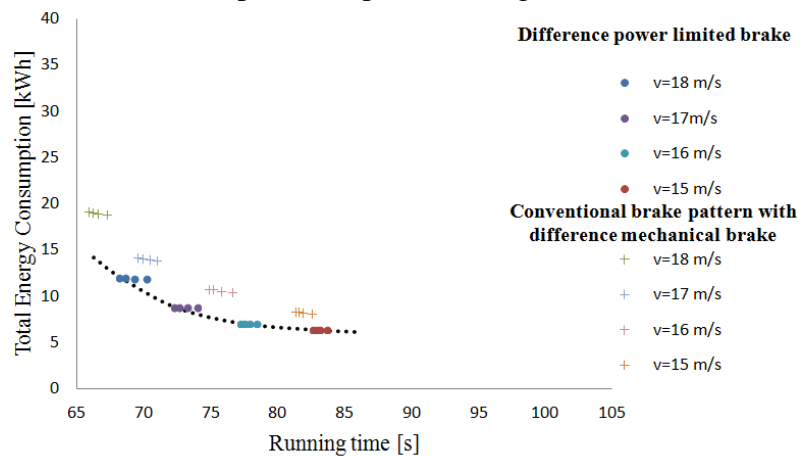
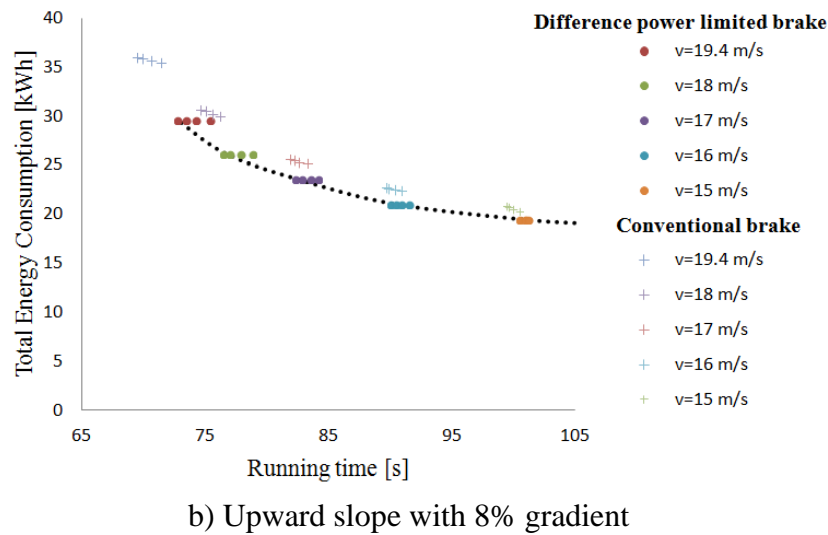
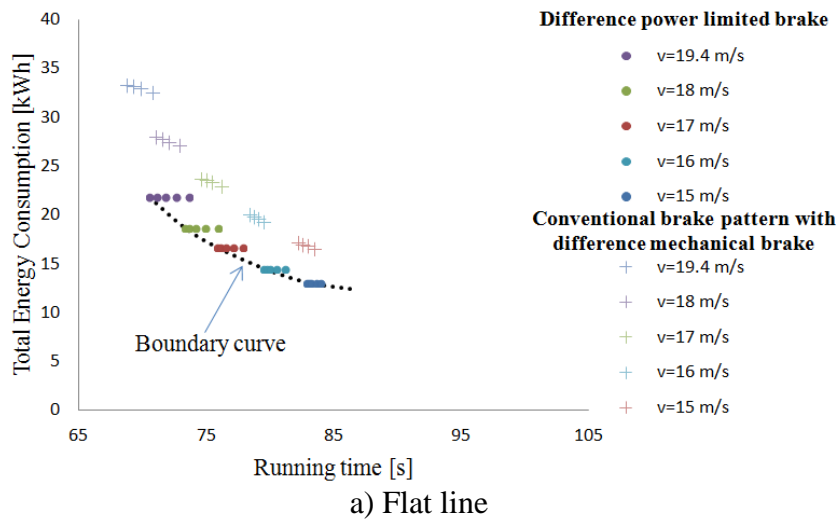


Fig.2.31. Net of energy consumption and running time at different line conditions

2.3.3.4. Possibility of energy saving through running curve design

Three energy saving principles on train operation can be concluded from simulation results:

- (1) At the same notch-off speed, regenerative energy can be obtained with nearly the same value;
- (2) Energy can be saved by increasing the running time and reducing notch-off speed;
- (3) With the same running time, energy can be saved by considering the mutual relation of notch-off speed and braking pattern.

While, conclusion (2) is well known in real train operation and running curve design, the result in (1) is significant for choosing braking pattern, and (3) can be illustrated as Fig. 2.32. The possibility of energy saving at the same running time is determined when considering the different energy between running curve <I>, highest powering energy and low braking power, and running curve <II>, low powering energy and highest braking power.

Up to nearly 15% of energy can be saved when considering the difference of running curve <I> and <II>. However, it must be noted that regenerative energy is difficult to obtain in real train operation. Low energy consumption in <II> means large braking power has been used and it creates the crisis on peak power of regenerative energy, Fig. 2.33. In addition, large braking power in short braking time may lead to waste of regenerative energy when there is no powering train at the same braking time. This result makes a requirement for running curve design to consider both powering energy and braking power.

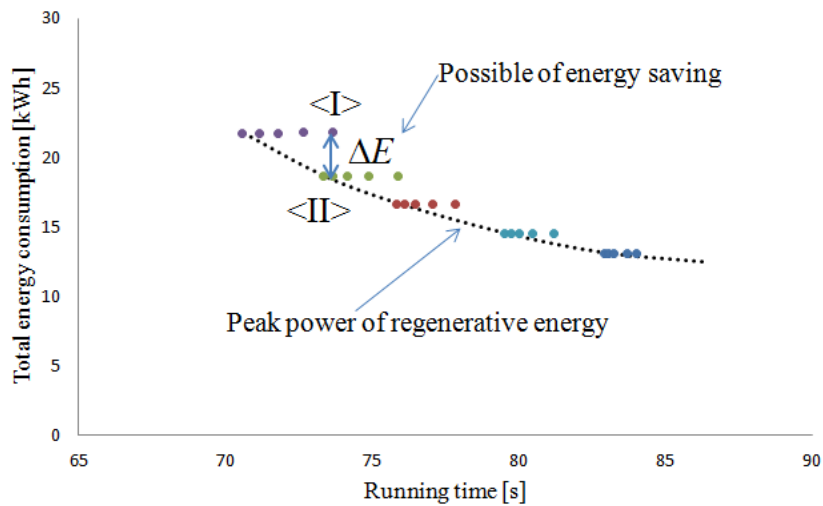


Fig.2.32. Total energy consumption and running time relations

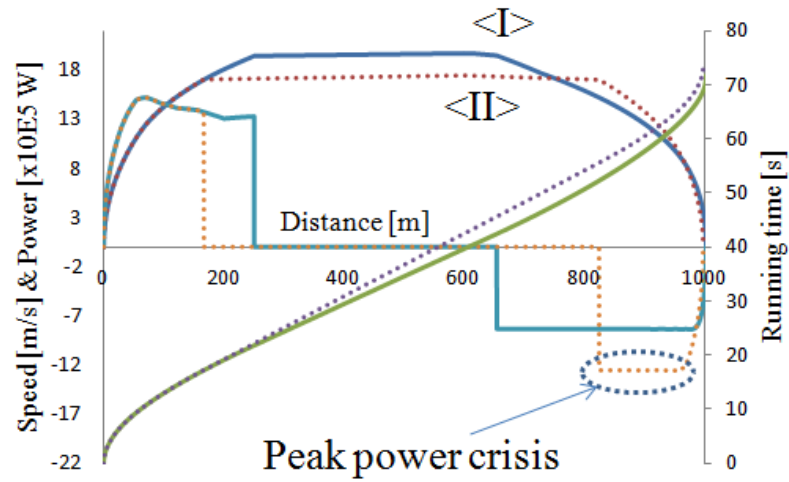


Fig.2.33. Running curve and peak power crisis

In addition, total energy consumption, maximal braking power and running time between two stations as Fig.2.34 imply a new approach to train scheduling in the whole line to improve the utilization of regenerative energy.

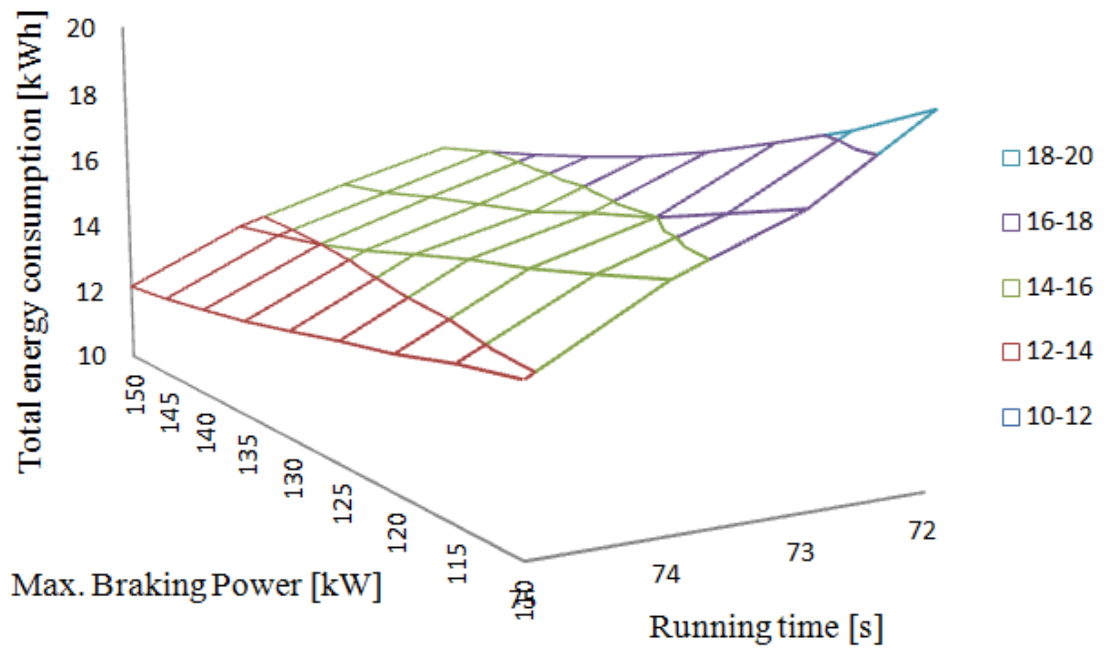


Fig.2.34. Total energy consumption and maximal braking power in running time relations

2.4. Parameter influence on ATO running curve design

Between an inter-station A-B, with planned running time, it is necessary to design the running curve that concerns the powering energy and braking power in order to reduce the total energy consumption and improve the utilization of regenerative energy. The braking time is required as maximum as possible in order to make sure that regenerative energy can be used.

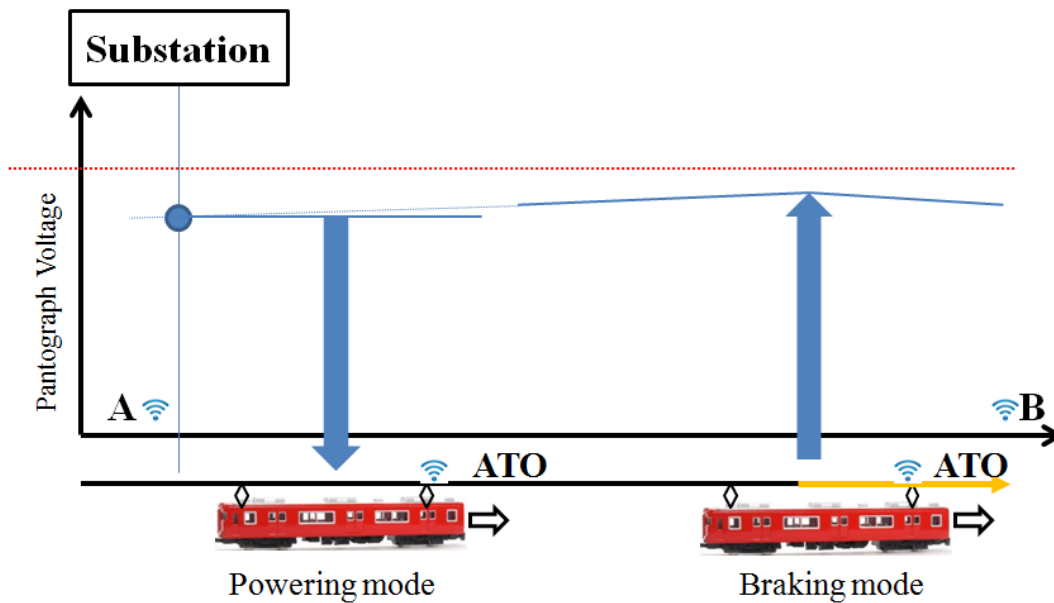



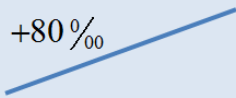
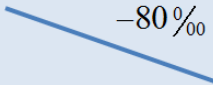
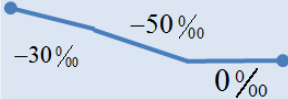
Fig.2.35. Running curve design based on ATO support

The problem can be explained as: at scheduled running time T , find the powering notch-off speed, braking power and braking time which satisfy 2 conditions:

- Lowest total energy consumption;
- Lowest braking power or longest braking time.

The influence of powering ratio and braking power ratio to total energy consumption and running time can be seen in Fig.2.26 and Fig.2.28 in the previous part. The influence of coasting length and notch-off speed on speed limitation, lower and upper speed at constant speed control as well as the combination of these parameters must be considered in ATO running curve design. With the same model as the last simulation, in order to consider the influence of each parameter, in this part the simulation are taken part when the train runs over four different line sections as described below:

Table 2.5. Line conditions for simulation

Line	Illustration	Description
L1	 0 ‰	Idealized line with a constant zero gradient
L2	 +80 ‰	Idealized line with constant upward gradient
L3	 -80 ‰	Idealized line with constant downward gradient
L4	 -30 ‰, -50 ‰, 0 ‰	Real line condition

2.4.1. Influence of coasting distance

As well known in real train operation, by choosing the coasting distance long enough, it is possible to do the action of power limited brake to avoid mechanical brake as well as to avoid powering in the whole time before braking.

At the same powering notch-off speed, influence of coasting distance on energy and running time are determined. Total energy consumption, regenerative energy and running time in different coasting are compared with the running curve when the maximal 150kW braking power is used.

Simulation results in Fig.2.36 show that when reducing braking power, regenerative energy can be obtained with the same value at different line conditions. In short, total energy consumption is necessary. When line conditions change from downward slope to upward slope, total running time also changes. Running time increases when reducing the braking power at upward gradient or idealized line with constant zero gradient (L1, L2 and L4). At an idealized line with constant zero gradient, braking power is reduced by 25% with running time increase of 2% only in comparison with a reference case having maximal braking power. The increase of running time is small when the train runs on the download gradient. It seems that like energy, running time does not change when the braking power at high upward gradient is reduced (L2).

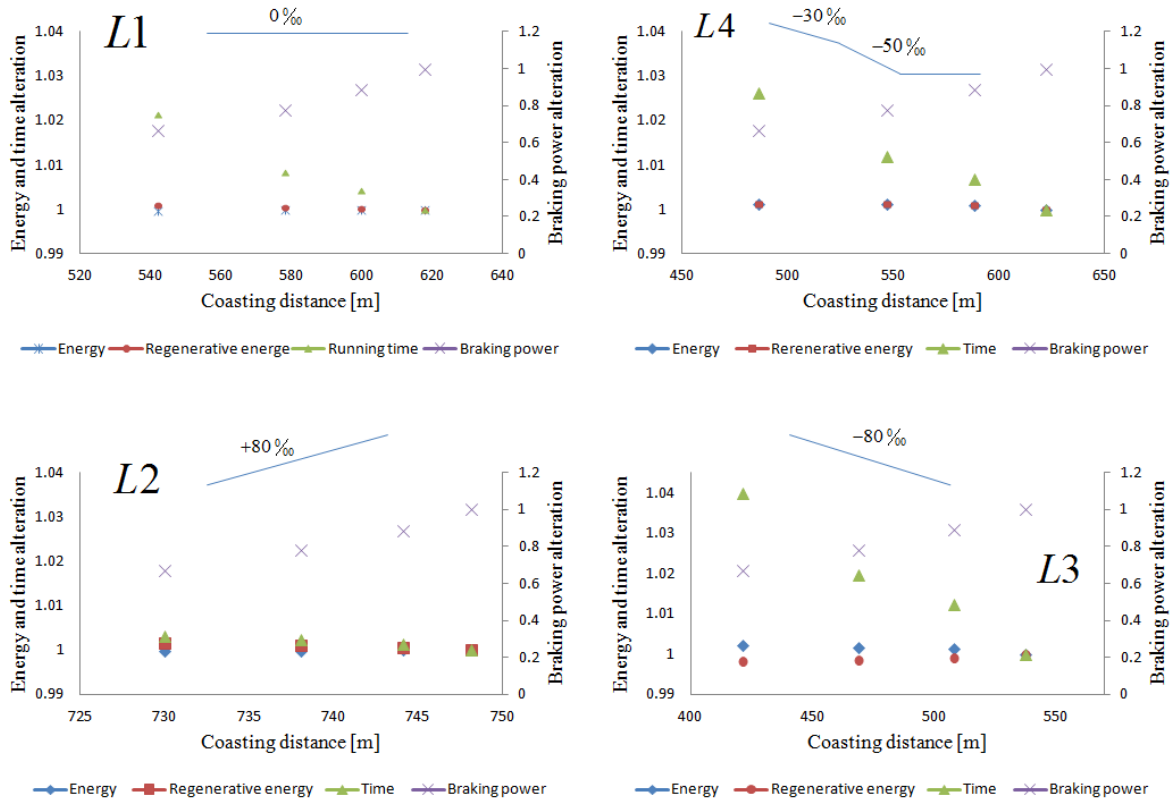


Fig.2.36. Influence of coasting distance at different running conditions

2.4.2. Influence of coasting and notch-off speed when considering speed limitation

In real system, for the safety purpose, speed must be limited at curving or gradient. In order to run according to planned running time, determining the power off and re-powering time is necessary. In this part, the possibility of energy saving through running curve design when considering the influence of speed limitation is based on primary notch-off speed and primary coasting distance. The condition is that speed must be limited at 17m/s at 230m from started station. Speed limitation, running curve and power distribution are expressed in Fig.2.37.

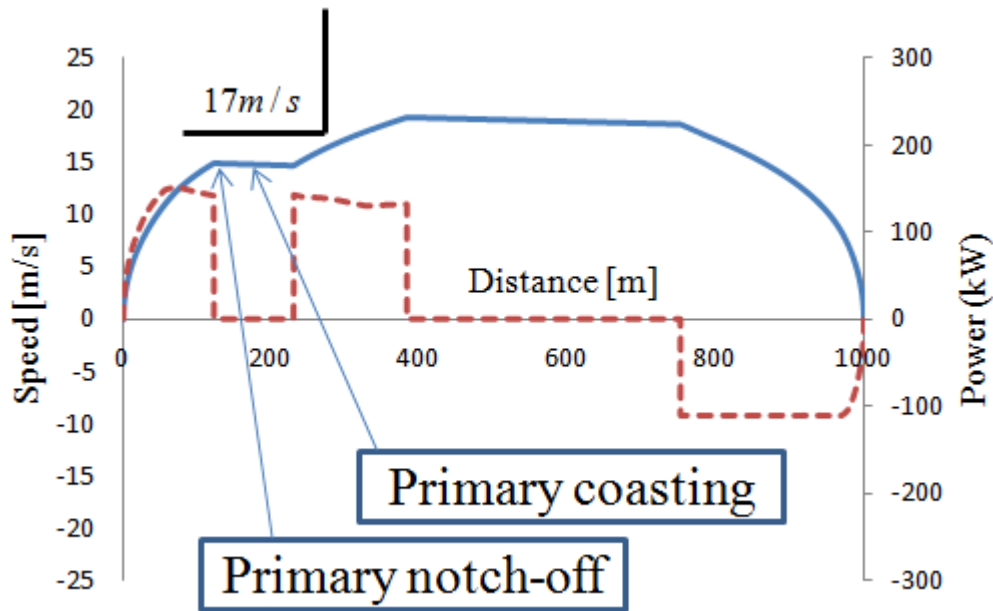


Fig.2.37. Running curve in case of speed limitation

2.4.2.1. Influence of primary coasting

The investigation of the influence of primary coasting is carried out in two cases.

a) At planned braking power

Depending on the other powering trains in the system, maximal braking power is kept constant in order to calculate the energy, regenerative energy, running time and coasting distance relation. Simulation conditions are expressed as below:

- Primary notch-off speed 15m/s
- Secondary notch-off speed 19.5 m/s
- Maximal braking power 120 kW (braking ratio 0.8)

Fig.2.38 shows the different running curves from the simulation made from idealized line with constant zero gradient (L1). The influence of primary coasting distance on running time, total energy consumption and regenerative energy in comparison with normal running curve (without speed limitation) are illustrated in Fig.2.39. Although regenerative energy slightly increases when primary coasting distance increases because of the increase of powering energy in secondary powering mode, total energy consumption also increases. Running time increases 3.6% of 71.5s (nearly 2.5s) and energy increases 2.9% of 21.8kW/h (0.63kW/h) at longest primary coasting distance simulation (180m).

This result shows that, with planned primary notch-off speed and braking power, running curve nearest to the limited point (red line in Fig.2.36) is the best choice for both of running time saving and energy saving.

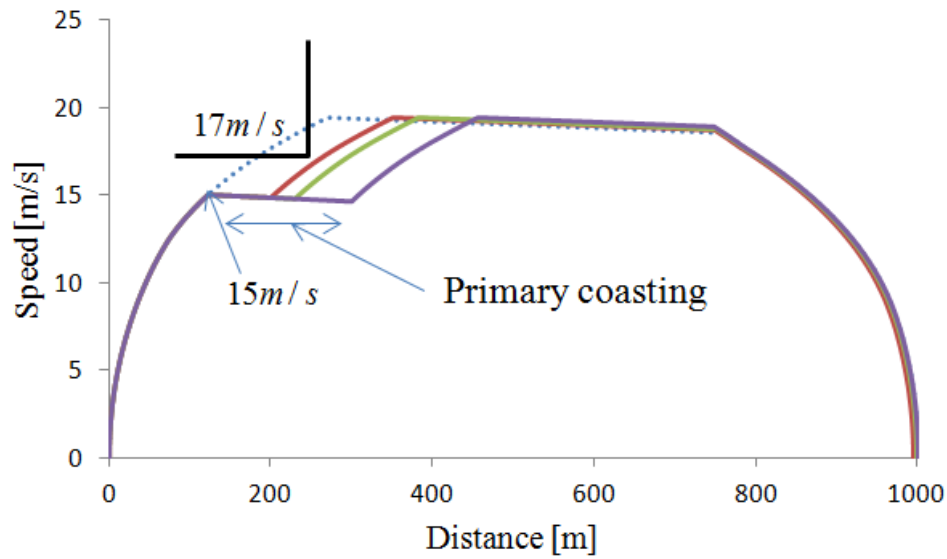


Fig.2.38. Different running curves at different primary coasting distance

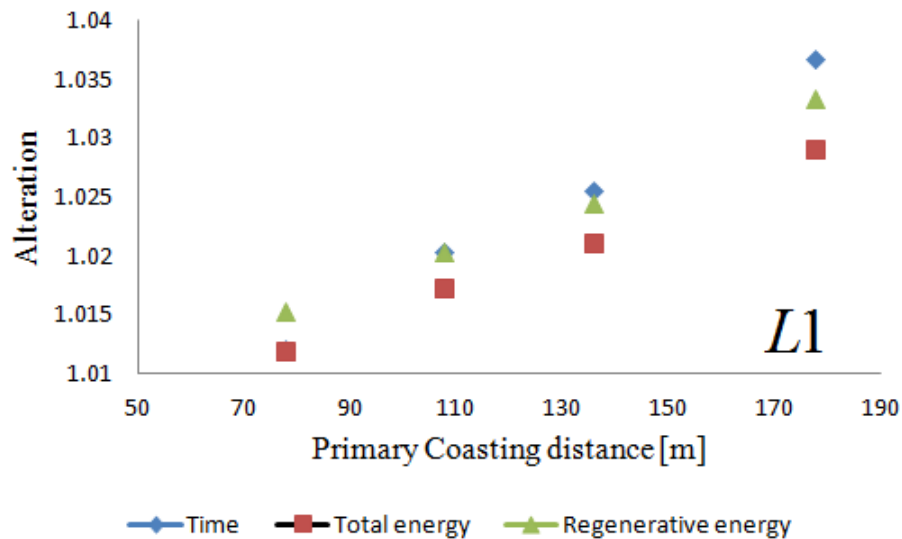


Fig.2.39. Influence of primary coasting distance at the same braking power

b) At planned running time

At planned running time and planned primary notch-off speed, running mode is defined with the following conditions:

- Primary notch-off speed 15m/s
- Total running time 72.5s (based on the running time of the red line in Fig.2.38)

Fig.2.40 shows different running curves at the same running time. At longer primary coasting distance, higher braking power in shorter time is necessary. The simulation results of comparison between different running curves with the running curve nearest to the limited point are shown in Fig.2.41 and Table 2.6.

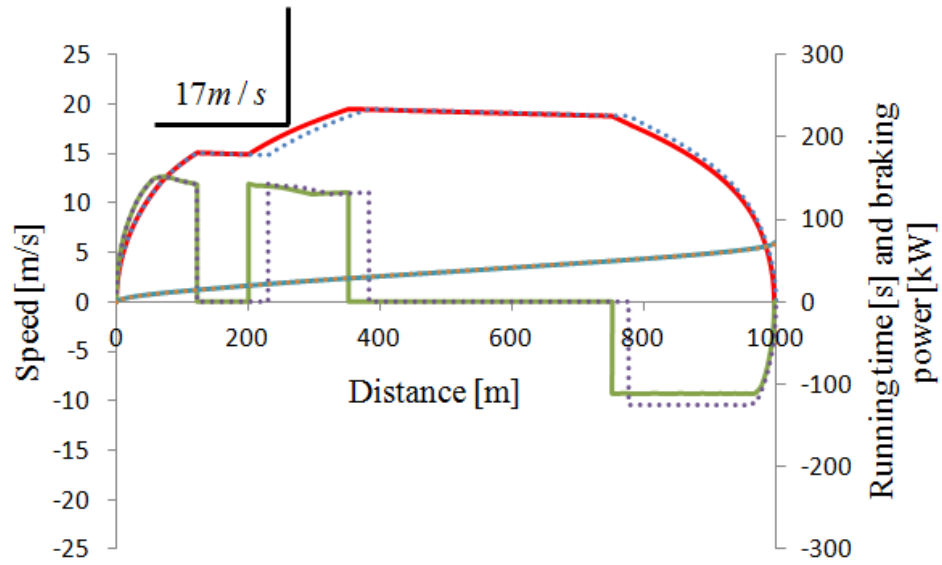


Fig.2.40. Different running curves at planned running time

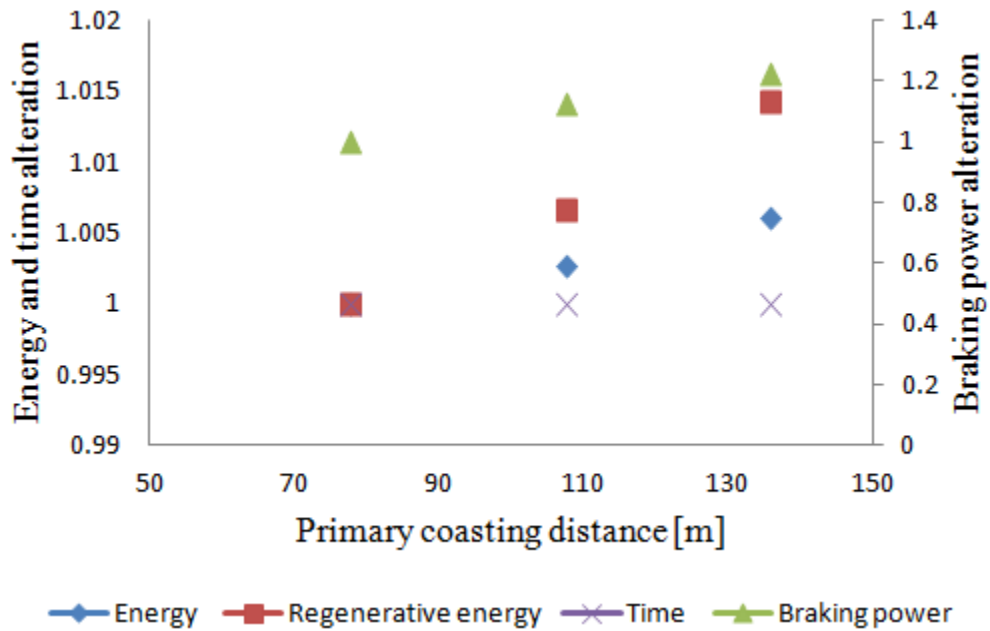


Fig.2.41. Influence of primary coasting distance at planned running time

Table 2.6. Simulation results at planned running time

Time [s]	Coa. Dis. 1 [m]	Pow. Ene.1 [kWh]	Pow. Ene. 2 [kWh]	Braking Power [kW]	Regenerative Energy [kWh]	Total Energy [kWh]
72.5	77.75	18.99	14.41	122	11.33	22.07
72.5	107.66	18.99	14.58	137	11.41	22.17
72.5	135.7	18.99	14.79	150	11.51	22.27

At planned running time, we can obtain more regenerative energy when we enlarge the primary coasting distance and increase the maximal braking power. However, because of the increase of energy in secondary powering mode, total energy consumption also increases. At maximal braking power (150kW), 1.4% of regenerative energy increases (0.17kWh) while 0.8% of total energy consumption also increases (0.2kW). Consequently, enlarging of the primary coasting power leads to increasing of both energy and braking power. For this reason, running curve nearest to the limited point is the best choice for both energy saving and reducing braking power.

2.4.2.2. Influence of primary notch-off speed

a) At planned maximal braking power

The simulations at planned maximal braking power are carried out at idealized line with constant zero gradient (L1) at different primary notch-off speeds. Based on the results of the last simulation, secondary powering mode is chosen nearest to the limited point (the red line in Fig.2.40) for energy saving. Running curves at different primary notch-off speeds are shown in Fig.2.42.

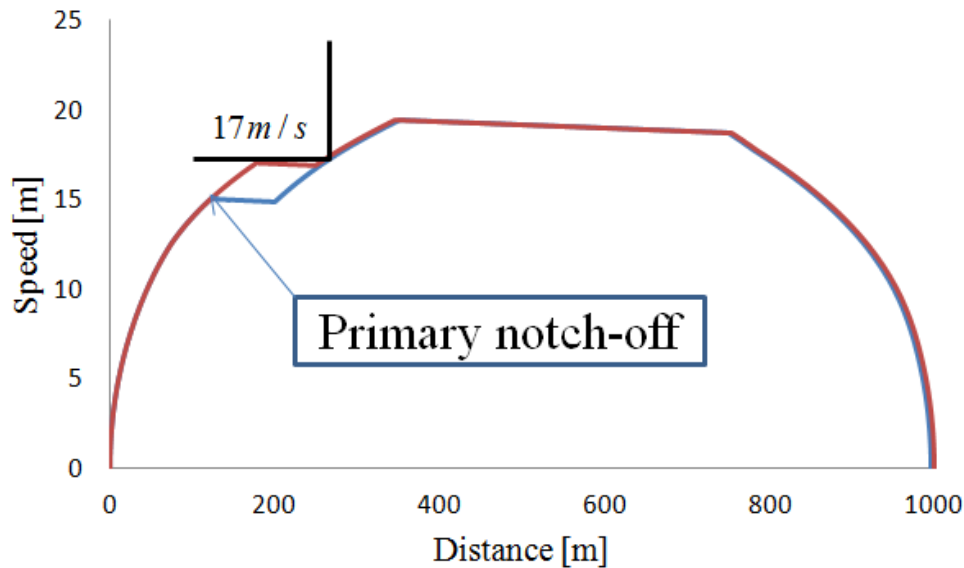


Fig.2.42. Running curve at different primary notch-off speeds

Simulations at different conditions based on:

- Secondary notch-off speed 19.5 m/s
- Maximal braking power 135kW (braking ratio 0.9)

Energy and running time alteration in comparisons with as maximal as possible primary notch-off speed, 17m/s (red line in Fig.2.42) are shown in Fig.2.43. While total energy consumption seems not to be affected and regenerative energy slightly increases when reducing the primary notch-off speed, running time is much more affected; specifically, running time increases 1.4% (1.02s of 71s) when maximal of primary notch-off speed reduces from maximal value of 17m/s to 15m/s.

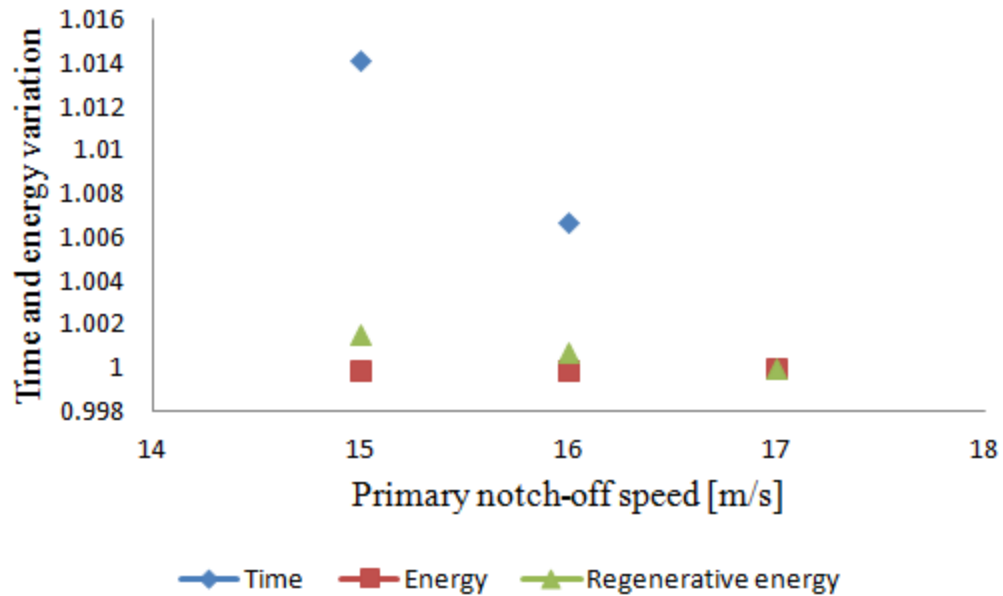


Fig.2.43. Influence of primary notch-off speed at planned braking power

b) At planned running time

At planned running time, running mode is defined based on the following conditions:

- Maximal primary notch-off speed 17m/s
- Secondary notch-off speed 19.5m/s
- Secondary powering mode follows to nearest limited point
- Running time 72.5s

Fig.2.44 shows the different running curves at the same running time. Low primary notch-off speed means more time for secondary powering mode. For this reason, higher braking power must be used in shorter braking time. Simulation results in comparison with the highest primary notch-off speed are shown in Fig.2.45 and Table 2.7.

Simulation results show that at planned running time, more regenerative energy can be obtained when reducing the primary notch-off speed. In addition, total energy consumption also slightly decreases when this value decreases. On the other hand, higher maximal braking power at shorter time is necessary. 0.12% of total energy consumption reduces, and 0.36% of regenerative energy increases when primary notch-off speed reduces

from 17m/s to 15m/s. Nevertheless, braking power increases from 100kw to 145kW in this case. Therefore, reducing the primary notch-off speed is not a good solution to reduce braking power.

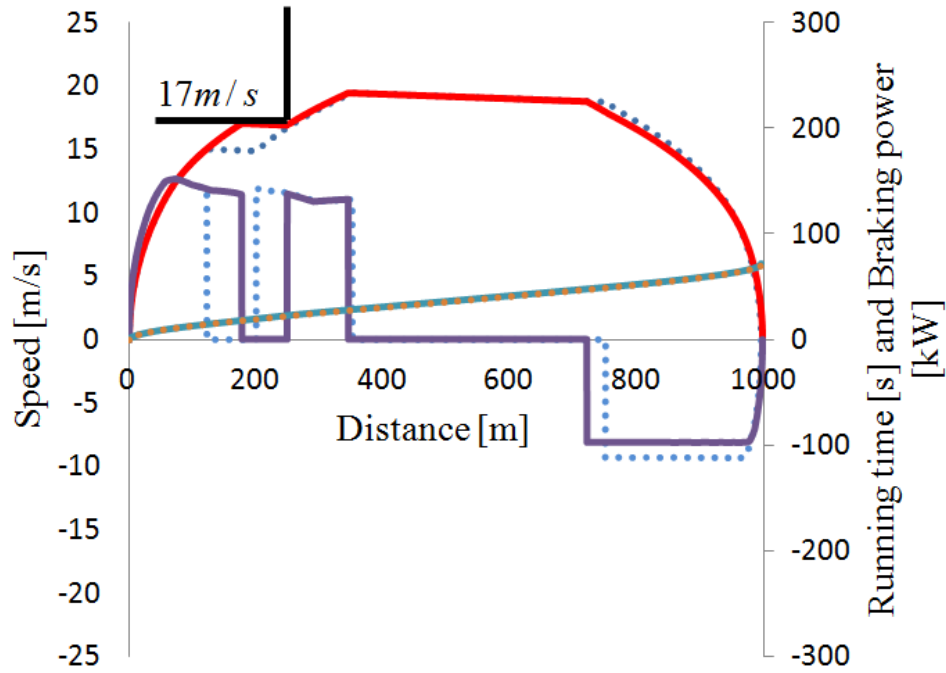


Fig.2.44. Speed, running time and braking power distribution

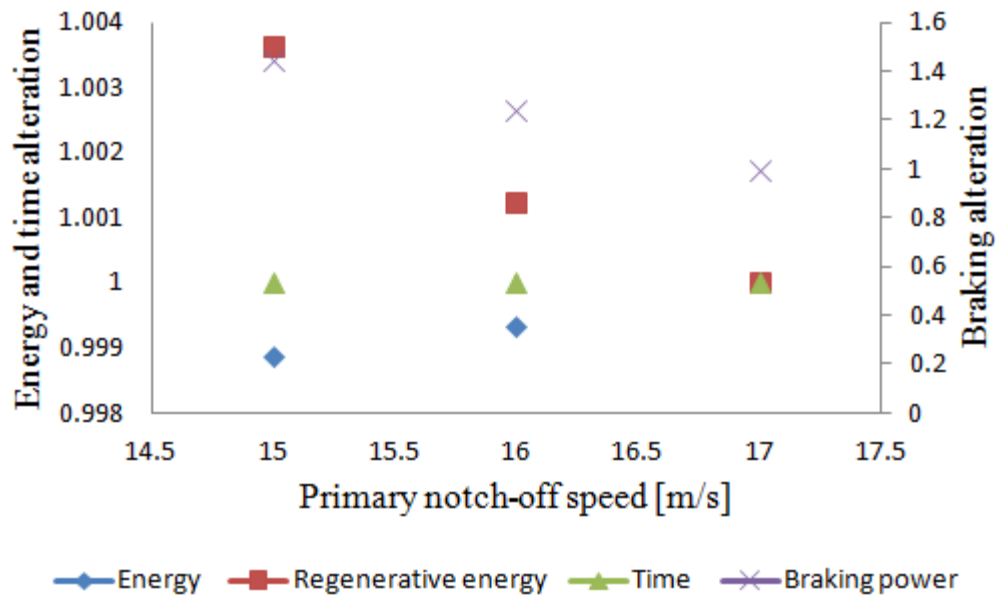


Fig.2.45. Energy, time and braking power variation at planned running time

Table 2.7. Performance at planned running time

Time [s]	Pri. Notch-off [m/s]	Pow. Ene.1 [kWh]	Pow. Ene. 2 [kWh]	Braking Power [kW]	Regenerative Energy [kWh]	Total Energy [kWh]
72.5	17	24.84	8.54	100	11.29	22.086
72.5	16	21.96	11.42	124	11.31	22.079
72.5	15	18.99	14.4	145	11.33	22.07

Hence, when considering the influence of speed limitation, simulations in different primary coasting distances and different primary notch-off speeds show that running curve at maximal primary notch-off speed and at the point nearest to the limited point (the red line in fig.2.46) is the best solution for reducing maximal braking power and increasing braking time. This is also a good solution for decreasing running time. Energy can be saved at the nearest limited point but it slightly increases at maximal notch-off speed. Consequently, it becomes the best running curve when total regenerative energy can be used and there is no peak power crisis on regenerative energy.

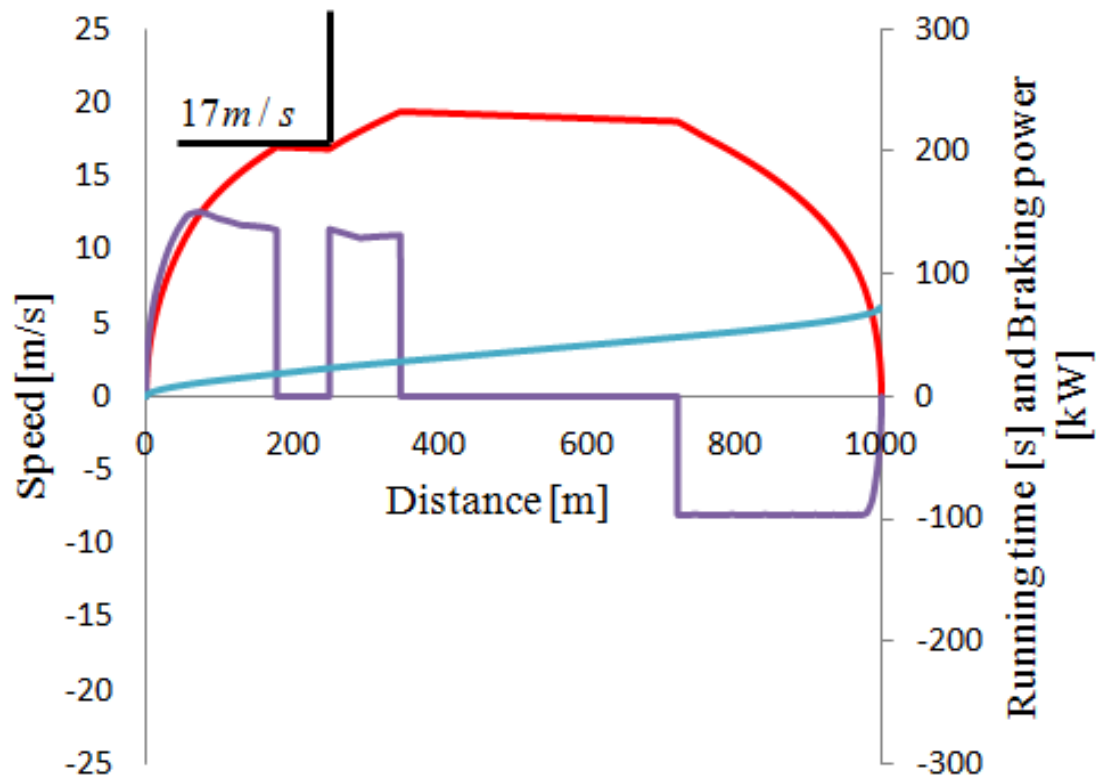


Fig.2.46. Best running curve in speed limitation

2.4.3. Influence of upper and lower speed at constant speed control

In ATO running curve, coasting can be a part of the constant speed control when it is kept around the nominal allowed speed. By altering the range of upper and lower speed around the constant value, it is possible to investigate the influence of upper and lower speed on energy consumption and running time.

The investigation of the upper and lower speed is performed on idealized line L1 and it is based on following conditions:

- Constant speed control at 18m/s
- Upper and lower speed are changed at each $\pm 0.2m/s$
- Maximal braking power 135kW

Fig.2.47 shows the running curve and power distribution when upper and lower speed oscillates at $\pm 0.2m/s$. In this figure, dotted lines (---) are speed and power at normal coasting running curve. The powering is reduced to zero when the speed reaches $18.2m/s$, which makes the train to start coasting. When the speed drops to $17.8m/s$, the powering is increased to maximum value due to the influence of running resistance.

Variation of running time, energy consumption and regenerative energy as a function of upper and lower speed in comparison with normal coasting mode (dotted-green line in Fig.2.47) are shown in Fig.2.48. This performance is also expressed in Table 2.8.

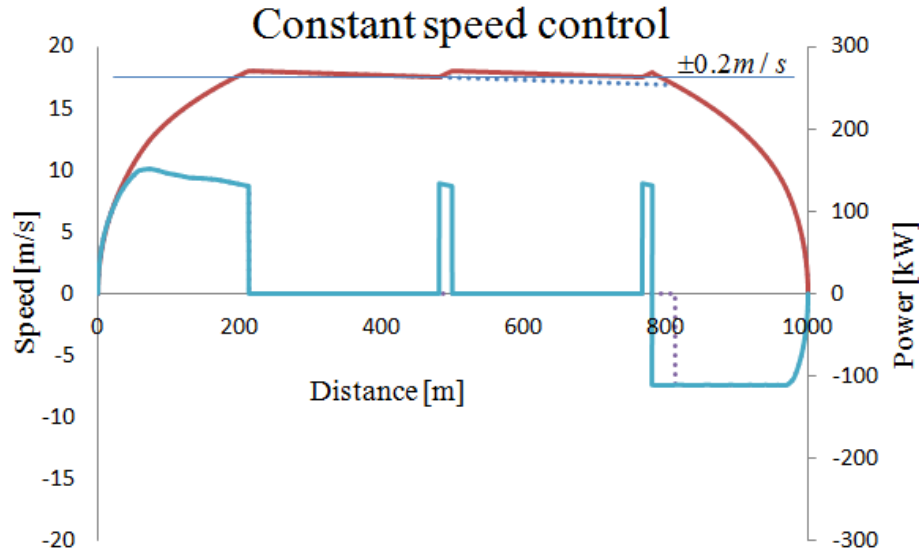


Fig.2.47. Running curve when considering constant speed control

Simulation results show that, a train running at a low value of upper and lower speed has lower energy consumption than a train running at a higher value of upper and lower speed. Running time can also be reduced when speed are controlled at a constant value during the coasting mode.

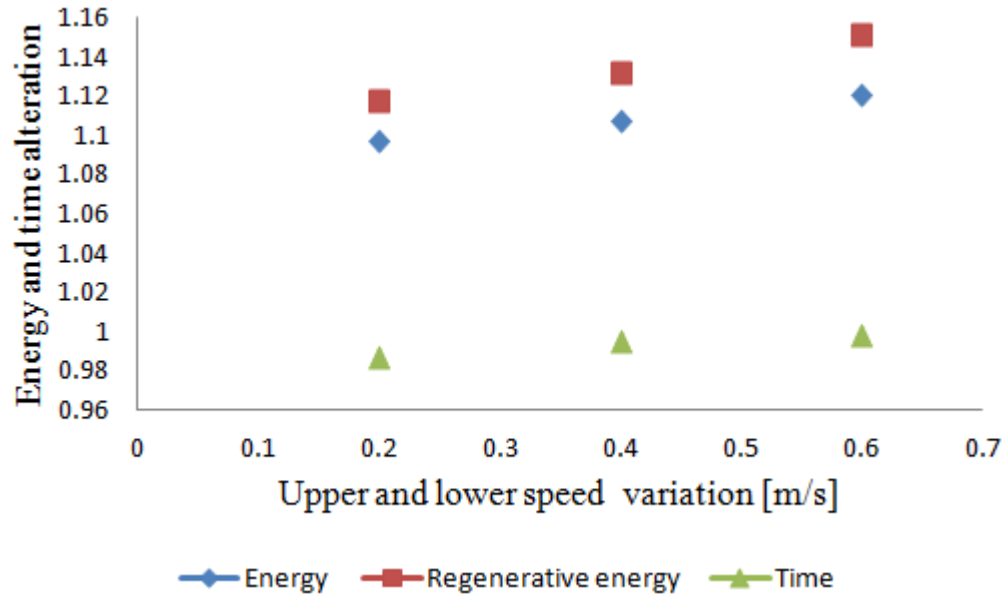


Fig.2.48. Time and energy variation

Table 2.8. Simulation results at different upper and lower speed

Time [s]	Speed variation [m/s]	Powering Energy [kWh]	Braking Power [kW]	Regenerative Energy [kWh]	Total Energy [kWh]
73.02	± 0.2	30.99	135	10.51	20.49
73.55	± 0.4	31.32	135	10.63	20.68
73.82	± 0.6	31.75	135	10.81	20.94

2.4.4. Influence of the combination of some different parameters

According to the simulation results from 2.4.1 to 2.4.3, running curve for energy saving and improving the utilization of regenerative energy are considered at some different parameters. Simulation is carried out at idealized line L1 according to the conditions below:

- Speed limitation at 230m and 17m/s during the powering mode
- Speed limitation at 700m and 13.5m/s during the braking mode
- Maximal braking power 135kW

Fig.2.49 shows a comparison between normal random running curve and optimal running curve (solid-red-line). While total energy consumption reduces from 22.65kWh to 22.21kWh, running time also reduces from 78.5s to 76.8s. The improvement of regenerative energy can be seen when maximal braking power reduces from 120kW and 135kW to 60kW and 112.5kW respectively.

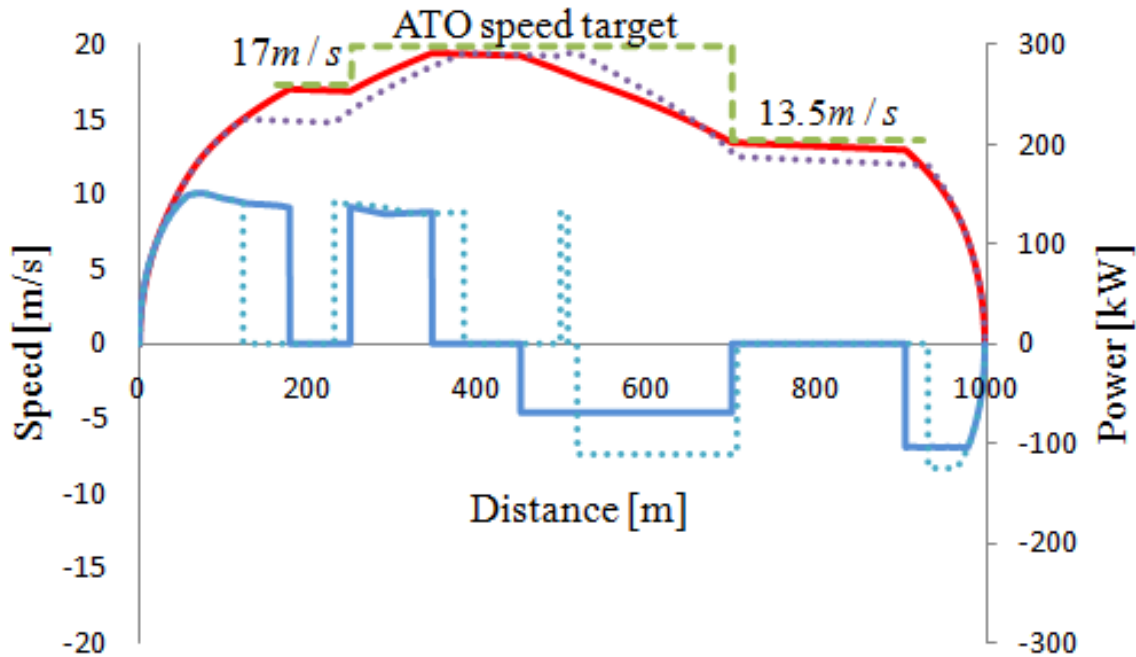


Fig.2.49. Running curve at different parameters

This case shows that it is possible to reduce energy consumption and improve the utilization of regenerative energy by combining the driving parameters.

Table 2.9. Simulation results at different running curves

Curve	Time [s]	Powering energy [kWh]	Regenerative energy [kWh]	Braking power 1 [kW]	Braking power 2 [kW]	Total energy [kWh]
Normal	78.5	34.28	11.62	120	135	22.65
Optimal	76.8	33.38	11.17	60	112.5	22.21

2.5. Chapter summary

In this chapter, different railway braking systems used in railway system are introduced. For better use of electrical brake, regenerative brake is used as power limited brake at high speed operation. The model of ATO running curve design is described based on real ATO operation principle. Thanks to that, simulation at an inter-station shows that at the same notch off speed regenerative energy can be obtained with the same value, energy can be saved by increasing the running time and reducing notch-off speed, and with the same running time energy can be saved by considering the mutual relation of notch-off speed and braking power.

Thanks to these design principle, in order to save energy for ATO running curve design, the influence of coasting length and notch-off speed on speed limitation and lower and upper speed at constant speed control as well as the combination of these parameters are determined. Finally, it shows the optimal running curve at real operation conditions.

Chapter III

Three-dimensional analysis for secondary reaction plate design of LIM

3.1. Introduction

Linear Induction Motor (LIM) is a suitable choice for railway application and has been applied for Linear Metro in Japan since the 1990s. It has many significant characteristics such as it is easy of manufacture, capable of direct force, independent of adhesion, the ability to transfer steep gradients and curves.

However, different from rotating motor, LIM has special characteristics and inherent problems because of non-continuity of the magnetic field. Longitudinal end effect and transverse edge effect are two major electromagnetic phenomena of LIM, which make the analysis, design and control of this motor difficult. While longitudinal end effect is strongly affected by slip frequency and the length of mechanical clearance, transverse edge effect is strongly affected by the construction of secondary reaction plate. Thus, in the transportation system using LIM, mechanical clearance and secondary reaction plate are important design factors thanks to their influence on not only the operation cost but also the construction cost [18][19].

In LIM, the experiments for analysis and design are difficult to carry out due to the construction requirements. Therefore, the analysis research of longitudinal end effect and transverse edge effect in LIM is generally based on an idealized mathematical model that has some restrictions [20]-[21]. The first restriction is that the longitudinal end effect is caused by the finite length of the primary part that requires LIM the full modeling in analysis. The second restriction is that two-dimensional (2-D) analysis cannot express the influence of transverse edge effect caused by the finite width of the primary and secondary part. Hence, in order to evaluate the characteristics of LIM, the three-dimensional (3-D) analysis with full-length model is necessary.

Purpose

In this chapter, from fundamental mathematics and formulation of the simplified field calculation, by using integral equation method for 3-D analysis, high accuracy LIM analysis will be examined to define the influence of the finite length of the primary part and the finite width of the secondary part.

Methodology

The study is carried out through literature review, calculation, simulations, and experiments.

3.2. Overview of LIM for Linear Metro

3.2.1. Construction and principle LIM

Fig.3.1 shows the concept of LIM from rotary motor. It is a conventional rotary motor whose stator, rotor and winding have been cut open, flattened and placed in the guided way [21]. Even though the operating principle is exactly the same as a rotary motor, LIM has a finite length of the primary or secondary part so it causes longitudinal end effect and transverse edge effect. Moreover, the large air gap causes lower efficiency and power factor in comparison with rotary induction motor. LIM is preferable for the urban railway transportation system because the construction cost is much lower than that of linear synchronous motor (LSM), although its efficiency and performance are not as good.

The operation principle of LIM is identical to a rotary induction motor. The force is produced by a linear moving magnetic field generated by conductors in the field. Any conductor, be it a loop, a coil or simply a piece of plate metal, called secondary reaction plate, that is placed in this field will have eddy currents induced in it, thus creating an opposing magnetic field in accordance with Lenz's law. The two opposing fields will repel each other, creating motion as the magnetic field sweeps through the metal, Fig.3.2.

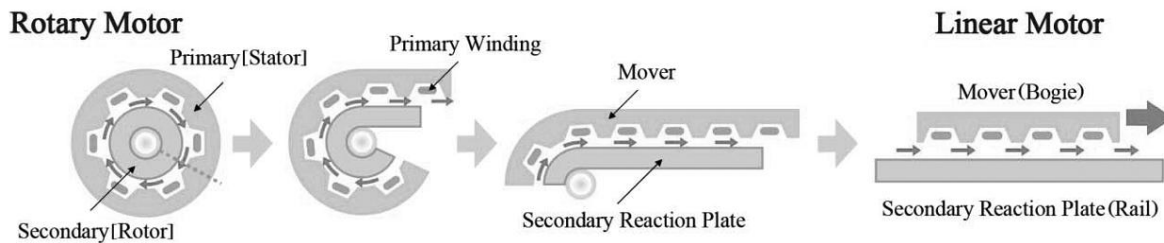


Fig.3.1. Concept of LIM from rotary motor

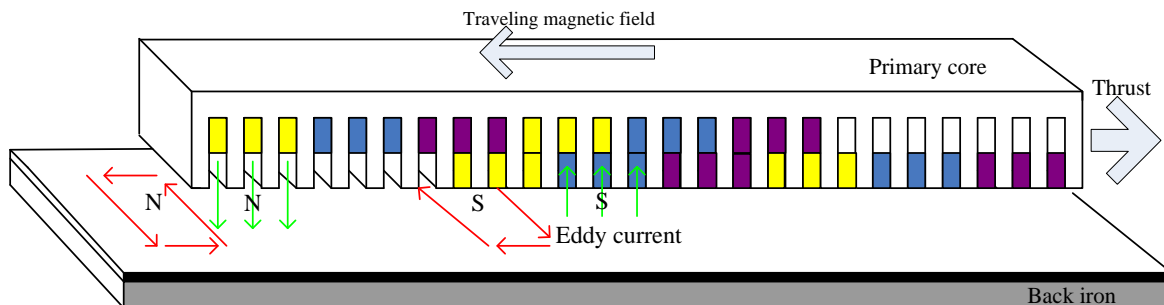


Fig.3.2. LIM's principle

3.2.2. LIM problems

As mentioned above, because of the non-continuity of the magnetic field, LIM has some problems with its performance. These shortcomings must be minimized as much as possible in design so that they do not drastically affect performance of the LIM.

3.2.2.1. End effect

One obvious difference between LIM and conventional rotary machines is that LIM has primary ends. This means that the travelling magnetic field cannot join up by itself, which is called end effect. The end effect is clearly exhibited in the form of a non-uniform flux density distribution along the length of the motor. For a given slip, the flux density builds up along the primary length, beginning with a small flux density at the entry end. Depending on the length of penetration of the entry end effect wave, the flux density may not even reach the nominal level that would be found in a motor without end effect.

In the design of LIM for linear metro, with a maximum speed of about 70km/h, other designs show that the pole pitch should be 20 to 30 times the mechanical clearance to increase the output to input of LIM, which has a long air gap. In addition, the motor's length should be from 2m to 2.5m, with a decrease in the stack high of the primary iron core in order to reduce the end effect as well as the cost of secondary ground materials [23].

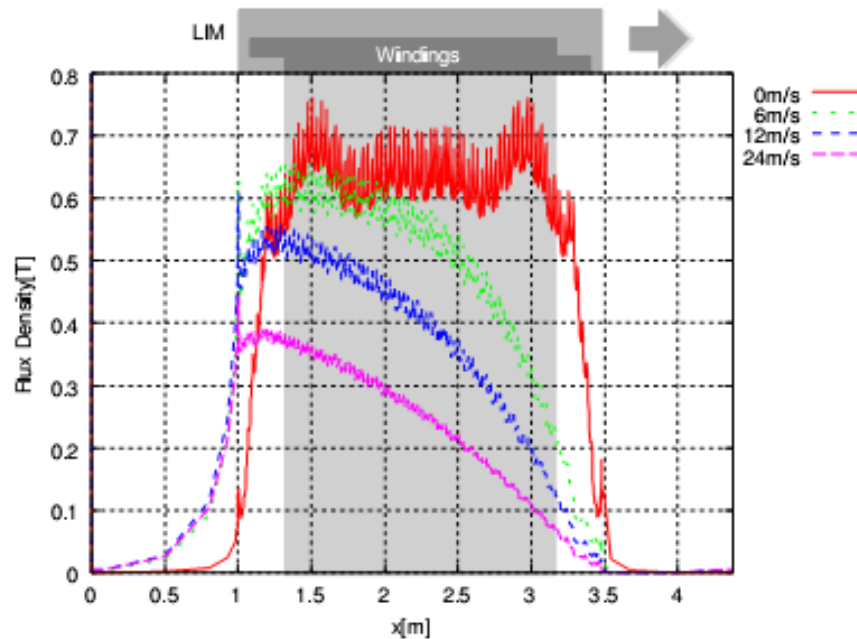


Fig.3.3. Flux density distribution along moving direction due to end effect [14]

3.2.2.2. Edge effect

The edge effect is generally described as the effect of having finite width of LIM. This effect is more evident with lower values of width compared to air gap ratio. Fig.3.4 illustrates the normal flux density in the transverse direction. The figure shows a dip at the center of the magnetic flux due to the edge effect as well as lateral parts of LIM. As a result, the edge effect will increase the secondary resistivity and lateral instability due to the uneven secondary overhang and a reduction in performance.

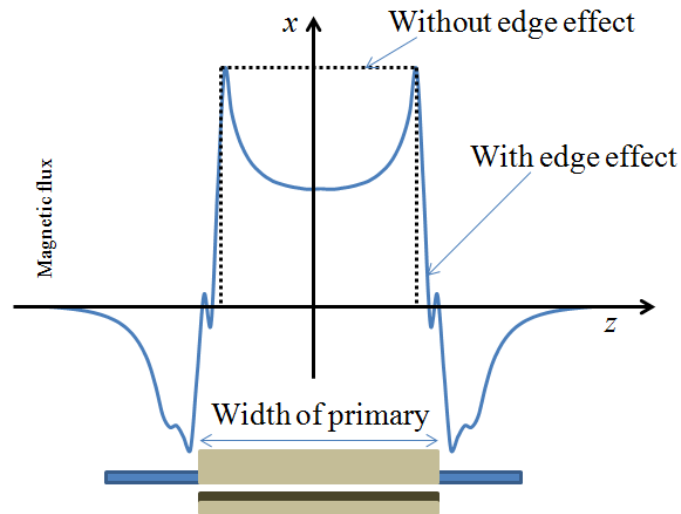


Fig.3.4. Edge effect in LIM

3.2.2.3. Eddy current problem

The combination between air gap magnetic flux and the eddy current, that follows the perpendicular of moving direction in the secondary reaction plate, will generate the thrust of LIM. However, LIM has the finite width of the secondary reaction plate so at the periphery of the plate, the current wrap occurs as show in Fig.3.5. Therefore, when eddy currents flows in other parts of the product thickness direction, the current component is not involved in generating thrust. In addition, by applying the alternating current in the primary part, eddy current will be generated in the secondary conductor and the thrust is generated through interaction with electromagnetic force. The alternative magnetic field is also osmosis to secondary back iron, so the primary and secondary part close the magnetism circuit. Therefore, the eddy current is generated even in the secondary core. As a result, when magnetic saturation occurs, the core will cause some direct influences. In order to restrain the eddy current in secondary back iron, steel lamination layer has been used.

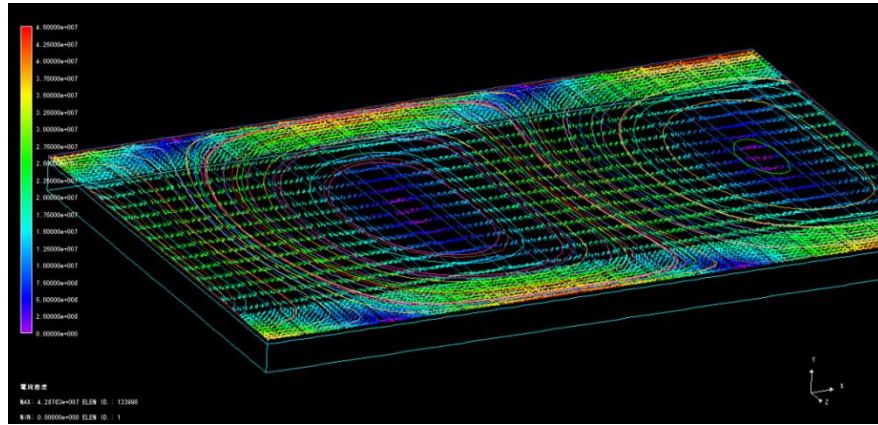


Fig.3.5. Distribution of eddy current in secondary reaction plate

3.3. Numerical analysis method for LIM analysis

Up to now, many numerical methods have been applied for LIM analysis. In order to analyze the characteristics of LIM when considering the influence of end effect, edge effect and the difficult of eddy current analysis, 3-D Integral Equation Method (IEM) using Magnetic Moment Method (MMM) has been used. For the purpose of comparison, 3-D results of this method have been shown with 2-D Finite Different Method (FDM) and actual LIM experiment results in [19].

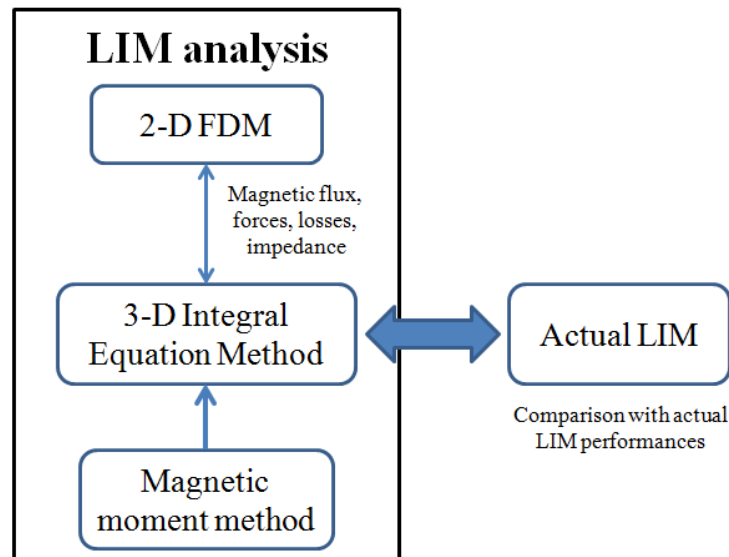


Fig.3.6. LIM analysis and experiment

Table 3. 1. Symbols and meaning

Symbols	Meaning
A	Magnetic vector potential
B	Magnetic flux density
E	Electric field
E_e	Electric field for the flow of eddy current
F	Forces
I	Current
J	Current density
J_e	Eddy current density
ϕ	Scalar potential
Φ	Inter-linkage flux
ω	Angular frequency
f	Frequency, magnetomotive force
g	Air gap length
m	Number of phase
n	Number of coil
S_c	Coil area
p	Number of pole
s	Slip
v	Speed
Z	Impedance
η	Efficiency
\mathcal{G}	Reductively
μ	Permeability
σ	Conductivity
τ	Pole pitch length
<i>Others</i>	Vectors are shown as bold-type (\mathbf{A} , \mathbf{B} , ...)

3.3.1. 2-D Finite Different Method

FDM is a numerical method to approximate the solutions to differentiate equations using finite different equations to approximate derivatives. In this method, the target area is divided into grid patterns as shown in Fig.3.7 [24].

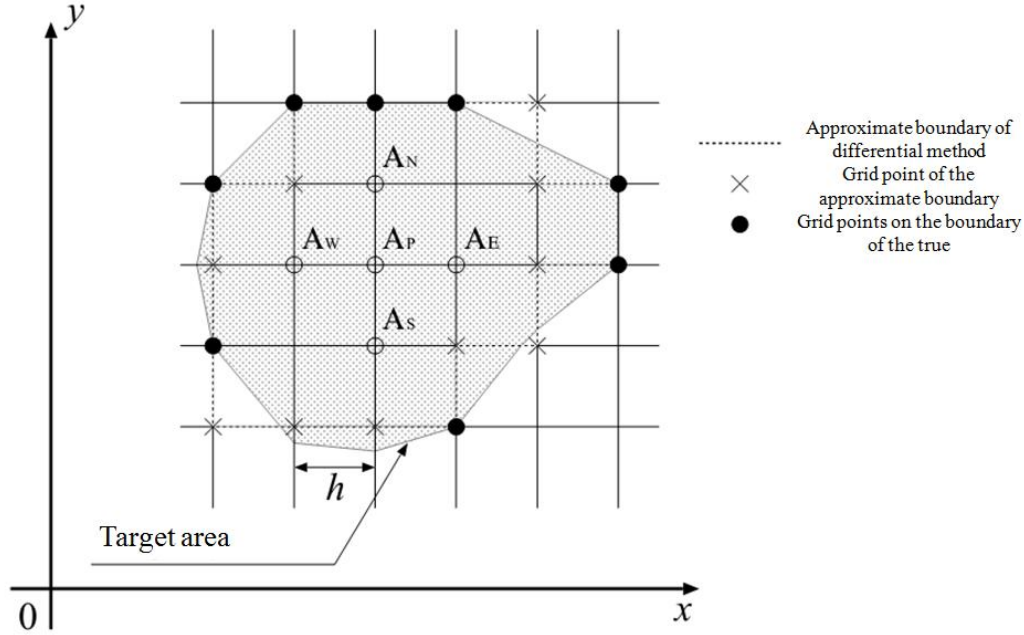


Fig.3.7. Finite Different Method

At each grid point, adjacent grid point potential of the electromagnetic field is calculated by its relation to the near grid point. For example, equations of the electromagnetic field can be assumed in the simplified of two-dimensional Laplace equation as in equation (3.1)

$$\frac{\partial^2 A}{\partial x^2} + \frac{\partial^2 A}{\partial y^2} = 0 \quad (3.1)$$

When solving a differential equation like (3.1) in the numerical calculations, it is necessary to discrete this equation. In the equally spaced grid as Fig.3.7, Taylor expansion is used around the points of A1 to A4 potentials. Following equation (3.2), we can obtain the potential by considering the second derivative equation.

$$\left\{ \begin{array}{l} A_E(x_0 + h, y_0) = A_P(x_0, y_0) + h \frac{\partial}{\partial x} A_P(x_0, y_0) + \frac{h^2}{2} \frac{\partial^2}{\partial x^2} A_P(x_0, y_0) \\ A_N(x_0, y_0 + h) = A_P(x_0, y_0) + h \frac{\partial}{\partial x} A_P(x_0, y_0) + \frac{h^2}{2} \frac{\partial^2}{\partial x^2} A_P(x_0, y_0) \\ A_W(x_0 - h, y_0) = A_P(x_0, y_0) + h \frac{\partial}{\partial x} A_P(x_0, y_0) + \frac{h^2}{2} \frac{\partial^2}{\partial x^2} A_P(x_0, y_0) \\ A_E(x_0, y_0 - h) = A_P(x_0, y_0) + h \frac{\partial}{\partial x} A_P(x_0, y_0) + \frac{h^2}{2} \frac{\partial^2}{\partial x^2} A_P(x_0, y_0) \end{array} \right. \quad (3.2)$$

Here, h is the distance between the gratings. From (3.1) and (3.2) we can neglect the term of h^2 as in (3.3):

$$A_0(x_0, y_0) = \frac{1}{4} (A_1(x_0 + h, y_0) + A_2(x_0, y_0 + h) + A_3(x_0 - h, y_0) + A_4(x_0, y_0 - h)) \dots\dots\dots(3.3)$$

To create grid points of the entire region (3.3), the potential of each grid point is determined by solving according to boundary conditions.

3.3.2. 3-D Integral equation method using Magnetic Moment Method

The advantages of Magnetic Moment Method (MMM) are mesh division is not needed for the free space, and it can easily treat the nonlinearity of magnetic properties of the magnetic materials. This method is considered fairly effective for the analysis of the problems with the open boundary, including LIM. In MMM method, the MMM yields fully populated matrices because of the integral-based formulation. Therefore, large memory and computational time have been required due to dense matrices [26].

Formulation of MMM [27][28],

Consider the following two regions:

- Region Ω_0 is the free space which extends to infinity with supply currents
- Region Ω_m with boundary Γ_m consists of a non-conducting magnetic substance whose permeability μ_m has a nonlinear characteristic

The magnetization \mathbf{M} satisfies the following integral equation (3.4)

$$\frac{M}{\mu_r - 1} = H_M + H_0 = - \int_{\Omega_m} \nabla \cdot M \nabla G d\Omega + \int_{\Gamma_m} M \cdot n \nabla G d\Gamma + H_0 \quad (3.4)$$

Where μ_r, G, H_M and H_0 are respectively the relative permeability, the Laplace Green's function, the induced magnetic field and the source field calculation by the Biot-Savart law.

Magnetic material is divided into hexahedral elements, and magnetic surface charge density is defined on a surface of each hexahedral element:

$$\sigma = M \cdot n \quad (3.5)$$

Thus, an element has six unknown points and six evaluation points of M . The midpoint between the gravity point of a hexahedral element and the center of its surfaces as evaluation points is selected. In the case of constant μ_r , in each hexahedral element, the divergence of M becomes zero and σ satisfies the following equation:

$$\int_{\Gamma_m} \sigma d\Gamma = 0 \quad (3.6)$$

Therefore, the right-hand first term of (3.4) can be eliminated.

Compared with FEM, MMM has the outstanding points that the data making is straightforward because it does not require the matching constraints at vertices and edges of each element. In addition, mesh division for the free space is not necessary.

3.3.3. LIM calculation using numerical analysis

By using numerical analysis based on FDM and MMM, the calculation of some important characteristics of LIM will be introduced in this section.

3.3.3.1. Derivation of basic equation

Eddy current flows in the conductor by the changing of magnetic flux \mathbf{B} and the generating of electromotive force and it can be expressed as:

$$\mathbf{J}_e = \sigma(\mathbf{E}_e + \mathbf{v} \times \mathbf{B}) \quad (3.7)$$

Where, \mathbf{E}_e is the electric field by eddy current by in the induction, \mathbf{v} is the velocity of the movement of LIM.

Vector potential \mathbf{A} is defined by the following equation:

$$\mathbf{B} = \nabla \times \mathbf{A} \quad (3.8)$$

From Maxwell equation we have:

$$\nabla \times \mathbf{E} = -\frac{d\mathbf{B}}{dt} \quad (3.9)$$

So,

$$\nabla \times \mathbf{E}_e = -\frac{d}{dt}(\nabla \times \mathbf{A}) \quad (3.10)$$

$$\mathbf{E}_e = -\frac{\partial \mathbf{A}}{\partial t} - \nabla \phi \quad (3.11)$$

Hence, the eddy current density in (3.7) can be rewritten as:

$$\mathbf{J}_e = \sigma \left(-\frac{\partial \mathbf{A}}{\partial t} - \nabla \phi + \nu \times (\nabla \times \mathbf{A}) \right) \quad (3.12)$$

Current density is sum of eddy current density and forced current density, or

$$\mathbf{J} = \mathbf{J}_0 + \mathbf{J}_e \quad (3.13)$$

From Maxwell equation we also have $\nabla \times \mathbf{H} = \mathbf{J}$, while $\mathbf{H} = \mathcal{G}\mathbf{B}$, so the derivation of basic equation can be written as:

$$\nabla \times \{ \mathcal{G}(\nabla \times \mathbf{A}) \} = \mathbf{J}_0 + \sigma \left\{ -\frac{\partial \mathbf{A}}{\partial t} - \nabla \phi + \nu \times (\nabla \times \mathbf{A}) \right\} \quad (3.14)$$

3.3.3.2. Magnetic flux density calculation

From the relation of magnetic flux and magnetic vector potential in (3.8), magnetic flux can be determined as:

$$\mathbf{B} = \nabla \times \mathbf{A} = \begin{vmatrix} i & j & k \\ \frac{\partial}{\partial x} & \frac{\partial}{\partial y} & \frac{\partial}{\partial z} \\ A_x & A_y & A_z \end{vmatrix} = \begin{bmatrix} B_x \\ B_y \\ B_z \end{bmatrix} \quad (3.15)$$

In case of two dimensional analysis, $\mathbf{A} = A_z$ or

$$\mathbf{B} = \nabla \times \mathbf{A} = \begin{vmatrix} i & j & k \\ \frac{\partial}{\partial x} & \frac{\partial}{\partial y} & \frac{\partial}{\partial z} \\ 0 & 0 & A_z \end{vmatrix} = \begin{bmatrix} \frac{\partial A_z}{\partial y} \\ -\frac{\partial A_z}{\partial x} \\ 0 \end{bmatrix} = \begin{bmatrix} B_x \\ B_y \\ B_z \end{bmatrix} \quad (3.16)$$

3.3.3.3. Forces calculation

From the magnetic flux density, the propulsion force and normal force are generated in LIM. Consider that B_x and B_y are magnetic flux densities at the center of the mechanical air gap propulsion force and normal force at that point can be expressed by the following equation, using the Maxwell stress tensor equation:

$$f_x = \frac{1}{\mu_0} B_y B_x \quad (3.17)$$

$$f_y = \frac{1}{2\mu_0} (B_y^2 - B_x^2) \quad (3.18)$$

These equations can be rewritten as:

$$f_x = \frac{1}{2\mu_0} \text{Re}(\dot{B}_x \dot{B}_y^*) \quad (3.19)$$

$$f_y = \frac{1}{4\mu_0} (\dot{B}_y \dot{B}_y^* - \dot{B}_x \dot{B}_x^*) \quad (3.20)$$

Propulsion force and normal force are finally determined as the integral along the primary length as:

$$F_x = \int_L \frac{1}{2\mu_0} \text{Re}(\dot{B}_x \dot{B}_y^*) ds \quad (3.21)$$

$$F_y = \int_L \frac{1}{4\mu_0} (\dot{B}_y \dot{B}_y^* - \dot{B}_x \dot{B}_x^*) ds \quad (3.22)$$

3.3.3.4. Impedance calculation

As the calculation of magnetic flux density and forces, impedance of LIM is calculated from magnetic vector potential \mathbf{A} . LIM model for impedance calculation is illustrated in Fig.3.8. From Maxwell equation, the inter-linkage flux Φ of the exciting coil can be determined by direct integration over the coil length of the distribution of magnetic vector potential as:

$$\Phi = \frac{n}{S_c} \int_{V_c} \mathbf{A} \cdot \mathbf{n}_s dv \quad (3.23)$$

Hence, \mathbf{n}_s is the unit vector along the direction of the exciting current

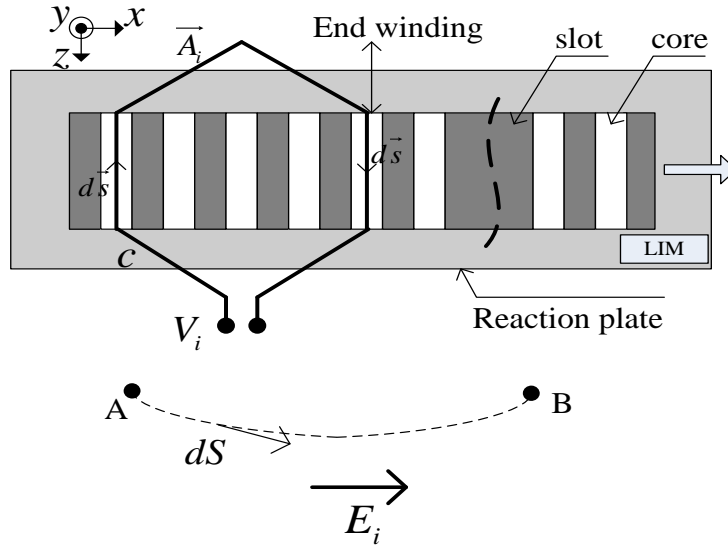


Fig.3.8. Impedance calculation model

In the simulation with current source, the exciting current I_0 is represented using the exciting current density J_0 as:

$$J_0 = \frac{n}{S_c} I_0 \mathbf{n}_s \quad (3.24)$$

So the inter-linkage flux of the exciting coil is rewritten as:

$$\Phi = \int_{V_c} \frac{1}{I_0} \mathbf{A} \cdot J_0 dV \quad (3.25)$$

Then, the induced primary voltage in each coil at time t can be determined as:

$$V_i(t) = \frac{\Phi(t) - \Phi(t - \Delta t)}{\Delta t} \quad (3.26)$$

Thus, absolute value of impedance is calculated as:

$$Z = \frac{|V_i|}{|I_i|} \quad (3.27)$$

In addition, out put power, power factor and motor efficiency are determined as:

$$P_0 = F_x v \quad (3.28)$$

$$p.f = \frac{\text{Re}(Z)}{|Z|} \quad (3.29)$$

$$\eta = \frac{P_0}{P_0 + P_2} \quad (3.30)$$

3.4. 3-D Integral Equation Method model and results

3.4.1. LIM model for 3-D IEM analysis

The model of LIM for analysis is the same with LIM used in current Linear Metro systems. Three-dimensional analysis of this model is expressed in Fig.3.9 while other parameters and analysis conditions are shown in Table 3.2. In Fig.3.9, x -direction is moving direction, y -direction is height direction, and z -direction is lateral direction.

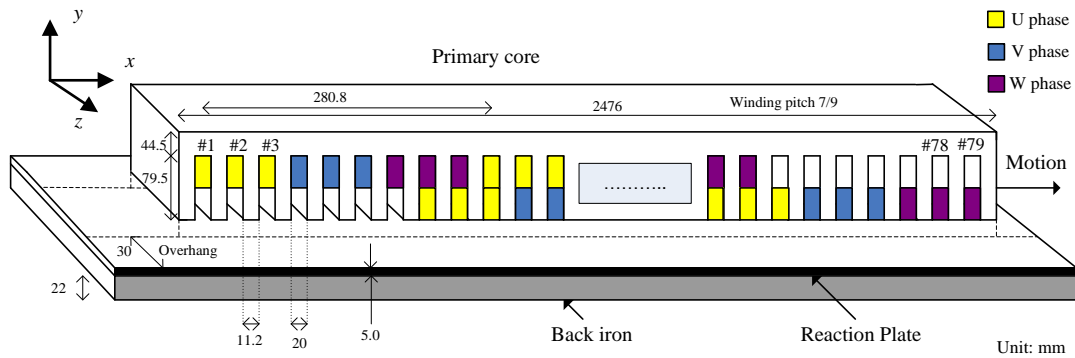
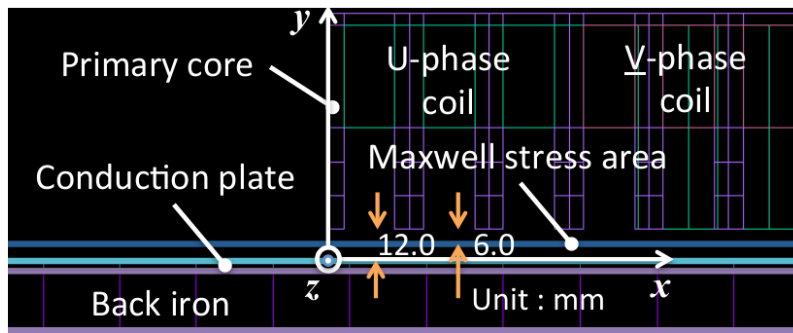


Fig.3.9. LIM model

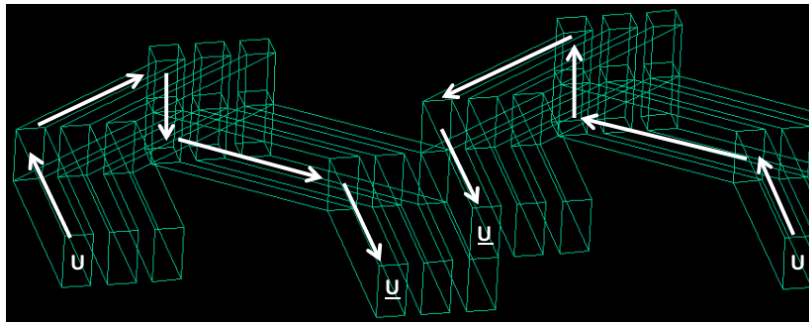
Table 3.2. Analysis conditions

Parameter	Linear metro
Normal frequency [Hz]	21
Slip frequency [Hz]	3
Synchronous speed [km/h]	70
Maximum current [A]	170
Relative permeability in primary/back iron	1000
Conductivity in primary/back iron	0
Material of conduction plate	Cu

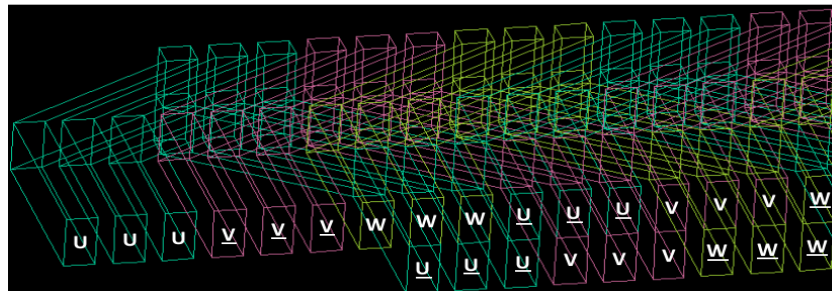
Fig.3.10 shows more details of the construction of this model in ELF/MAGIC software simulation



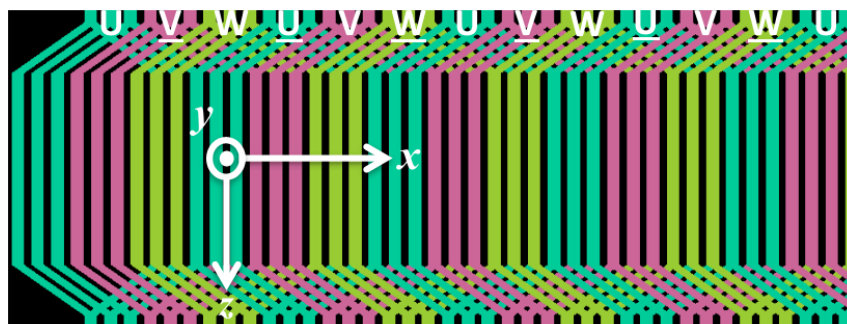
a. Front view



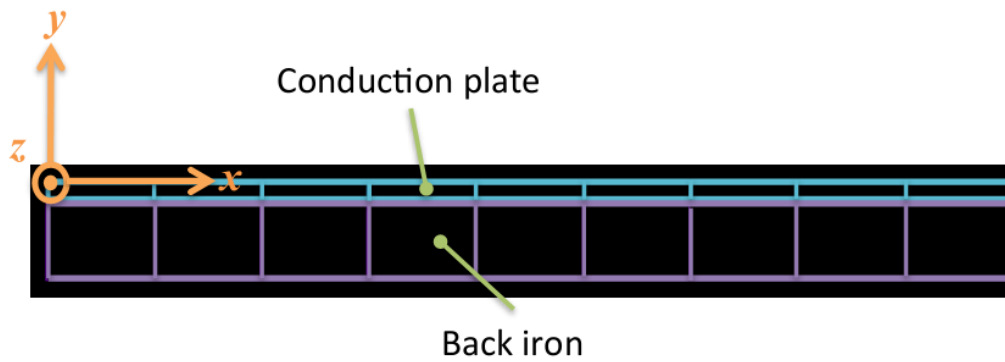
b. Construction of U-phase coil and current direction



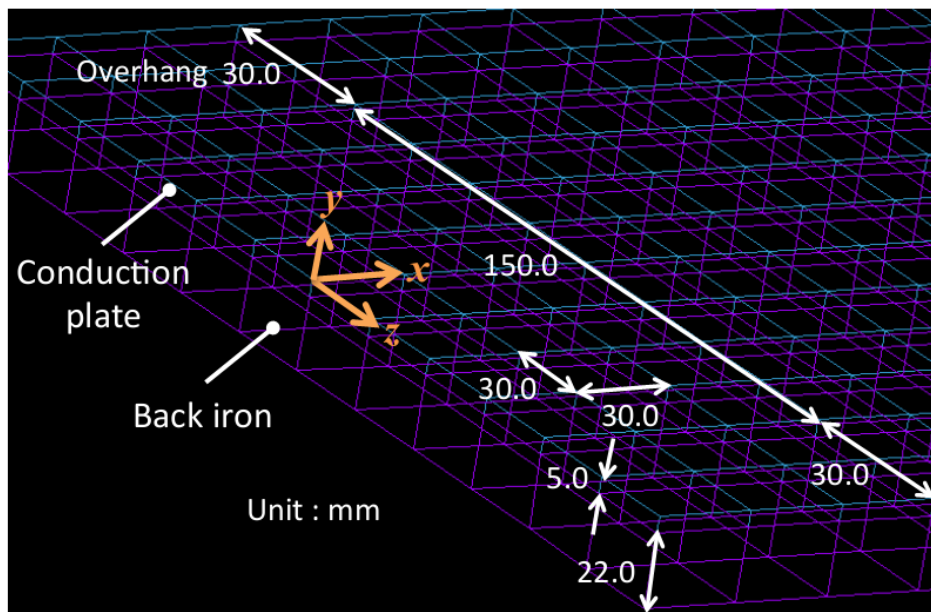
c. 3-phase construction



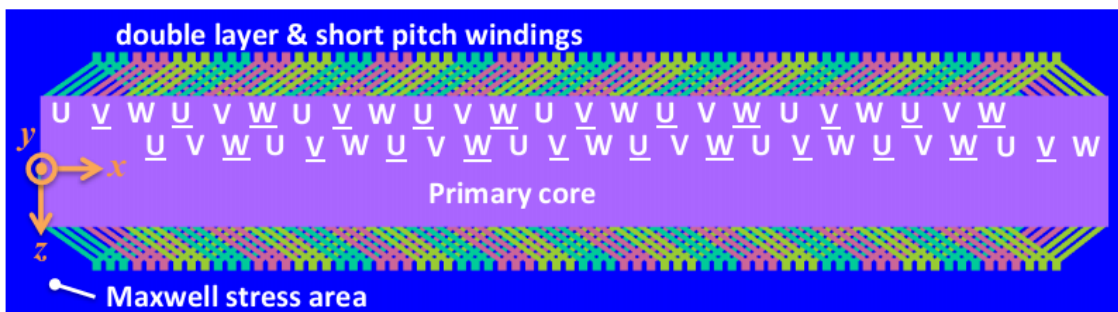
d. Coil construction from upper view



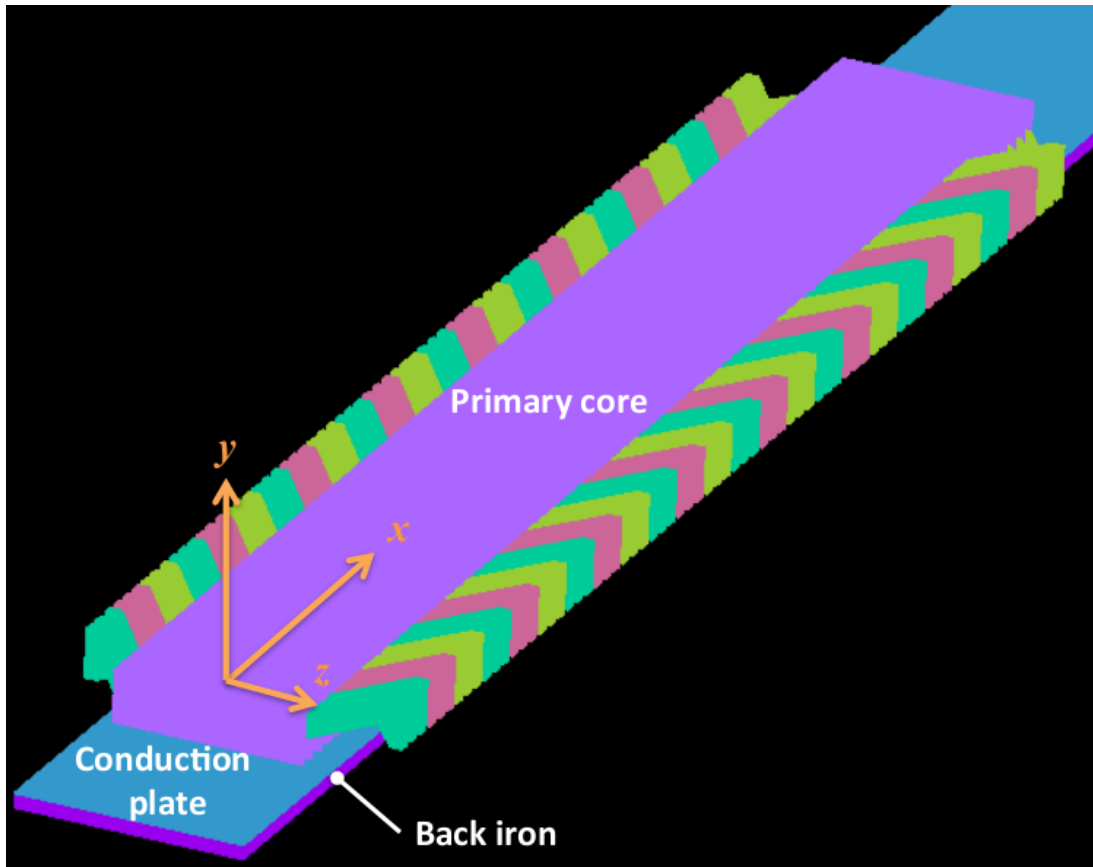
e. Front view of secondary construction



f. Element division of the secondary side



g. Maxwell stress surface from upper view



h. Overview of analysis model

Fig.3.10. Elements division and configuration of a basic analysis model

3.4.2. Numerical results

In this section the performance of LIM, including air-gap magnetic flux density, two-dimensional forces, inter-linkage flux, and eddy current with different slip frequency input will be obtained from IEM-MMM analysis.

3.4.2.1. Air-gap magnetic flux density

Along the width direction, magnetic flux is obtained at three different points along the moving direction: at the center of primary part ($z=0$), at the end of primary core ($z=150$) and at the end of the secondary part ($z=180$). To imagine the distribution of air gap flux density, the distribution of magneto-motive force (MMF) at *timestep*=9 are also illustrated in Fig.3.11.

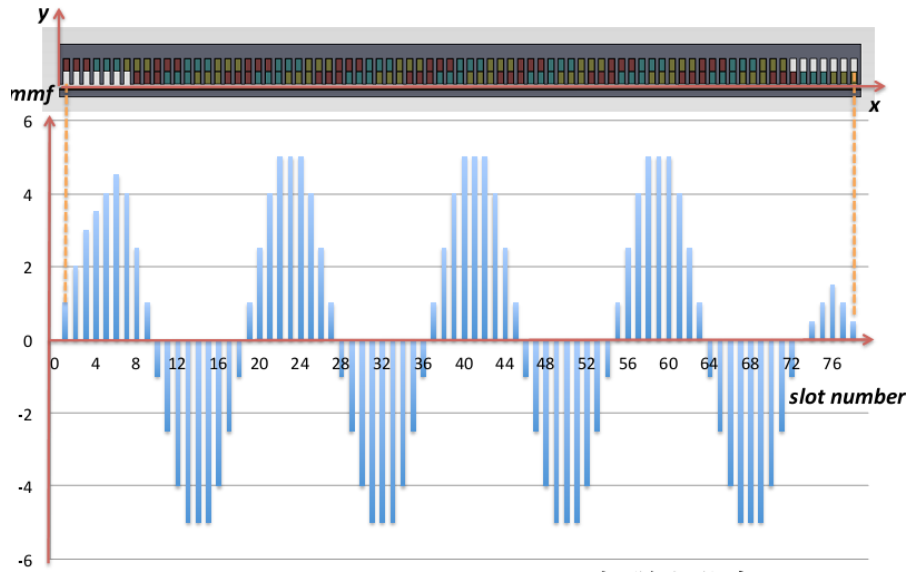
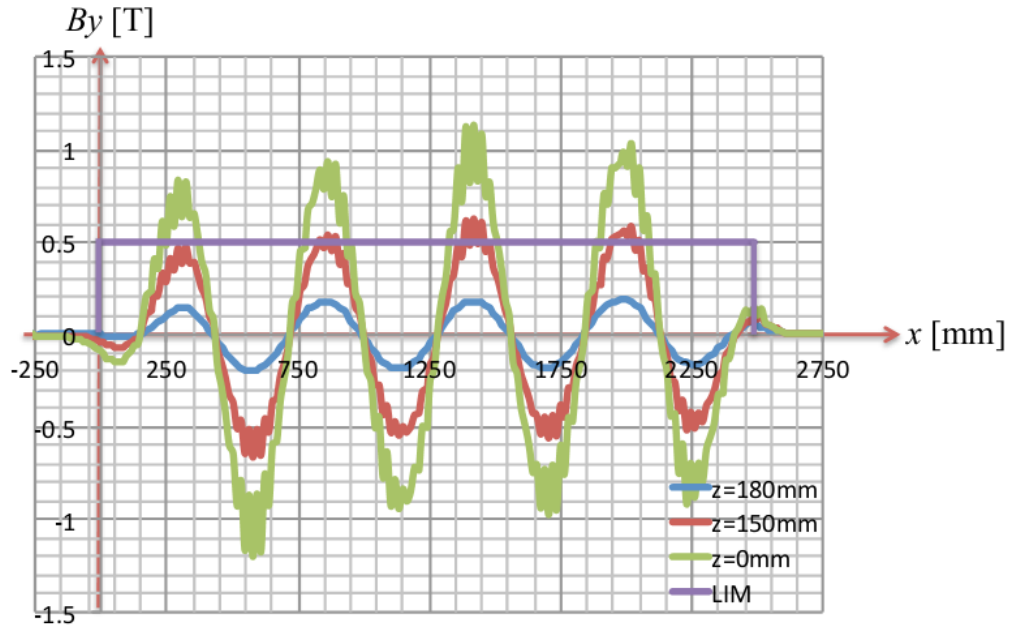
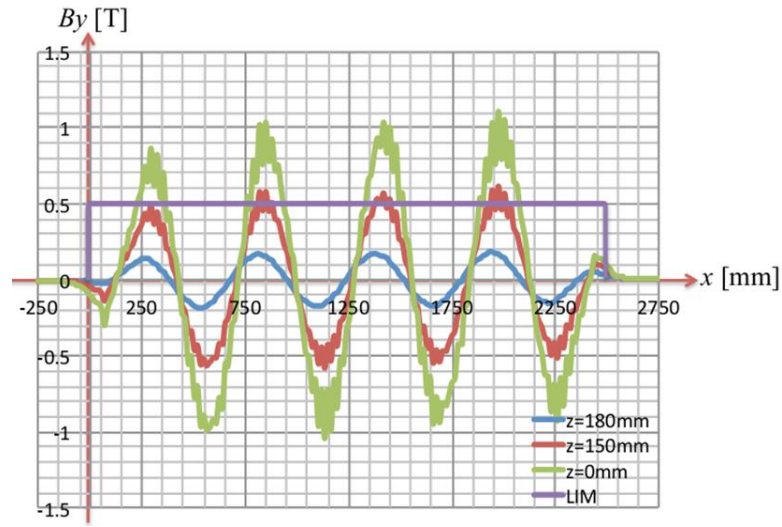


Fig.3.11. Distribution of MMF at $timestep=9$

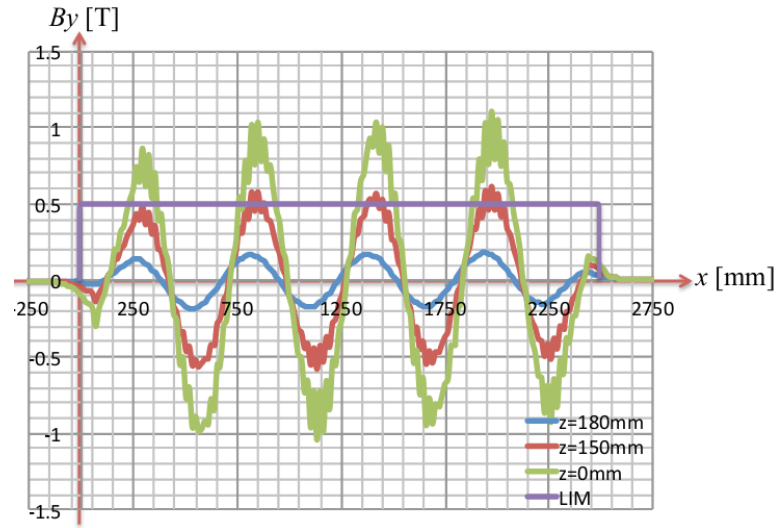
Fig.3.12 and Fig.3.13 show the distribution of air gap magnetic flux at different slips: 0.0, 0.5, and 1.0 at the same $timestep=9$. In addition, at $timestep=9$, air-gap magnetic flux along z -direction is illustrated in Fig.3.14. Magnetic flux at the entrance, exit of primary part along the moving direction and lateral part along the z -direction show the effect of end effect and edge effect on LIM's performance.



a. $slip=0$

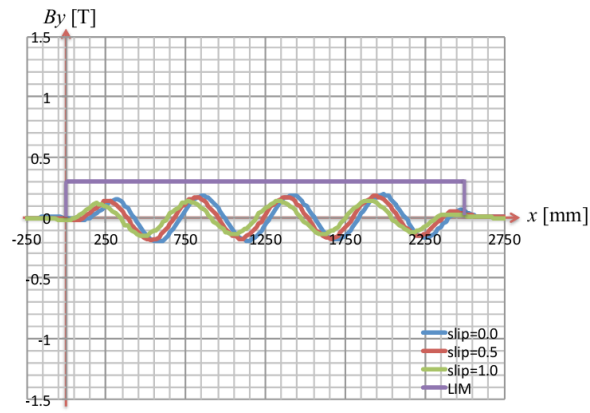


b. $slip=0.5$

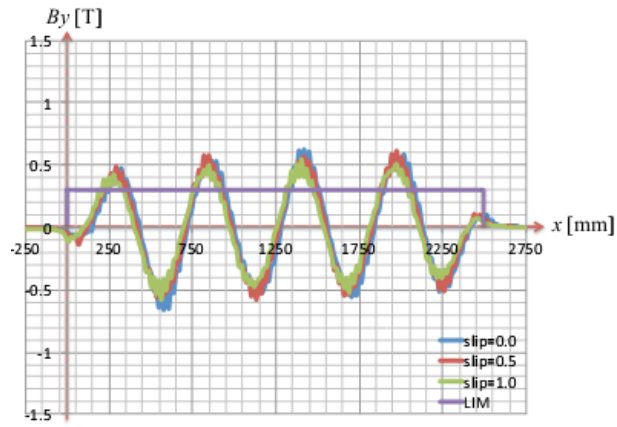


c. $slip=1$

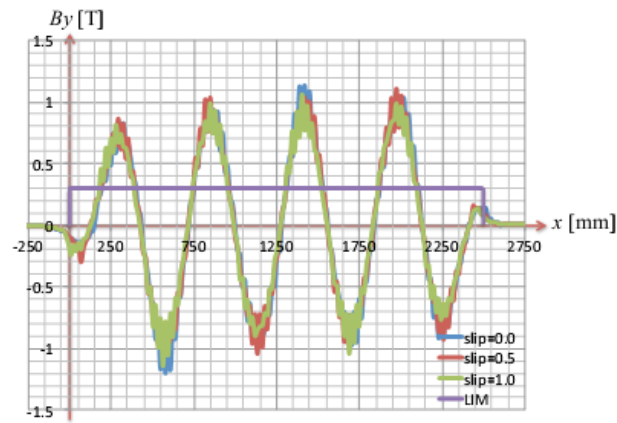
Fig.3.12. Distribution of air gap magnetic flux at different slips



a. $z=180$ (at the end of secondary part)



b. $z=150$ (at the end of primary core)



c. $z=0$ (at the center of primary core)

Fig.3.13. Air gap flux distribution at different positions along z -direction

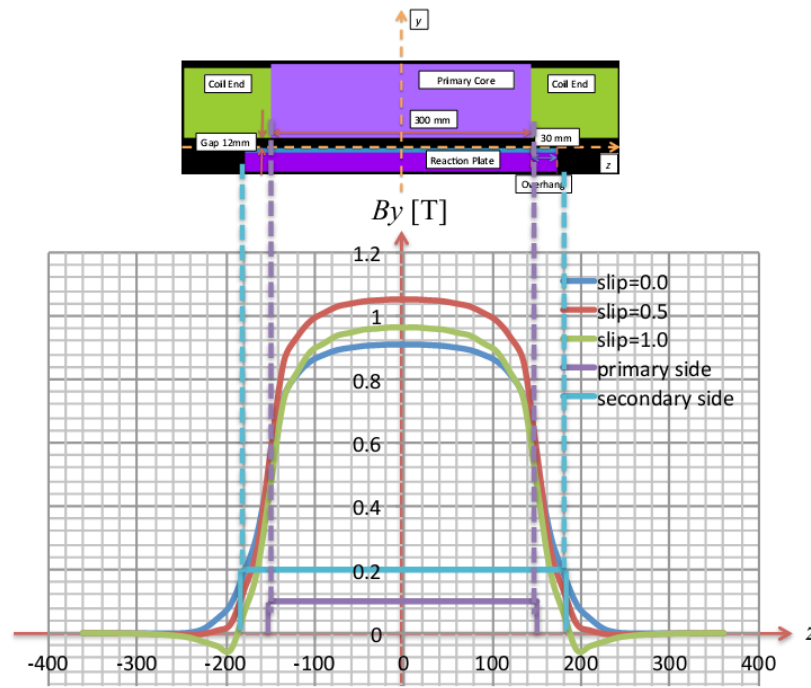


Fig.3.14. Air gap magnetic flux along z -direction

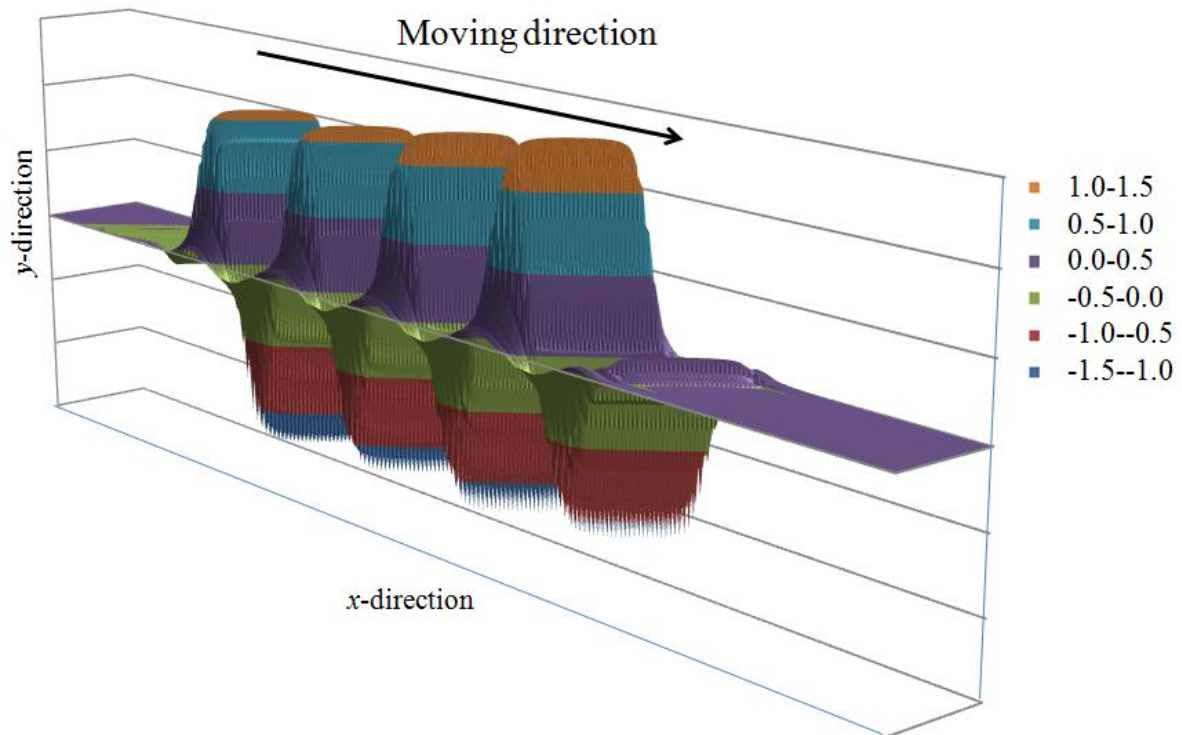


Fig.3.15. Distribution of B_y in three dimensions

3.4.2.2. Two-dimensional forces

Fig.3.16 shows the characteristics of two-dimensional forces of LIM, including longitudinal and normal force variations in time steps. With the initial current input, in order to suppress the rapid decrease of magnetic flux interlink between the primary and secondary part, eddy current in the secondary side becomes larger. This process makes the transient response bigger and the 2-D force at steady state smaller in comparison with that value of the transient process. In this model, it is found that we need 150-200 step calculations in order to obtain thrust at a steady state.

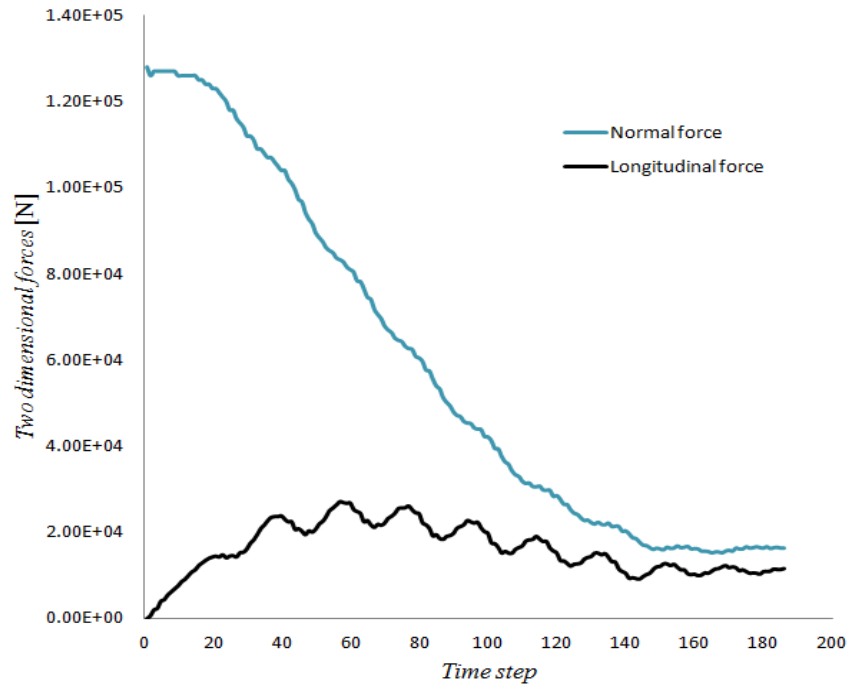


Fig.3.16. 2-D force characteristics of LIM at motor starting transient

3.4.2.3. Inter-linkage flux

Fig.3.17 demonstrates one cycle of electrical angle of scalar potential (corresponding to the flux linkage of the coil), which is obtained by vector potential A along coil line and the applied current at the steady state. Assume that each phase of scalar potential in Fig.3.16 is a sine wave; its effective value is used to calculate the induced single phase terminal voltage $V_i (i = u, v, w)$ and then power factor and efficiency as in 3.29 and 3.30. Because of the non-uniform flux density due to end effect, three-phased inter-linkage flux is also non-uniformed.

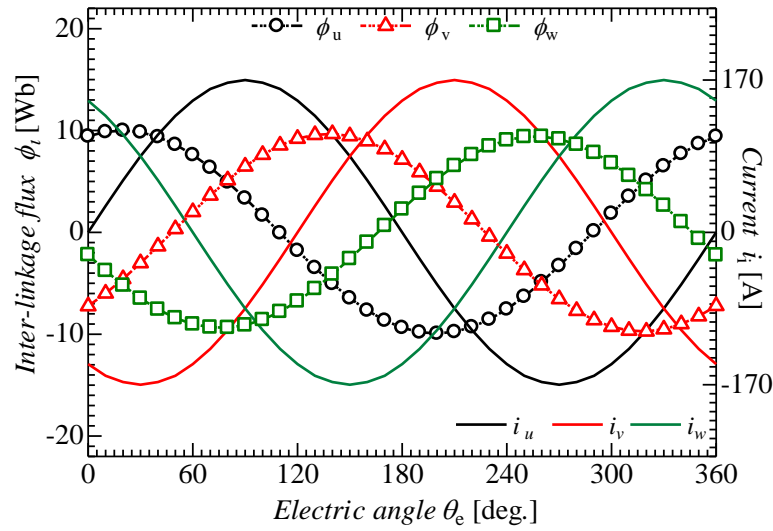


Fig.3.17. Absolute value and phase relation between inter-linkage flux and applied current in steady state

3.4.2.4. Eddy current distribution

Fig.3.18 is the distribution of eddy current in secondary reaction plate at stand-still $slip=1$. Eddy current along x -direction in the overhang part increases due to the influence of edge effect.

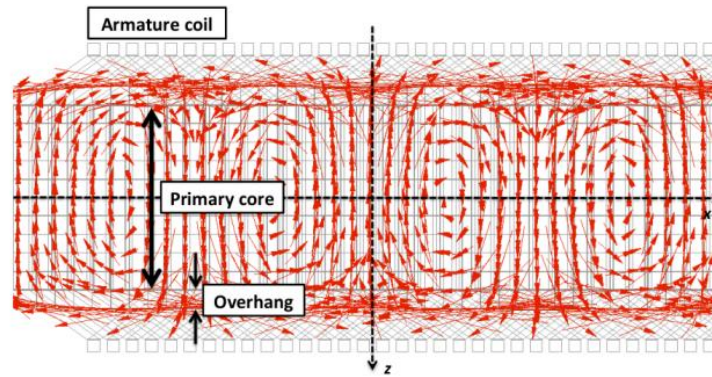


Fig.3.18. Distribution of eddy current in secondary reaction plate at steady state

3.4.2.5. 2-D FEM and 3-D IEM results comparison

By using the calculation method described above, the performance of LIM has been evaluated through numerical analysis in the comparison between 2-D FDM (without end & edge effect) and 3-D IEM (with end & edge effect) analysis including thrust, power factor, secondary loss, and efficiency, Fig.3.19.

Because of the calculating restriction on 3-D numerical analysis, LIM in 3-D model is only taken into account in three different values of slip frequency that are nearly equal to rated slip frequency. The results of 3-D analysis concerning the influence of edge elements have shown the strong dependence of thrust on operational speed according to the effect of end and edge effect. In addition, the large value of secondary loss can be seen according to the effect of secondary eddy current. While power factor is determined by the impedance value, efficiency can be calculated from output power and secondary loss as shown in 3.30. In 3-D IEM analysis, the rated slip becomes larger than in 2-D FDM. At higher slip or lower speed operation, performances of LIM in both 3-D IEM and 2-D FDM are the same.

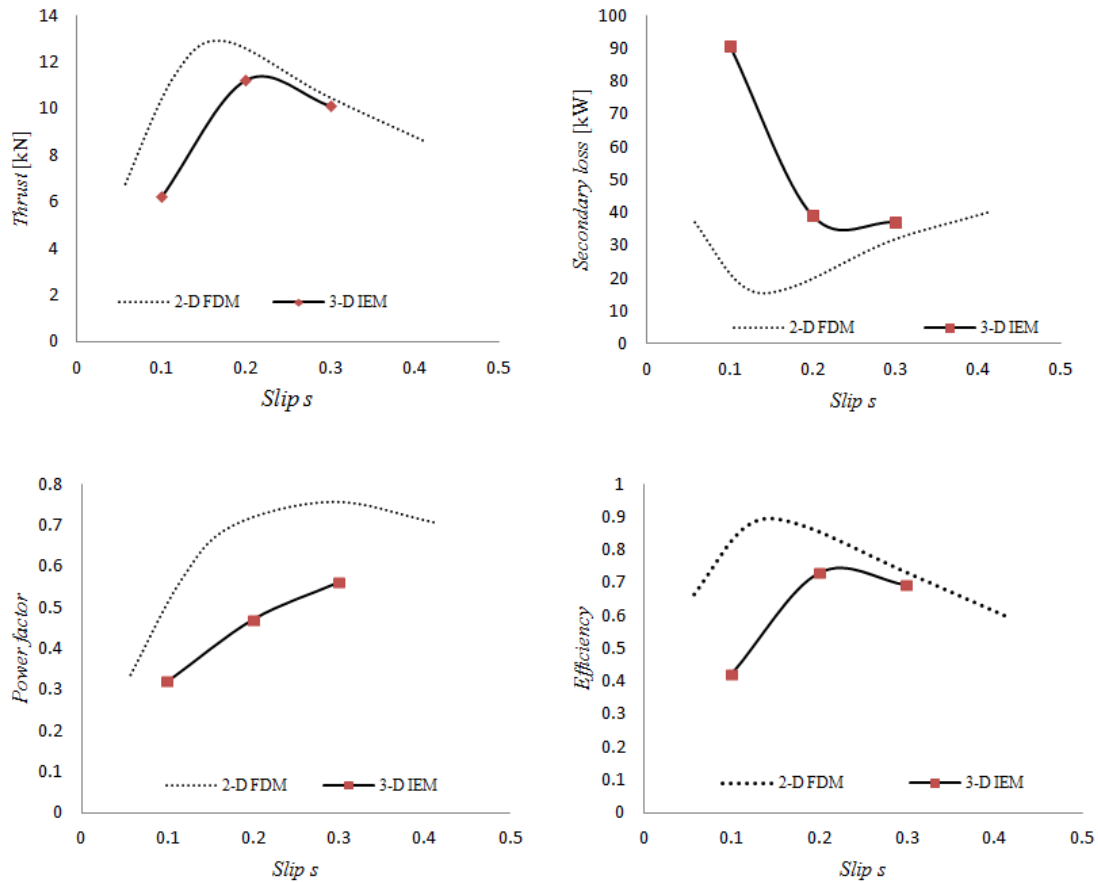


Fig.3.19. 2-D FDM and 3-D IEM results

Some significant points of IEM in ELF/MAGIC in comparison with FDM/FEM :

- Boundary conditions are unnecessary: specification of boundary conditions are not required for differential equation because it contains an infinity in analysis area in the integral equation method
- Space mesh is unnecessary: it is not necessary to create an air-element analysis of the object. It allows calculation of the magnetic flux density in any arbitrary point in the space. In FDM, elements in the space and air gap are necessary
- Handling of motion is easy: because of unnecessary of meshes in space, it is not necessary to consider the displacement of the meshes
- Analysis with complicated coil is easy: because there is no meshes in space, arbitrary shape of coil or free current direction can be applied
- It is possible to consider the eddy current and induced current in the coil;
- High speed three-dimensional calculation (corresponding to parallel core): in 3-D FDM, degree of freedom and number of elements become large in comparison with 2-D so more calculation time is necessary. On the other hand, in 3-D IEM in ELF/MAGIC, although variables increase, it can be calculated at high speed because the number of element divisions in the depth direction is small
- High accuracy even in rough element division
- Space magnetic field is highly accurate
- Analysis of the steady state is a disadvantage.

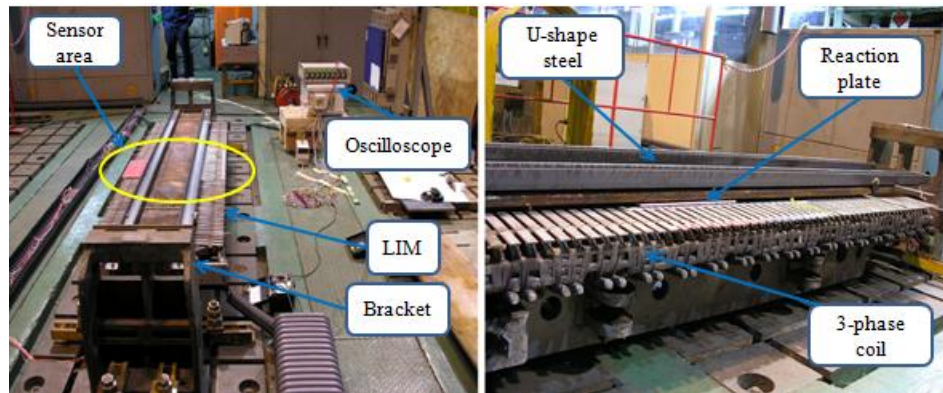
3.5. Actual LIM experiment and comparisons

In order to evaluate the exactitude of 3-D IEM, simulation results are compared with actual LIM experiment in [19]. Fig.3.20 (a) and (b) are the arrangement of test devices. For safety purpose, the primary side is fixed under the secondary side. Secondary side - copper reaction plate - is also fixed by U-shape steel and bracket. This means the experiments are carried out with different frequency inputs and $slip = 1.0$.

To measure the magnetic flux in the air gap, Hall sensors have been used. In order to get the accurate measured values of magnetic flux density distribution, instantaneous values are obtained through Hall sensors. In addition, since the temperature of the reaction plate can make change to the characteristics of the LIM, it is necessary to perform the flux density measurement in a short time.

Fig.2.31 shows the arrangement of Hall sensors along the moving direction. Measured range is conducted at two-pole near the center of LIM. The sensors are arranged at each 20mm along this two-pole.

Differences of LIM experiment and analysis conditions are expressed in Table 3.2.



a. Equipment of actual LIM test

b. Actual LIM

Fig.3.20. Experimental equipment of actual LIM

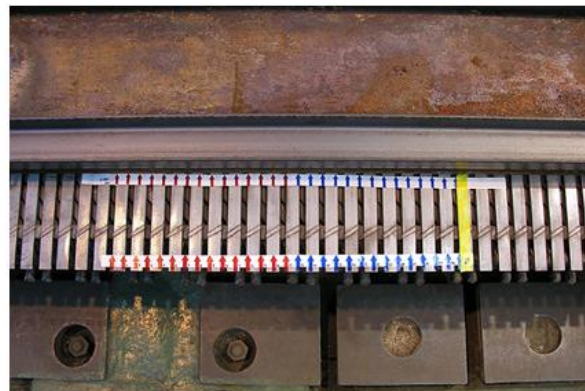
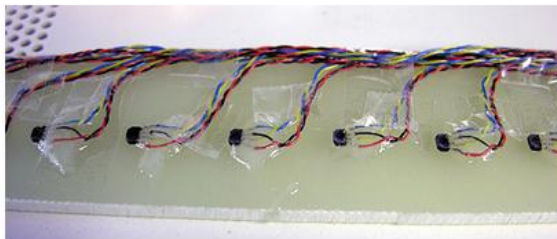


Fig.3.21. Sensors arrangement

Table 3.3. Experiment and analysis conditions

Parameter	Actual LIM	3-D IEM
Slip	1	1
Primary speed [km/h]	0	0
Relative permeability in primary iron	1000	1000
Relative permeability in back iron	300	1000
Conductivity in primary/back iron ($\times 10^7 S/m$)	0.6	0
Material of conduction plate	Cu	Cu

Air gap magnetic flux density

Air gap magnetic flux density along the moving direction obtained by experiment and 3-D IEM analysis at the same primary frequency of 21Hz are plotted in Fig.3.22. It can be seen that there is no plain difference between magnetic flux along two poles of LIM and calculated results. Therefore, the validity of the 3-D IEM analysis with current input can be approved.

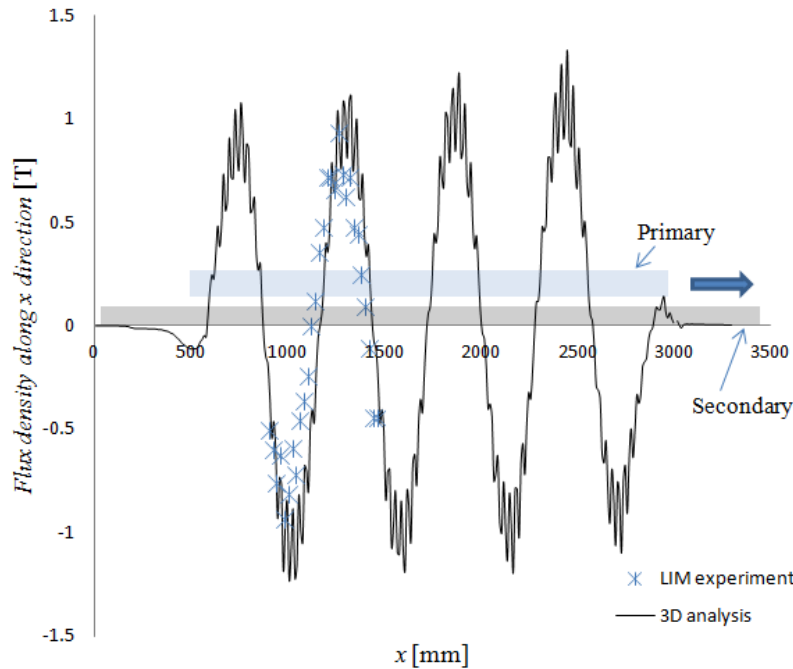


Fig.3.22. Air gap flux density

Impedance and power factor

In addition, in case of copper reaction plate, absolute value of impedance and power factor obtained from voltage and current measurement are compared with 3-D IEM analysis results. Because of the restriction in experiment conditions, all of the experiments with different primary frequency are taken at the same slip frequency of 1.0. While absolute value of impedance and power factor in 3-D analysis with current sources are determined from the calculation method as described above, these values are obtained from voltage and current measurement in experiment. There is no plain difference between simulation and experiment in absolute value of impedance (Fig.3.23.a), but in case of power factor, the difference becomes large when primary frequency increases, Fig.3.23.b. The reason can be explained as follow: In LIM with only conductor plate and iron plate in secondary side, because of the strong influence of skin effect, magnetic saturation occurs easily, especially in high primary frequency, so it affects physical properties such as permeability and conductivity. Because of the ignorance of this problem in 3-D analysis, at high primary frequency, a larger difference between analysis and experiments occurs. The restriction is that there is necessity to consider the non-linear characteristics with magnetic saturation.

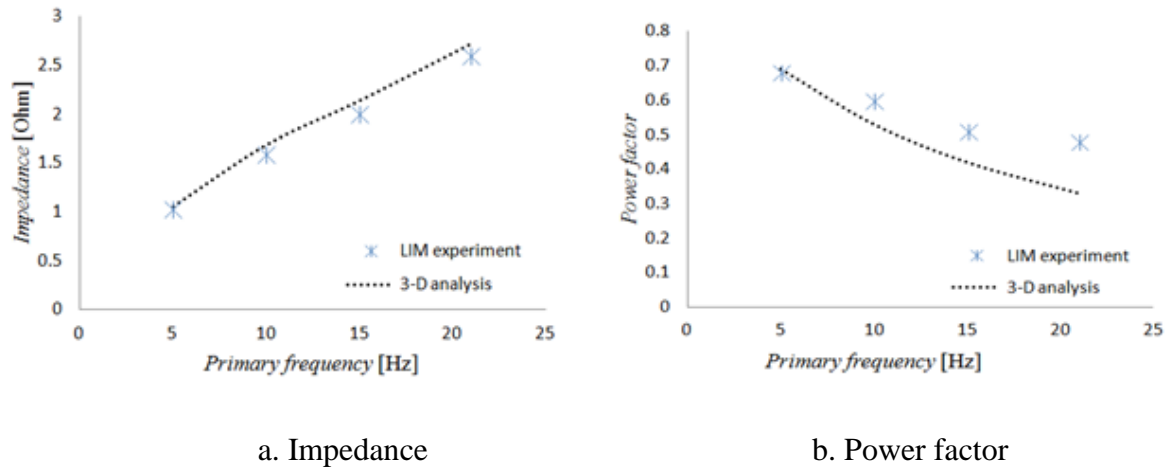


Fig.3.23. Impedance and power factor with different primary frequencies

3.6. Chapter summary

In this chapter, the model of LIM for Linear Metro and its problems, and the analysis methods for determining the LIM characteristics have been introduced. While classical 2-D FDM method can be used to analyze the characteristics of the full length of LIM with the influence of end-effect, it cannot be used to analyze the influence of edge effect caused by lateral elements. To solve this problem, 3-D IEM has been used for the requirement of full three-dimensional model for accurate analysis of LIM. Because of the unnecessary on boundary condition or space mesh, calculating time can be reduced. Full analysis model and performance of LIM with different slips have been shown.

In order to evaluate this analysis method, simulation results have been compared with actual LIM performances. As a result, a large difference was not seen in the magnetic flux distribution of measurements and numerical calculations. In addition, the results are the same in case of absolute value of the impedance, but in case of power factor, difference of measurement and numerical analysis increases when primary frequency increases. This result implies that the non-linear of secondary core must be concerned in analysis.

With high accuracy in simulation results, 3-D IEM can be used to design the secondary side that causes edge effect for high performance of LIM.

Chapter IV

Conclusion and Future work

4.1. Conclusion

This thesis contributes to improving the performance of linear metro in the following aspects:

1. ATO running curve design

The model and operation of ATO running curve design are introduced. Power limited brake has been used for better usage of regenerative brake. ATO running curve are calculated based on maximal principle: maximal powering, longest coasting and maximal braking power. This model has been used for calculating the relationship of total energy consumption, maximal braking power and running time of a train in an inter-station.

Different from normal running curve design, when design the running curve with ATO support, the designing method in this thesis considers both energy consumption and braking power for improving the regenerative energy utilization. Thus, we must also decide the influence of different parameters on running curve design. In real operation conditions with speed limitation, maximal principle is still correct in both of reducing total energy consumption and reducing the maximal braking power.

2. 3-D IEM for LIM analysis

Longitudinal end effect and transverse edge effect are two main problems of LIM. 3-D with full-length model is necessary to find accurate LIM performance and further for LIM design. 3-D Integral Equation Method using Magnetic Moment Method to analyze the full model of LIM is introduced. In comparison with 2-D FDM, the influence of end-effect and edge-effect that have strong effect on LIM performance are also mentioned in this method. We can obtain high accuracy calculation results with different slips or different primary speeds. In addition, significant points on analysis conditions of IEM in comparison with FDM/FEM are also introduced.

For evaluating this analysis method, we conduct the experiments in steady state to obtain the air gap flux density, impedance and power factor at different primary frequency.

4.3. Future work

Based on the achievements and limitations of this thesis as well as on the requirement of my future career, not only for linear metro but also for normal railway system, the future works are proposed as the followings:

1. Energy saving on train operation

- Based on the energy saving principle on ATO running design, I would like to conduct the experiment in real railway system with ATO support. With planned running time, using low notch-off speed and low braking power at long braking time for a train in an inter-station. In addition, re-calculate running time for a train in the whole line based on energy-braking power-running time relation will be considered.
- In current railway system, substation voltage is kept at constant value 1500V. In order to transfer more energy from braking train to accelerating train, depending on braking power the research for adjusting substation voltage will be concerned.

2. Power electronic for railway

- Due to the limitation of experiment condition and high requirement of safety, in actual LIM operation, measurement of thrust and normal force were not carried out. Other precise measurements will be examined to evaluate numerical analysis. For high LIM efficiency and power factor, by using the 3-D IEM, different secondary reaction plates will be considered. In addition, the research on independent drive for each LIM in order to reduce the influence of end effect is also concerned.
- In addition, according to the requirement of future career, I will conduct the researches on power equipments such as the latest SiC inverter and new permanent magnet motor.

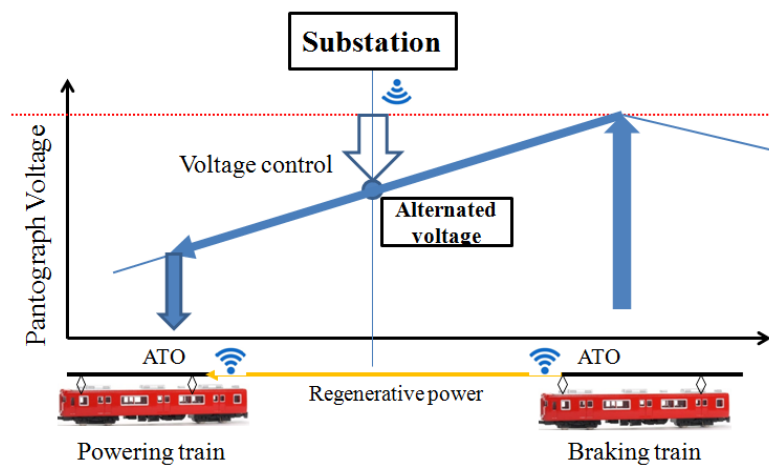


Fig.4.1. Framework of better use of regenerative energy for train operation research

References

- [1] T. Koseki, *Technical trends of railway traction in the world*, International power electronic conference, 2010.
- [2] E. Isobe, J. Cho, I. Morihisa, T. Sekizawa, R. Tanaka, *Linear metro transport systems for the 21st century*, Hitachi Review, 1999.
- [3] J. Ohya, S. Iba, H. Nakazawa, *Automatic train operation systems for subway trains*, Toshiba Review, 2008.
- [4] 福岡市高速鉄道3号線（七隈線）3000系電車 (In Japanese)
http://subway.city.fukuoka.lg.jp/subway/about/vehicles_3.html
- [5] T. Koseki, Z. Yang, K. Hisatomi, T. Mizuma, *Approximate constant power braking in high speed and onboard driver assistance for energy saving electric train operation*, 2012.
- [6] Z. Yang, *Smart Braking Control for Energy-saving Train Operation – Experimental Implementing of Driver Assistance* —, The University of Tokyo, Master Thesis, 02.2013 (In Japanese)
- [7] E. Khmelnitsky, On an optimal control problem of train operation, IEEE Transactions on Automatic Control, Vol. 45, pp. 1257, 2000.
- [8] P. Howlett, *The optimal control of train*, Annuals of operations research, Vol. 98, pp. 65 (2000)
- [9] R. Franke, P. Terwiesch, M. Meyer, *An algorithm for the optimal control of the driving of trains*, IEEE Transaction on decision and control, Vol 1 (2000)
- [10] H. Ko, T. Koseki, M. Miyatake, *Application of dynamic programming to the optimization of the running profile of a train*, Computers in railways IX, Vol. 15, pp. 103-112 (2004)
- [11] M. Dominguez, A. F. Cardador, A. Cucala and R. Pecharroman, *Energy saving in metropolitan railway substations through regenerative energy recovery and optimal design of ATO speed profiles*, IEEE Transactions on Automation Science, Vol.9, No. 3, 06. 2012
- [12] M. Miyoshi, T. Takeba, M. Miyatake, *Development of an energy efficient train traffic control system for saving electricity*, Computers in railways XIII, Vol 127 (2012)
- [13] I. Hasegawa, S. Uchida, *Braking system*, Japan railway & Transport review 20, June, 1999.
- [14] 回生エネルギーを最大限に活かし、さらなる省エネへ、Mitsubishi Electric Review, 21.2013 (In Japanese)
<http://www.mitsubishielectric.co.jp/corporate/randd/spotlight/spotlight23.html>
- [15] O. Junko, I. Satoshi, N. Hiroji, *Automatic train operation system for subway trains*, Toshiba Review, 21.2008
- [16] H. Ko, T. Koseki, M. Miyatake, *Application of dynamic programming to optimization of running profile of a train*, 2004

- [17] Pontryagin's maximum principle
<http://www.statslab.cam.ac.uk/~james/Lectures/oc16.pdf>
- [18] T. Koseki, *Flux synthesizing Linear Induction Motor*, The University of Tokyo, PhD. Thesis, 1991.12.
 URL:<http://repository.dl.itc.u-tokyo.ac.jp/dspace/handle/2261/1186?mode=full>
- [19] Y. Nozaki, *Identification of linear induction motor plant model with significant consideration of end-effect*, The University of Tokyo, PhD. Thesis, 2007. 12 (In Japanese)
- [20] S. Yamamura, *Theory of linear induction motor*, The University of Tokyo Press, 09.1977
- [21] S. G. Lee, H. W. Lee, S. H. Ham, C. S. Jin, H. J. Park, J. Lee, *Influence of the construction of secondary reaction plate on the transverse edge effect in linear induction motor*, IEEE Trans. Mag., Vol. 45, No. 6, June 2009.
- [22] H. Lee, S. G. Lee, H. J. Park, *Characteristic analysis of a linear induction motor for a lightweight train according to various secondary schemes*, IJR International Journal of Railway, Vol. 1, No. 1, pp. 6-11, March, 2008.
- [23] T. Yamaguchi, Y. Kawase, M. Yoshida, and Y. Ohdachi, *3-D finite element analysis of a linear induction motor*, IEEE Trans. Magn., vol.37, no. 5, pp. 3668-3671, Sep. 2001.
- [24] Finite Difference Method
<http://www.mathematik.uni-dortmund.de/~kuzmin/cfdintro/lecture4.pdf>
- [25] H. W. Lee, C. Park, K. H. Han, B. Lee, S. Y. Kwon and H. J. Park, *Optimal air gap control of a linear induction motor for Korean railway transit*, WCRR 2008.
- [26] *Three-dimensional non-linear dynamic magnetic field analysis with ELF / MAGIC*
 URL: <http://www.elf.co.jp/product/elfmagic.html>
- [27] L. D. Tung, O. Chadebe, J. Guichon, G. Meunier and Y. Lembeey, *Coupling between PEEC and magnetic moment method*, The international journal for computation and mathematics in electrical and electronic engineering, Vol. 32, No. 1, pp. 383-395, 2013.
- [28] Y. Takahashi, *Large scale electromagnetic field analysis by using integral equation method for practical electric machine design*, Waseda University, PhD. Thesis, 2008 (In Japanese)
 URL: <http://dspace.wul.waseda.ac.jp/dspace/bitstream/2065/28676/3/Honbun-4773.pdf>
- [29] Y. Yamamoto, N. V. Cuong, T. Koseki, *Performance improvement and power saving of linear induction motor for urban rail-guided transport considering their lateral edge effect*, Japan railway technology symposium (J-Rail), Tokyo-Japan, 2012 (In Japanese)
- [30] S. P. Bhamidi, *Design of a single sided linear induction motor using a user interactive computer program*, University of Missouri Columbia, Master Thesis, 2005.

Publications

- [1] N. V. Cuong, Y. Yamamoto, T. Koseki, *3-D numerical analysis for impedance calculation and high performance consideration of linear induction motor for rail-guided transportation*, The 2nd Advanced Electromagnetic Symposium, AES 2013, Sharjah-UAE, pp. 62-67, 03.2013
- [2] N. V. Cuong, S. Watanabe, T. Koseki, *A fundamental study on energy saving on automatic train operation for linear metro*, Linear drive/ Transportation and Electric Railway Joint Study Symposium, Iwate-Japan, pp. 41-44, 08. 2013.
- [3] N. V. Cuong, T. Koseki, E. Isobe, *Numerical analysis for influence of construction of the secondary reaction plate in the characteristics of linear induction motor - for urban rail-guided transportation-*, The 39th Annual Conference of the IEEE Industrial Electronics Society, IEEE IECON, Vienna, Austria, 11.2013.
- [4] N. V. Cuong, S. Watanabe, T. Koseki, *A proposal of simultaneous monitoring of total energy and peak braking power for the design of energy-saving ATO running curve*, Japan railway technology symposium (J-Rail), Tokyo, 12.2013.
- [5] N. V. Cuong, T. Koseki, *Maximal braking power consideration in energy saving ATO running curve design*, 電気学会全国大会, Eihime, 03.2014. (Accepted)
- [6] N. V. Cuong, T. Koseki, *Influence of different parameters on total energy consumption, braking power and running time of ATO running curve design*, 第7回鉄道分野の新技术に関するシンポジウム、NU-Rail 2014, Tokyo, 03.2014 (Accepted)

Co-authored paper

- [1] Y. Yamamoto, N. V. Cuong, T. Koseki, *A numerical study on variation of forces and impedance of a single side linear induction motor to lateral displacement*, 電気学会全国大会, Hiroshima, 03. 2012. (In Japanese)
- [2] Y. Yamamoto, N. V. Cuong, T. Koseki, *Performance improvement and power-saving of linear induction motors for urban rail-guided transport considering their lateral edge effect*, Japan railway technology symposium (J-Rail), Tokyo, Japan, 12. 2012. (In Japanese)
- [3] T. Koseki, S. Watanabe, N. V. Cuong, T. Mizuma, E. Isobe, *Dead time compensation of braking operation with an on-board drive assistance and a proposal of power limiting braking in an Automatic Train Operation*, Linear drive/ Transportation and Electric Railway Joint Study Symposium, Iwate-Japan, pp. 45-50, 08. 2013. (In Japanese)